FROM SIGNALING TO STRUCTURE: REGULATION OF EXTRACELLULAR MATRIX IN *C. elegans*

A Dissertation

by

ROBBIE DIANA SCHULTZ

Submitted to the Office of Graduate and Professional Studies of
Texas A&M University
in partial fulfillment of the requirements for the degree of

DOCTOR OF PHILOSOPHY

Chair of Committee,	Sarah E. Bondos
Co-Chair of Committee,	Tina L. Gumienny
Committee Members,	L. Rene Garcia
	Bruce Riley
	Emily Wilson
Intercollegiate Faculty Chair,	Craig Coates

May 2015

Major Subject: Genetics

ABSTRACT

The extracellular matrix is a meshwork of molecules that reside in the microenvironment between cells. Extracellular matrix, while historically known as an inert scaffold, is critical in regulating cell communication, shape, migration, and adhesion. Using *C. elegans*, we characterized regulation of extracellular matrix. First, we showed how activity of a cell-cell communication pathway is regulated and how pathway signaling affects composition and organization of an extracellular matrix. Next, we characterized an extracellular matrix component that is critical for cell adhesion and described how loss of this protein affects a spectrum of phenotypes, including cell shape, sensory perception, and extracellular matrix function.

DEDICATION

This work is dedicated to Emmett and Oris Baker. May your never-ending love and support always guide me.

ACKNOWLEDGEMENTS

I would like to thank my advisor, Dr. Tina L. Gumienny for all your support and guidance. I am grateful to Dr. Sarah Bondos for your encouragement and allowing me the opportunity to finish my research. I would also like to thank my committee members, Dr. Bruce Riley, Dr. L Rene Garcia, and Dr. Emily Wilson, for providing valuable direction and support throughout the course of this research.

Thanks also go to my friends and colleagues and the department faculty and staff for making my time at Texas A&M University a great experience. I especially would like to thank Dr. Suparna Taneja-Bageshwar and Kathy Beifuss for making time in lab enjoyable and always being happy to lend a helping hand.

Finally, thanks to my mother and father, sister, and aunt and uncle for all your love and encouragement. Finally, I would like to thank my husband for your patience and love.

NOMENCLATURE

AJM-1	*C. elegans* apical junction molecule
BMP	bone morphogenetic protein
BMP4	bone morphogenetic protein 4
CAV-1	*C. elegans* homologue of caveolin
CFCS	conserved furin cleavage sequence
COL-19	*C. elegans* cuticle collagen
Cyto	cytoplasmic domain
DAF-1	*C. elegans* type I receptor for DAF-7
DAF-4	*C. elegans* type II receptor for DAF-7 and DBL-1
DAF-7	*C. elegans* homologue of BMP
DBL-1	*C. elegans* homologue of BMP
DIC	differential interference contrast
DiI	1,1'-dioctadecyl-3,3,3'3'-tetramethylindocarbocyanine perchlorate
DPY-13	*C. elegans* cuticle collagen
DYF-7	*C. elegans* ZP-domain protein
DYN-1	*C. elegans* homologue of dynamin
EGL-4	*C. elegans* cyclic GMP dependent protein kinase
GFP	green fluorescent protein
eGFP	enhanced green fluorescent protein
IP2P	1-phenoxy-2-propanol

IPTG	isopropyl-beta-D-thiogalactopyranoside
ISW-1	*C. elegans* modifier of germline chromatin
LIN-35	*C. elegans* synMuv B protein
LON-2	negative regulator of DBL-1 signaling
MES-6	*C. elegans* modifier of germline chromatin
M_r	molecular mass
mRFP	monomeric red fluorescent protein
MW	molecular weight
N2	wild-type *C. elegans* Bristol strain
ND	not determined
NGM	nematode growth media
PCR	polymerase chain reaction
PiMP	photobleaching microscopy with non-linear processing
Pro	prodomain
RNAi	RNA interference
RRF-3	*C. elegans* RNA-directed RNA polymerase
SAX-7	*C. elegans* homologue of L1CAM
SB	scale bar
SEM	standard error of the mean
sfGFP	superfolder GFP
SMA-3	*C. elegans* Smad transcription factor in the DBL-1 signaling pathway
SMA-6	*C. elegans* type I receptor for DBL-1

SPP-9	*C. elegans* homologue of saposin
SRF-5	*C. elegans* surface antigenicity protein
SS	signal sequence
synMuv B	synthetic multivulva class B
TEM	transmission electron microscopy
TGF-β	transforming growth factor-β
TM	transmembrane domain
Vab	variably abnormal phenotype
VHA-5	*C. elegans* homologue of V-ATPase
WGA	wheat germ agglutinin
ZP	zona pellucida

TABLE OF CONTENTS

Page

LIST OF FIGURES

LIST OF TABLES

1. INTRODUCTION

The extracellular matrix is a meshwork of molecules that reside in the microenvironment between cells. The extracellular matrix components are secreted from nearby cells and are assembled into a meshwork that is often closely associated with the cells of origin. Extracellular matrix composition is complex; components include polysaccharides, fibrous proteins such as collagen, fibronectin, and elastin, adhesive proteins such as integrin and cadherin, and zona pellucida-domain proteins. The relative amounts and organization of these macromolecules vary between extracellular matrices, leading to a diverse array of forms and functions. Bone, cartilage, tendon, basement membrane, zona pellucida, and exoskeleton are all variations in extracellular matrix forms. While the extracellular matrix is historically known for its structural role acting as a scaffold to support cells and tissue, more recently extracellular matrix has been recognized to be critical in regulating cell communication, shape, migration, and adhesion (Brazil et al., 2015; Ferreira et al., 2014). Defects in organization of extracellular components are associated with disease, including infertility, deafness, and bone deformities (Brazil et al., 2015; Ferreira et al., 2014; Plaza et al., 2010). Mechanisms regulating function of extracellular matrix function need to be further studied.

I am interested in studying mechanisms regulating extracellular matrix using the *C. elegans* model system. Using molecular and cell biological approaches, I showed how a cell-signaling molecule is regulated and how activity of this signaling pathway affects

composition and organization of the extracellular matrix. Next, I characterized an extracellular matrix component and showed how loss of this protein affects cell shape, adhesion, sensory perception, and other organismal phenotypes.

Advantages of using *C. elegans*

Caenorhabditis elegans is a small, free-living nematode often found in rotting vegetation. The *C. elegans* system is advantageous because of its invariant, well-studied cell lineage and simple anatomy where adult hermaphrodites have only 959 somatic cells, including 302 neurons (Sulston *et al*., 1983). The *C. elegans* genome is fully sequenced and highly annotated, and many genes found in humans are conserved in *C. elegans*. Its small body size (about 1 mm), short generation time (about 3.5 days), and large brood size make maintenance within a laboratory amenable. *C. elegans* feeds on microbes and is often grown on agar plates seeded with a lawn of *E. coli* in laboratory settings, making propagation cost efficient. Further, animals can be frozen for long periods of time, eliminating the need for continuous propagation. While the typical *C. elegans* life span is 3 weeks, animals can survive harsh environmental conditions by entering an alternate life stage called dauer where they can survive in these harsh conditions for several months (Cassada and Russell, 1975). *C. elegans* has two sexes: hermaphrodites and males. Hermaphrodites are self-fertilizing, which allows for maintenance of genetically identical progeny. Hermaphrodites can also be mated with males to generate cross progeny. In addition, simple transgenic techniques provide a powerful tool to study the function of introduced transgenes in animals. As *C. elegans* is

transparent, microscopy in live or fixed animals can be used to study protein expression and cell structure and morphology using fluorescent and differential interference contrast (DIC) microscopy. These properties make *C. elegans* a powerful tool for studying how genes function and act to regulate organismal phenotypes.

Life cycle

The *C. elegans* life cycle comprises an embryonic stage, four larval (L1 – L4) stages, and an adult stage. Each larval stage is punctuated by a molt in which a new cuticle is formed and the old cuticle is shed. Standard reproductive development from embryogenesis to adulthood takes about 64 hours at 20°C. Harsh environmental conditions can arrest *C. elegans* development.

The nematode's default state is to pause at the first larval stage until favorable conditions are confirmed (Figure 1.1). L1 diapause occurs without any type of morphological modification. Post-embryonic development is only initiated upon feeding (Baugh and Sternberg, 2006; Fukuyama et al., 2006; Hong et al., 1998). Environmental factors including nutrient availability and temperature contribute to the decision to exit L1 arrest. Molecular mechanisms involved in the decision to exit from L1 arrest and continue with larval development include insulin pathway signaling, cell cycle regulators, and synMuv B gene products.

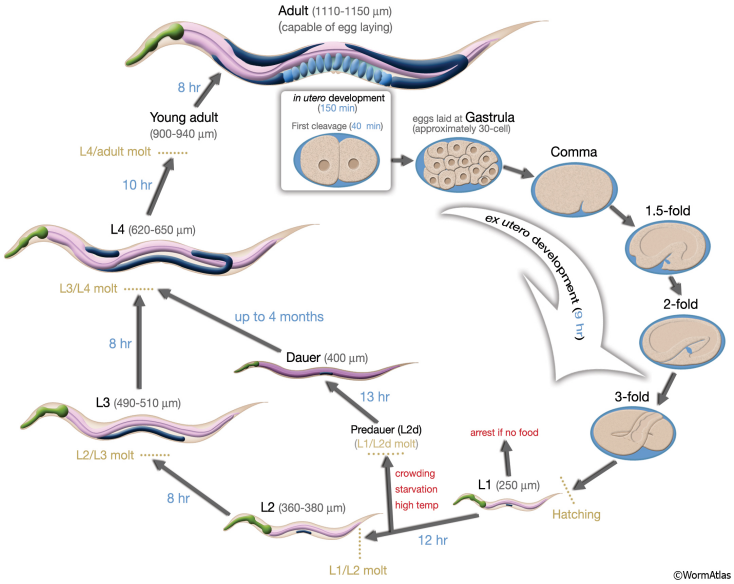

Figure 1.1 The *C. elegans* life cycle. The life cycle of *C. elegans* includes embryogenesis and four successive larval molts before reaching adulthood. Harsh environmental conditions prevent animals from exiting L1 arrest upon hatching or promote exit of standard reproductive development and entry into dauer arrest. Image adapted from WormAtlas.org.

Insulin signaling is a key regulator of arrest at both L1 and dauer stages. Animals mutant for *daf-2* insulin/IGF receptor constitutively arrest at L1 even in the presence of food (Baugh and Sternberg, 2006). Penetrance of the L1 arrest phenotype of *daf-2* mutants increases with temperature, suggesting that animals with loss of *daf-2* signaling display a physiological state at high temperature that mimics that of starvation (Baugh and Sternberg, 2006). *daf-2* regulates L1 arrest through control of the FOXO-family transcription factor, *daf-16*. Animals lacking DAF-16 continue to develop normally even in the absence of food, indicating that *daf-16* promotes L1 arrest through transcriptional

regulation of genes involved in development. Providing a mechanistic link between insulin signaling and cell cycle arrest, transcriptional targets of *daf-16* include cell cycle genes *cki-1* and *lin-4* (Baugh and Sternberg, 2006). *cki-1,* a cyclin-dependent kinase inhibitor, regulates post-embryonic development through control of cell division (Hong et al., 1998), while *lin-4,* a microRNA, regulates the progression from L1 to L2 (Feinbaum and Ambros, 1999; Olsen and Ambros, 1999). *daf-2* insulin signaling acts upstream of the *age-1* and *akt-1* to regulate developmental arrest in the germline independent of *daf-16* (Baugh and Sternberg, 2006; Fukuyama et al., 2006). The AGE-1/AKT-1 pathway is repressed by DAF-18/PTEN signaling to regulate quiescence in L1 in the absence of food (Fukuyama et al., 2006).

Misregulated L1 arrest has also been described for animals lacking function in specific synMuv B genes. While synMuv B genes derive their name from their synthetic multivulval phenotype that arises when they are combined with a synMuv class A or class C mutation (Fay and Yochem, 2007), it has recently been shown that specific synMuv B genes also regulate L1 arrest (Petrella et al., 2011). synMuv B genes are involved in regulation of chromatin structure and have no direct effect on sensory perception. Mutants lacking specific synMuv B gene function arrest at L1 when grown at 26°C, a temperature that is higher than normal growing conditions. High temperature L1 arrest by synMuv B mutant animals can be suppressed by mutations in genes that modify germline chromatin (Petrella et al., 2011). While it is known that both insulin signaling and synMuv genes play a role in L1 arrest and recovery, the specific cells involved in advancement from this sensory checkpoint are still unknown.

A second developmental checkpoint occurs after the L1 stage. If the animal senses that the environment is favorable enough for larval survival but not reproductive fitness, it enters an alternative, environment-resistant stage called dauer ("enduring" in German) (Figure 1.1) (Hu, 2007). Unlike animals in L1 arrest, which display no morphological modifications, dauer animals survive harsh environmental conditions by altering their internal physiology. Environmental conditions including food supply, temperature, and overcrowding contribute to the decision to enter dauer (Golden and Riddle, 1984). Both extrinsic and intrinsic cues mediate pathways that regulate dauer formation. Key regulators that mediate dauer developmental include neural signaling (Vowels and Thomas, 1992) and hormone signaling pathways including BMP (Ren et al., 1996), insulin (Kimura et al., 1997), and guanylyl cyclase signaling (see below) (Birnby et al., 2000). Mutations in dauer development genes can cause animals to inappropriately and constitutively enter the dauer state under non-inducing conditions (dauer constitutive) or to fail to enter the dauer state under inducing conditions (dauer defective).

Environmental cues are transformed into neuroendocrine signals by environmentally exposed neurons in the head. Signaling from hormonal pathways act to regulate dauer formation by inhibiting dauer development under favorable conditions. The DAF-7 TGF-β mediated pathway acts through ASI, ADF, and ASG chemosensory neurons (Schackwitz et al., 1996). When environmental conditions are favorable, the DAF-7 TGF-β ligand is produced in ASI neurons and acts on the DAF-1 type I and DAF-4 type II receptors, allowing the animal to continue with reproductive development

(Figure 1.2). However, if cues indicate an unfavorable environment, DAF-7 is no longer produced and, in the lack of DAF-7 pathway signaling, the animal will arrest in dauer. Likewise, when guanylyl cyclase signaling from the ASJ and ASK neurons (Schackwitz et al., 1996) or insulin pathway signaling from the ASI, ASJ, and other cells is present (Gottlieb and Ruvkun, 1994), dauer development is inhibited, thereby promoting a reproductive fate.

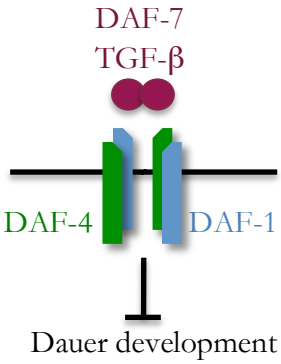

Figure 1.2 DAF-7 pathway signaling. *daf-7* acts upstream of receptor genes *daf-4* and *daf-1* to regulate entry into the alternate larval stage, dauer.

Despite being resistant to the external insults of detergents, dehydration, low oxygen, and some of the internal insults of aging, animals in the dauer stage are still highly sensitive to changes in their environment that signal them to resume reproductive

development and exit dauer (Figure 1.1). While dauer entry has been widely studied, little is known about dauer maintenance and recovery. We do know dauer maintenance is regulated by *glp-1* Notch signaling in AWC neurons (Ouellet et al., 2008). Dauer recovery is dependent on a second Notch ligand, *lin-12,* and insulin pathway signaling (Ouellet et al., 2008). While ASJ chemosensory neurons are critical for dauer recovery, it is unknown if the *lin-12* Notch pathway acts on ASJ neurons in its role in dauer recovery (Bargmann and Horvitz, 1991; Ouellet et al., 2008).

Extracellular matrix in *C. elegans*

There are two main types of extracellular matrix in *C.* elegans: basement membrane and the cuticle. Basement membrane is a thin network of molecules that surrounds epithelial tissue, separating tissue from the pseudocoelomic body cavity. Basement membrane is closely associated with its secreting tissue and covers many surfaces, including muscle, intestine, pharynx, and hypodermis. Many components of mammalian basement membrane are conserved in *C. elegans* (Hutter et al., 2000). Basement membranes display stage and tissue-specific differences in composition and organization.

The cuticle is a secreted extracellular matrix comparable to bone and serves as an exoskeleton to provide protection from the environment and allows the animal to move (Kramer et al., 1988; Page and Johnstone, 2007). The cuticle, which is secreted by underlying hypodermal tissue, is composed of multiple layers that can be distinguished using transmission electron microscopy (TEM) techniques (Figure 1.3). The composition

of the cuticle includes collagens, various heavily cross-linked collagen-like proteins called cuticulins, and lipids in the outmost layer (Cox et al., 1981a). The cuticle is patterned by ultrastructure, including annuli, which are circumferential ridges that line the entire length of the animal, and stage-specific alae, which are longitudinal lateral ridges (Cox et al., 1981b). Mutation in collagens, including *dpy-7* and *dpy-13,* results in disruption of matrix substructure within the cuticle, causing defects in organization of the annuli (McMahon et al., 2003). Disruption of cuticular cuticulin components, including ZP-domain proteins CUT-1, CUT-3, and CUT-5, affects both body shape and alae formation (Sapio et al., 2005).

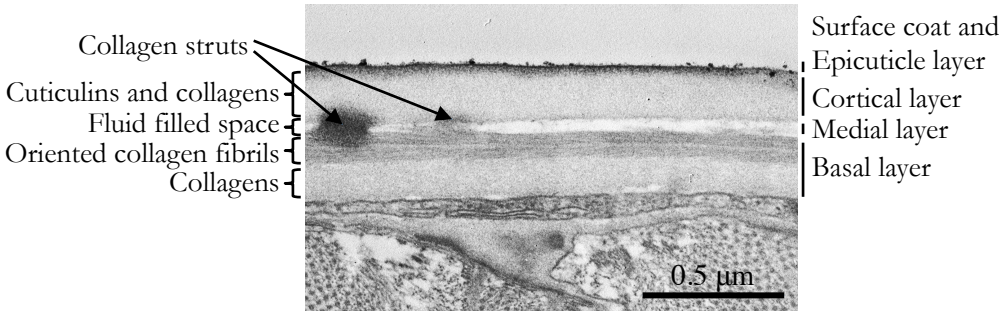

Figure 1.3 The *C. elegans* cuticle. The cuticle is composed of multiple layers. Each layer (indicated on the right side of the figure) has a unique composition (indicated on the left side of the figure).

Epithelia

The *C. elegans* epithelial system includes the pharynx, intestine, interfacial cells, somatic gonad cells, and epidermis. The epidermis can be further divided into two

categories: the hypodermis and specialized epithelial cells. The pharynx is the foregut and is part of the alimentary system. It is posteriorly connected to the intestine. The intestine is responsible for digesting food and absorbing nutrients. The hypodermis covers the main body cavity, head, and the tail. The hypodermis, along with specialized epidermal seam cells, secretes components of the cuticle. Some features are often common between various epithelial tissues in *C. elegans*: apical junction structures establish cell adhesion throughout the epithelia, epithelia secrete extracellular matrix components and are surrounded by a basally localized basement membrane, and epithelia have an apical surface that often faces a lumen.

DBL-1 BMP signaling

Bone morphogenetic proteins (BMPs) are members of the transforming Growth Factor-β (TGF-β) superfamily of intercellular signaling molecules and comprise an import means of cell-to-cell communication in eukaryotic animals. Misregulation of these pathways leads to developmental defects and diseases, and is associated with a host of cancers, vascular defects, and bone abnormalities (Padua and Massague, 2009; Wu and Hill, 2009). While there are over thirty TGF-β superfamily members in mammals (Wu and Hill, 2009), *C. elegans* have only five TGF-β ligands with non-redundant functions (Gumienny and Savage-Dunn, 2013).

DBL-1 is a secreted, dose-dependent ligand that belongs to the BMP family in *C. elegans*. While DBL-1 is secreted from nervous tissue (Morita et al., 1999; Suzuki et al., 1999), it must be trafficked to the epidermis where it binds to receptors (Krishna et al.,

1999). Upon activating receptors, the DBL-1 BMP pathway activates a signaling cascade that regulates transcription of many genes. Extracellular proteins are involved in regulation of the *dbl-1* pathway, including *lon-2,* a negative regulator of *dbl-1* signaling (Figure 1.4) (Gumienny et al., 2007). The DBL-1 ligand acts on the *daf-4* type II and the *sma-6* type I receptor complex (Figure 1.4). The receptors then act on receptor Smads, *sma-2* and *sma-3*, which complex with the co-SMAD, *sma-4*. The SMAD complex can then translocate into the nucleus to regulate transcription (Krishna et al., 1999; Morita et al., 1999). Genes that are either activated or repressed by the DBL-1 pathway then affect a variety of processes, including body length and male tail development. Alteration of the DBL-1 pathway in *C. elegans* alters body length in a dose-dependent manner, providing a sensitive *in vivo* readout of ligand activity (Figure 1.5).

ZP-domain proteins

Zona pellucida-domain (ZP-domain) proteins are a family of extracellular molecules defined by their zona pellucida-domain, a protein-protein polymerization motif that allows ZP-domains to self-assemble into fibrils and even matrices. This family of extracellular proteins was first identified in the zona pellucida, an extracellular matrix surrounding the mammalian egg (Bork and Sander, 1992). Since that time, ZP-domain proteins have been characterized in diverse processes, ranging from cellular adhesion, organization of extracellular matrices, establishment of cell shape, and mechanotransduction. Disruption of ZP-domain protein organization can lead to deafness (Verhoeven et al., 1998), infertility (Dean, 1992), and vascular defects

(McAllister et al., 1994). In *C. elegans*, there are approximately 40 predicted ZP-domain proteins of largely unknown function (Sapio et al., 2005).

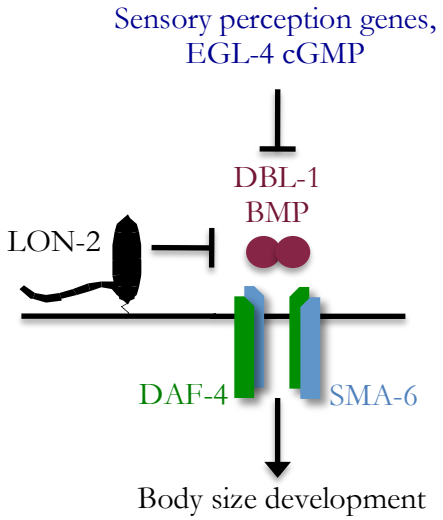

Figure 1.4 EGL-4 and DBL-1 pathway signaling. EGL-4 acts upstream of the DBL-1 pathway to regulate body length. The DBL-1 ligand activates a signaling cascade by binding to DAF-4 and SMA-6 type II and I receptors respectively. LON-2 is a negative regulator of DBL-1 pathway signaling.

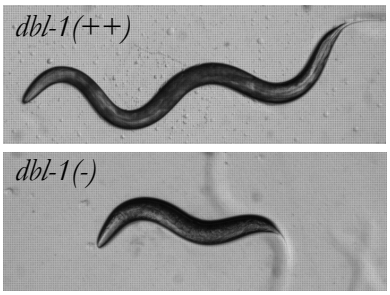

Figure 1.5 DBL-1 regulates body size development. DBL-1 is a dose dependent regulator of body length. Animals overexpressing DBL-1 (*dbl-1(++))* are long and animals lacking DBL-1 (*dbl-1(-)*) are small.

Regulation of body size development

Body size determination is a process that is precisely controlled by regulating either cell size and/or cell number. Body height in mammals is precisely controlled by multiple molecular mechanisms, including BMP, insulin, and hormone signaling, which in turn control cellular processes, including cell size, long bone growth, and response to environmental cues including nutritional status (Le Goff and Cormier-Daire, 2012; Visser et al., 2009). Some of these factors also govern body size regulation in *C. elegans*. In *C. elegans*, body size is dependent on BMP pathway signaling and organization of the cuticle. Unlike mammals, whose size is also determined by cell number, all congenic *C. elegans* have the same number of cells (Nagamatsu and Ohshima, 2004).

DBL-1 is the BMP superfamily member that positively regulates body size in *C. elegans*. While DBL-1 is secreted from nervous tissue (Morita et al., 1999; Suzuki et al., 1999), it must be trafficked to the epidermis where it binds to receptors, activating a signaling pathway to regulate body size development (Figure 1.4) (Krishna et al., 1999). DBL-1 is a dose dependent regulator of body size, where animals with increased signaling display a long body length and animals with decreased signaling display a small body length, providing a sensitive *in vivo* readout of ligand activity (Figure 1.5). *egl-4*, a cGMP dependent protein kinase, promotes a reduced body size through inhibition of the DBL-1 BMP pathway (Figure 1.4) (Fujiwara et al., 2002; Hirose et al., 2003), where loss-of-function mutations in *egl-4* produce an animal with a large body size (Daniels et al., 2000) and gain-of-function mutations result in an animal that is smaller than wild-type (Raizen et al., 2006).

Animals that cannot sense their environment are also typically smaller than wild type (Fujiwara et al., 2002). While the role of sensory perception genes in body size regulation is not well understood, studies have shown that while these animals cannot properly sense their environment, the small body size of these mutant animals is not caused by an inability to locate food (Fujiwara et al., 2002). These results suggest that sensory perception may regulate neuroendocrine function to determine body size. Epistasis analyses have placed genes involved in sensory perception upstream of *egl-4* and *dbl-1* BMP signaling (Figure 1.4) (Fujiwara et al., 2002).

C. elegans body shape can also be influenced through organization of the cuticle. The cuticle is primarily composed of collagen and collagen-like proteins, called

cuticulins. Genes affecting collagen organization can affect both the size and shape of the animal (Fernando et al., 2011; Sapio et al., 2005; von Mende et al., 1988).

Uniting regulatory mechanisms of DBL-1 signaling and cuticular organization, underlying hypodermal tissue secretes cuticular components that affect the shape and therefore size of the animal (Singh and Sulston, 1978), and DBL-1 affects the ploidy of hypodermal nuclei (Flemming et al., 2000; Fung et al., 2007). DBL-1 BMP signaling mutant animals have decreased hypodermal ploidy, yet animals with defects in a cuticular collagen, *dpy-2,* have wild type hypodermal DNA content indicating that reduced hypodermal ploidy is not conserved among all small animals (Flemming et al., 2000; Fung et al., 2007). These results could indicate that hypodermal ploidy is not the sole mechanism responsible for changes in body size. Further, microarray analyses have identified genes that are up- or down-regulated by DBL-1 BMP pathway signaling, including cuticle collagen genes (Liang et al., 2007; Mochii et al., 1999; Roberts et al., 2010).

Environmental perception

The small roundworm *C. elegans* is exquisitely sensitive to its surroundings and is developmentally responsive to environmental cues that signal survival potential. *C. elegans* sense their environment in part through environmentally exposed neurons in the head, called amphids. The dendrites of amphid neurons are established through retrograde extension, where the dendrite is anchored at the nose tip and the cell body extends posteriorly during embryonic development (Heiman and Shaham, 2009).

Adherence of dendrites to the nose tip is crucial for proper dendrite extension. Dendrites of amphid neurons are anchored through the ZP-domain protein DYF-7, as defects in DYF-7 cause loss of neuronal adhesion to the basement membrane, resulting in unattached, truncated dendrites (Heiman and Shaham, 2009).

Animals that fail to perceive environmental cues are often unable to take up lipophilic dye in environmentally exposed neurons, displaying the Dyf (dye-filling defective) phenotype. Further, sensory perception mutant animals are typically dauer defective because they fail to sense environmental stimuli that signal for an animal to enter the dauer pathway (Starich et al., 1995).

2. REGULATION OF EXTRACELLULAR MATRIX ORGANIZATION BY BMP SIGNALING IN *CAENORHABDITIS elegans**

Introduction

Intercellular signaling by bone morphogenetic proteins (BMPs), members of the Transforming Growth Factor-β (TGF-β) superfamily of signaling morphogens, is critical for a variety of normal developmental and homeostatic processes, including extracellular matrix deposition and remodeling. BMPs are critical for proper limb outgrowth during development (Bandyopadhyay et al., 2006). Recombinant human BMPs are used clinically to repair and replace bone (Lo et al., 1998). Perturbation of BMP signaling levels can contribute to pathogenic conditions including bone disorders and cancers (Miyazono et al., 2010).

In the invertebrate *Caenorhabditis elegans*, BMP member DBL-1 (Drosophila Dpp and BMP-like-1) regulates post-embryonic body size and other phenotypes (Morita et al., 1999; Savage-Dunn et al., 2000; Suzuki et al., 1999). Animals with increased DBL-1 signaling are longer than wild-type animals, while loss of signaling results in smaller animals (Table 2.1). The body length phenotype develops during postembryonic development, and is not based on cell number, as this eutelic species has a fixed somatic cell number among its members (Flemming et al., 2000; Nagamatsu and Ohshima, 2004; Suzuki et al., 1999). Studies to address how DBL-1 signaling regulates body size has

*Reprinted with permission from "Regulation of extracellular matrix organization by BMP signaling in *Caenorhabditis elegans*" by Schultz, R. D., Bennett, E. E., Ellis, E. A. and Gumienny, T. L., 2014. *PLoS one* 9, e101929. Copywright 2014 by Public Library of Science. DOI 10.1371/journal.pone.0101929.

revealed a canonical BMP signaling pathway exists to transmit the secreted DBL-1 signal from the cell membrane through a set of conserved receptors to the nucleus by Smad transcriptional regulators (Savage et al., 1996). The cellular focus of the body size phenotype is the hypodermis, an epidermal tissue that surrounds the animal's internal tissues and synthesizes the nematode cuticle, a sturdy, protective extracellular matrix (Schulenburg et al., 2004; Wang et al., 2002; Yoshida et al., 2001). The DBL-1 receptors, Smads, other regulatory factors, and a multitude of pathway targets are expressed in this tissue. Previous work to address the question of how DBL-1 regulates body size has provided evidence of a partial contribution by endoreduplication within these hypodermal cells (Flemming et al., 2000; Lozano et al., 2006; Morita et al., 2002; Nagamatsu and Ohshima, 2004; Nyström et al., 2002; Wang et al., 2002). Multiple studies show that expression of a number of transcriptional targets, including cuticular components, is altered by changes in DBL-1 signaling (Fernando et al., 2011; Liang et al., 2007; Mochii et al., 1999; Roberts et al., 2010). Loss of single cuticular proteins can also alter nematode body length (Brenner, 1974; Fernando et al., 2011; Page and Johnstone, 2007).

Table 2.1 DBL-1 is a dose-dependent regulator of body length and annular width.

Genotype	Body length	P-value	n	Annular width	P-value	n
Wild type	100±2	-	30	100±4	-	33
dbl-1(nk3)	79±2	<0.0001[A]	30	82±3	<0.0001[A]	32
dbl-1(nk3); dbl-1(++)	97±2	<0.0001[B]	30	N.D.	-	-
dbl-1(++)	110±2	<0.0001[A]	30	112±4	<0.0001[A]	30
lon-2(e678)	119±2	<0.0001[A]	29	N.D.	-	-

Body length and annular width represent average measurements relative to wild type ± the 95% confidence interval. P-values compare data to wild type ([A]) or *dbl-1(nk3)* ([B]) using the unpaired t-test. N.D. is not determined.

Loss of DBL-1 signaling increases sensitivity to different drug types in *C. elegans* (Almedom et al., 2009; Vashlishan et al., 2008). While mutation of drug target genes can affect drug sensitivity of the animal, alteration of some permeability barrier components also generally increases sensitivity of animals to anesthetics (Partridge et al., 2008; Ruiz-Lancheros et al., 2011). It has been proposed that DBL-1 also affects drug entry, rather than affecting the function of the drug targets themselves (Almedom et al., 2009).

Based on the observations that (1) the cuticle-secreting tissue is responsible for DBL-1-mediated body size regulation (Nyström et al., 2002; Wang et al., 2002; Yoshida et al., 2001), (2) cuticle-specific genes are highly regulated by DBL-1 signaling (Liang et al., 2007; Roberts et al., 2010; Wang et al., 2002), and (3) changes in cuticle can affect

both body morphology and drug response (Page and Johnstone, 2007; Partridge et al., 2008; Ruiz-Lancheros et al., 2011), similar to DBL-1 variations in signal strength, we hypothesized that these DBL-1-mediated phenotypes are consequences of altered cuticle. We asked if the cuticle was affected in nematodes with genetically manipulated levels of DBL-1 signaling. Animals overexpressing tagged DBL-1 are more resistant to drugs, showing a dose-dependent response to anesthetics by DBL-1. Using a novel microwave-based permeability assay for live animals and by genetically disrupting cross-linkages within the cuticle, we show that DBL-1 regulates cuticular barrier function. We show that this physiological change in cuticular permeability underlies the drug response phenotype displayed by DBL-1 pathway mutant animals. Loss of DBL-1 also permits tails to become entangled, forming "worm-stars". This oriented aggregation is phenocopied in wild-type animals that have had their surface coat stripped, further confirming that *dbl-1* mutant animals have altered surface properties. Quantitative differences in the spacing of annuli, circumferential ridges in the *C. elegans* cuticle, correlate with body length changes and DBL-1 dose. Using transmission electron microscopy, we discovered substantial cuticular changes that correlate with DBL-1 signaling levels, including deposition of surface lipids and organization of cuticular layers.

We propose that a common physiological mechanism, alteration of the cuticle, largely explains both the body length and drug response phenotypes, and underlies the worm-star aggregation defect we identified in *dbl-1* loss-of-function populations. Furthermore, this work shows that BMP pathway signaling, which in mammals affects

bone and other extracellular matrix growth and remodeling processes, also affects extracellular matrix in the invertebrate *C. elegans*, revealing a conserved function for the BMP family of cell signaling molecules. Lastly, this work provides a basis for revealing novel conserved regulators of BMP-mediated extracellular matrix patterning.

Materials and methods

Strains and maintenance

C. elegans strains used in these studies were derived from the wild-type variety Bristol strain N2 and were cultured on nematode growth media (NGM) plates as previously described (Brenner, 1974). All strains were cultured on *E. coli* strain OP50 at 20˚C, except where noted. Strains used include: N2, TLG634 *sma-3(wk30)* III; *him-5(e1490)* V, TLG182 *texIs100 [dbl-1p::dbl-1:gfp + ttx-3p::rpf]* IV (referred to as *dbl-1(++)* in this paper), TLG269 *texIs100* IV; *dbl-1(nk3)* V, TP12 *kaIs12 [col-19p::col-19:gfp]*, which we discovered appears to be linked to *texIs100* on chromosome IV (Thein et al., 2003), NU3 *dbl-1(nk3)* V, CL261 *him-5(e1940)* V; *srf-5(ct115)* X (Link et al., 1992), and CB678 *lon-2(e678)* X.

We sequenced the *dbl-1(nk3)* lesion (previously called *cet-1(kk3)* (Morita et al., 1999)) and identified a 5595 bp deletion that removes the 5' untranslated region and all but 33 bp of *dbl-1* 3' coding sequence. The flanking sequence is CTGCGCCTCC ... GACATGCGGG.

Molecular biology

To generate a clone with *egfp* fused to the mature *dbl-1* sequence downstream of the *dbl-1* prodomain, we first used a sequential PCR fusion technique using cosmid T25F10 as template for the *dbl-1* reactions (Horton et al., 1990). Using the Gateway® recombinational cloning system (Walhout et al., 2000), we then inserted the PCR product into a Gateway® donor vector with BP Clonase® II (Life Technologies, Grand Island, NY) to generate *gfp:dbl-1* in pDONR™221. Next, we PCR amplified and inserted 2 kb sequence 5' to the start site of *dbl-1* into pDONR™P4-P1R. Finally, we performed a multisite Gateway® reaction between the *gfp:dbl-1* in pDONR™221, the *dbl-1* promoter in pDONR™P4-P1R, and the pDEST™6-R4-R2 destination vector (gift of I. Hope, University of Leeds, Leeds, UK) using LR Clonase® II Plus (Life Technologies, Grand Island, NY) (Hope et al., 2004). The resulting construct contained *dbl-1p::gfp:dbl-1* and was named pK13-1.2. Primers used are available upon request.

Generation of transgenic strains

Initial germline transformation of nematode strains with plasmid DNAs was performed by microinjection (Mello and Fire, 1995). The *gfp*-tagged *dbl-1* construct pK13-1.2 was injected into N2 at 50 ng/μL with 50 ng/μL co-injection marker *ttx-3p::rfp*, which is expressed in the two AIY head neurons (gift of O. Hobert, Columbia University Medical Center, New York, NY, and C. Rongo, Rutgers University, Piscataway, NJ) (Wenick and Hobert, 2004). We then created an integrated transgene from a strain expressing GFP-tagged DBL-1. Low copy integrated lines (generously

created for us by B. Grant, Rutgers University, Piscataway, NJ) did not express visible levels of tagged DBL-1, nor did they affect body size (data not shown). UV/TMP integration of a multicopy extrachromosomal array yielded *texIs100* and four other alleles, which were backcrossed five times to remove extraneously UV/TMP-induced mutations and mapped. *texIs100* was selected for further studies based on its relatively high expression level, activity (body length phenotype), and location (chromosome IV).

Body length measurements

Body measurements of animals were performed as previously described (Taneja-Bageshwar and Gumienny, 2012). Specifically, about 30 staged young adult animals were transferred to 2% agar pads on glass slides and were imaged when moving forward at 60x magnification using iVision-Mac™ software (BioVision Technologies, Exton, PA) and a Retiga-2000R CCD camera (QImaging Corporation, Surrey, BC, Canada) mounted on a Nikon SMZ1500 dissecting microscope (Nikon Instruments, Inc., Melville, NY).

Lengths of animals were determined using the length measurement image tool within iVision-Mac™ software (BioVision Technologies, Exton, PA). Average body length values of strain populations were converted to percent wild-type average body lengths using staged wild-type control populations that were imaged the same day as the experimental strain(s). 95% confidence intervals were calculated using Prism (GraphPad Software, Inc., La Jolla, CA). P-values (using the unpaired t-test) were determined using Excel (Microsoft Corporation, Redmond, WA).

Drug sensitivity assays

Sensitivity to drugs was assayed as previous described (Gottschalk et al., 2005). Briefly, about 40 staged young adult animals were transferred to NGM plates containing 0 - 1 mM levamisole HCl, 0.2% (wt/vol) tricaine (ethyl 3-aminobenzoate methanesulfonate), 0.2% (vol/vol) IP2P (1-phenoxy-2-propanol), or 1 mM sodium azide. For standard drug sensitivity assays, the number of animals moving was scored by visual inspection every 15 minutes and was defined as response (movement) to prodding. For levamisole dose-curve assays, the number of animals moving was scored by visual inspection at 60 minutes and was defined as response (movement) to prodding. Three independent trials were performed and the results were pooled, with at least 117 animals total for each genotype at each time point. The average fraction of animals moving, standard error of the mean (SEM), p-values (using the unpaired t-test), and EC_{50} (by log transformation) were determined using Excel (Microsoft Corporation, Redmond, WA).

RNA interference

RNA interference (RNAi) was performed as previously described (Beifuss and Gumienny, 2012), with the exception that generations of animals were continuously grown on IPTG-containing NGM plates that were seeded with bacteria expressing gene-specific double stranded RNA. Briefly, single colonies of HT115 bacteria containing relevant plasmids (Thermo Fisher Scientific, Waltham, MA) were selected, isolated, and grown overnight in carbenicillin, then induced for 4 to 5 hours with IPTG to express double stranded RNA from the plasmid. Each bacterial growth was spotted onto NGM

plates containing carbenicillin and IPTG and dried. Animals were then transferred to and continuously cultured on NGM plates seeded with RNAi bacterial lawns at 15°C for use in either the drug sensitivity assays of fluorescent microscopy and imaging. Drug sensitivity scoring was performed as described above. Imaging was performed as described below.

Hoechst 33342 staining and quantification

To provide more consistent staining, L3 animals were staged by allowing gravid adults to lay embryos for about 16 hours on a plate. These animals that had never been starved or bleached were then washed in M9 buffer three times to remove residual bacteria. Next, animals were stained with the cuticle impermeable dye, Hoechst 33342 (2'-[4-ethoxyphenyl]-5-[4-methyl-1-piperazinyl]-2,5'-bi-1H-benzimidazole trihydrochloride trihydrate, Life Technologies, Grand Island, NY) by microwave irradiation treatment. Using the PELCO BioWave® microwave (Ted Pella, Redding, CA), live animals were stained by microwaving at 20°C with intermittent vacuum at 200 watts (W) for a 6-minute cycle (2 minutes on, 2 minutes off, 2 minutes on) in 1 μg/ml Hoechst 33342 in M9 buffer. Prior to imaging, animals were washed four times in M9 buffer. Imaging was performed as described below.

The number of animals displaying fluorescently stained hypodermal nuclei was scored by visual inspection. Three independent trials were performed and the results were pooled, with at least 218 animals per trial for each genotype. The average fraction

of stained animals, SEM, and p-values (using the unpaired t-test) were determined using Excel (Microsoft Corporation, Redmond, WA).

Worm-star formation assays and imaging

Staged adult animals were washed in M9 buffer three times to remove residual bacteria. Animals were then incubated for three hours at room temperature in 7.5 mL M9 buffer (without OP50 bacteria) in 60 mm petri dishes tilted at a slight angle to concentrate animals in a single area of the plate. The number of animals in worm-star aggregations, clusters of two or more animals entangled at their tails, was quantified for each genotype by visual inspection using a dissecting microscope. Three independent trials were performed and results were pooled, with approximately 150 to 400 animals per trial for each genotype.

To assay the effect of extracting surface lipids in wild-type populations, mixed stage animals that had been washed in M9 buffer three times to remove residual bacteria were briefly washed in 30% ethanol in M9 buffer. Animals were washed three additional times in M9 buffer to remove all traces of ethanol. Animals were then incubated overnight at room temperature in 7.5 ml M9 buffer in 60 mm petri dishes tilted at a slight angle to concentrate animals in a single area of the plate. The number of animals in worm-star aggregations was quantified by visual inspection using a dissecting microscope. Four independent trials were performed and results were pooled, with at least 150 animals per trial for each genotype. Worm-stars were imaged using the same imaging system used for body length measurements.

Annuli staining and measurements

The cuticle of staged adult animals was stained with DiI (1,1'-dioctadecyl-3,3,3',3'-tetramethylindocarbocyanine perchlorate, Biotium Inc., Hayward, CA) as previously described (Schultz and Gumienny, 2012). Specifically, staged young adult animals were washed once with M9 buffer with 0.5% (vol/vol) Triton X-100, then two times in M9 buffer. Next, animals were stained in 30 µg/ml DiI in M9 for approximately three hours while shaking at high speed at 20°C. Prior to imaging, animals were washed in M9 buffer to remove residual DiI. Confocal imaging was performed as described below.

Annuli widths were determined using the length measurement image tool within iVision-Mac™. The width of ten annuli was measured for each animal to compensate for any minor deviations in individual annuli size. Average width values from each strain were converted to percent wild-type average widths using staged wild-type control populations that were imaged the same day as the experimental strains. 95% confidence intervals were calculated using Prism (GraphPad Software, Inc., La Jolla, CA). P-values (using the unpaired t-test) were determined using Excel (Microsoft Corporation, Redmond, WA).

Wheat germ agglutinin staining

Lectin staining was performed as previous described (Link et al., 1988). Briefly, populations of staged adult animals were washed three times in M9 buffer to remove any residual bacteria. To further remove any residual bacteria from the cuticular surface,

animals were incubated in M9 buffer for an hour while gently shaking at 20°C. Animals were then stained in 200 μg/ml rhodamine-conjugated wheat germ agglutinin (WGA) (Vector Laboratories, Inc., Burlingame, CA) in M9 buffer for one hour while gently shaking at 20°C. Prior to imaging, animals were washed four times in M9 buffer. Imaging was performed as described below.

Confocal microscopy and imaging

Animals were immobilized in 2.5% (wt/vol) 0.1 μm diameter polystyrene beads (00876-15, Polysciences Inc., Warrington, PA) in 1 mM levamisole on 10% agarose pads (Fang-Yen et al., 2012). Fluorescent images were acquired on a Retiga-SRV CCD camera (Quantitative Imaging Corporation, Surrey, BC, Canada) mounted on a BD Carv II™ spinning disk confocal (BD Biosystems, San Jose, CA) on a Zeiss A1 compound microscope base (Carl Zeiss, Inc., Jena, Germany) fitted with GFP HQ, Rhodamine HQ, and DAPI filters. 10x/0.3 NA Plan-Neofluar and 63x/1.4 NA oil Plan-Apochromat objectives (Carl Zeiss, Inc., Jena, Germany) and iVision-Mac™ software (BioVision Technologies, Exton, PA) were used for image acquisition.

Transmission electron microscopy and imaging

As the cuticle of *C. elegans* is extremely tough, we optimized methods for transmission electron microscopy (TEM) sample preparation using the PELCO BioWave® microwave with ColdSpot® technology (Ted Pella, Redding, CA). For typical bench-top methods, the cuticle of each nematode is sliced during fixation to

allow the fixative past the impenetrable cuticle (Hall et al., 2012). Consistent with previous findings (Jones and Gwynn, 1991), we found that treatment with microwave irradiation allows the fixative and other treatments to penetrate the cuticle and infiltrate the tissue, eliminating any need to cut the cuticle.

Adult animals were washed in M9 buffer two times to remove residual bacteria. Next, animals were immersed in fixative (2.5% glutaraldehyde, 2% paraformaldehyde, and 0.1% (wt/vol) malachite green in working buffer (0.1 M HEPES, pH 7.4, containing 2 mM $MgCl_2$)). Malachite green was included as an additive to the primary fixative to preserve and stain lipids that are normally stripped from specimens during standard TEM fixation procedures (Teichman et al., 1972). For all microwave steps, specimens were microwaved at 20°C with a 37°C cut-out temperature and intermittent vacuum at 250 W unless otherwise noted. While immersed in fixative, animals were microwaved for an initial 6-minute cycle (2 minutes on, 2 minutes off, 2 minutes on), incubated at room temperature for about an hour, then microwaved again for another 6-minute cycle (2 minutes on, 2 minutes off, 2 minutes on). Animals were then washed three times in working buffer, microwaving each wash for one minute. To provide more contrast, specimens were post-fixed in 1% (wt/vol) osmium tetroxide with 1.5% (wt/vol) potassium ferricyanide in working buffer for 15 minutes at room temperature and then microwaved at 100 W for one minute. Samples were then washed two times in water, microwaving each wash one minute. Animals were next stained *en bloc* with 0.5% aqueous uranyl acetate at room temperature over night. Specimens were washed in water one time with a one-minute microwave cycle. The samples were then dehydrated

through a graded methanol series, starting at 5% (vol/vol) and continuing to 100% (vol/vol) methanol at 5% intervals, microwaving for one minute at each grade. Finally, animals were suspended in propylene oxide, infiltrated (each infiltration step was accompanied by a 6-minute microwave cycle (2 minutes on, 2 minutes off, 2 minutes on)), and embedded in a Quetol 651-modified Spurr low viscosity epoxy resin (Ellis, 2006). Transverse gold sections were taken from the midsection of young adult hermaphrodites and post-stained with 2% (wt/vol) aqueous uranyl acetate followed by Reynolds lead citrate (Reynolds, 1963). At least six animals of each genotype were examined and photographed on a JEOL 1200EX transmission electron microscope (JEOL Ltd., Tokyo, Japan) at an accelerating voltage of 100 kV.

TEM measurements

The depth and length of cuticular components were determined from micrographs of cross-sections using the tape measure tool within SIA Micrograph MaxIm DL5 software (Diffraction Limited, Ottawa, Canada). Components of at least six animals were measured per genotype. Averages of depth or length, SEM, and p-values (using the unpaired t-test) were determined using Excel (Microsoft Corporation, Redmond, WA).

Results

GFP-tagged DBL-1 is functional

We made a strain expressing transgenic GFP-tagged DBL-1 (allele name *texIs100*) and randomly integrated this transgene into in a wild-type background. As these animals express both endogenous DBL-1 and the GFP-tagged DBL-1, we call this overexpressing strain *dbl-1(++)*. The transgene is expressed from 2 kb sequence of the *dbl-1* 5' untranslated region, which expresses in cholinergic motor neurons previously identified to express DBL-1 (Figure 2.1A and data not shown) (Morita et al., 1999; Suzuki et al., 1999). DBL-1 expressed from the *texIs100* transgene is bioactive, as transgenic animals in a wild-type background are longer than normal, and animals lacking endogenous *dbl-1* product are restored to a more normal body length with *texIs100* (Table 2.1 and Figure 2.1B-E).

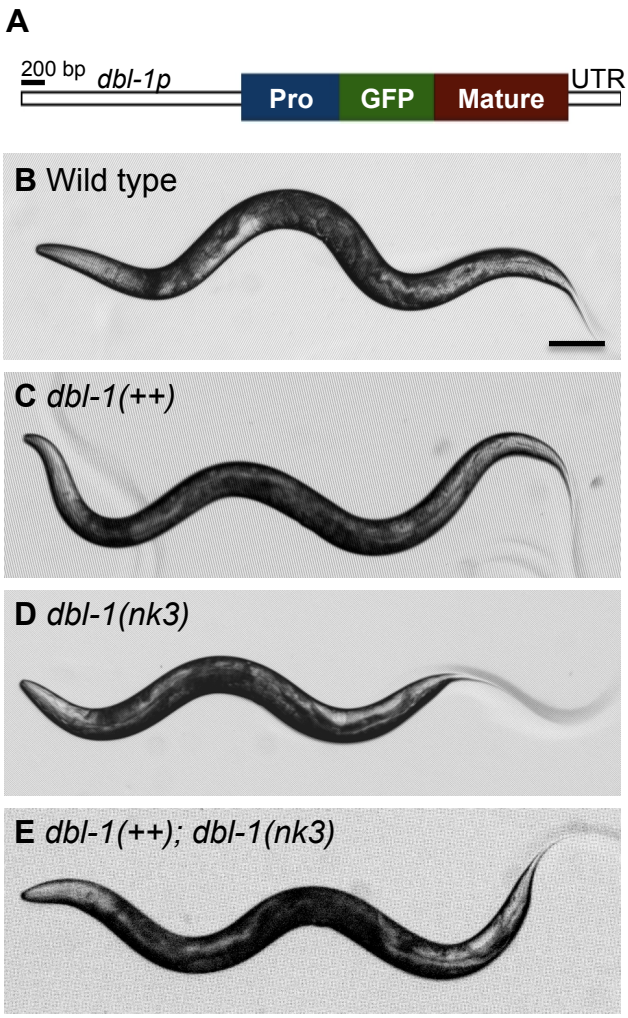

Figure 2.1 GFP-tagged DBL-1 is bioactive. (A) Schematic diagram of GFP-tagged DBL-1 expressed from the *dbl-1* promoter (*dbl-1p*). The GFP-tag (green) is inserted downstream of the prodomain (blue) and upstream of the DBL-1 mature domain (red). The construct also contains the *dbl-1* specific 3' untranslated region (UTR). (B–E) Body lengths of wild-type (B), *dbl-1(++)* (C), *dbl-1(nk3)* (D), and *dbl-1(nk3)* mutant animals expressing the GFP-tagged DBL-1 transgene (E). Scale bar = 100 μm.

Increased DBL-1 pathway signaling results in drug resistance

Animals deficient in DBL-1 signaling are hypersensitive to the anesthetizing effects of the cholinergic agonists levamisole and nicotine and the cholinesterase inhibitor aldicarb, which prevents breakdown of acetylcholine (Almedom et al., 2009; Vashlishan et al., 2008). Confirming these results, we also found that *dbl-1(nk3)* mutant animals are hypersensitive to levamisole-induced paralysis (Figure 2.2A). To test if this response was DBL-1 dose-dependent, we assayed paralysis in animals with increased DBL-1 signaling levels. After incubating animals on plates containing 0.5 mM levamisole for 75 minutes, over half of wild-type animals were immobilized and all *dbl-1(nk3)* animals were paralyzed (Figure 2.2A). However, only 20% of the *dbl-1(++)* population was anesthetized (Figure 2.2A). To confirm that this levamisole resistance phenotype is specific to increased DBL-1 pathway signaling, we also tested animals lacking the DBL-1 negative regulator LON-2. *lon-2(e678)* mutants showed results similar to overexpressing the DBL-1 ligand (data not shown). These results reveal animals with increased DBL-1 signaling display resistance to levamisole-induced paralysis, showing that DBL-1 is a dose-dependent regulator of levamisole response.

We reasoned the altered sensitivity to levamisole could be caused by specific modulation of acetylcholine receptor signaling pathway or by altered accessibility of the drug to its receptors in the DBL-1 variant backgrounds. To distinguish between these models and investigate the specificity of altered drug sensitivity due to dose of DBL-1, we analyzed the effects of three additional nematode anesthetics with different modes of action and molecular weights. We tested tricaine, which has a higher molecular weight

of 261 as compared to 241 for levamisole. Further distinguishing the two anesthetics, tricaine suppresses the nervous system by reducing transmission of action potential of the nerve (Carmichael, 1985). Using 0.2% tricaine, we tested the response of DBL-1 variants to this larger anesthetic over time. We found that tricaine affects DBL-1 over- and under-expressing animals in manner similar to levamisole, where *dbl-1(++)* animals are resistant, while *dbl-1(nk3)* animals are more sensitive to tricaine-induced paralysis (Figure 2.2B). IP2P, a smaller anesthetic with a molecular weight of 152, acts as an anesthetic by eliminating neural activity and blocking muscular contraction (Wyeth et al., 2009). We asked if DBL-1 variant animals would display altered sensitivity to this lower molecular weight anesthetic. We used 0.2% IP2P to measure the response of *dbl-1(nk3)* and *dbl-1(++)* animals to this anesthetic. We found that *dbl-1* mutant animals are more sensitive to IP2P than wild-type animals (Figure 2.2C). Notably, we discovered that long *dbl-1(++)* animals are as sensitive as wild-type animals to the paralyzing effects of IP2P (Figure 2.2C). Unlike the other anesthetics tested here, the nematode anesthetic sodium azide acts by inhibiting the electron transport chain (Duncan and Mackler, 1966; Herweijer et al., 1985; Van der Bend et al., 1985). Further differentiating these anesthetics, sodium azide is much smaller, having a molecular weight of 65. We asked if DBL-1 variant animals display an altered response to this low molecular weight anesthetic. While sodium azide is commonly used for imaging at doses of 10-25 mM, which anesthetizes nematodes quickly (Shaham (ed.), 2006; Sulston and Hodgkin, 1988), we chose a lower dose, 1 mM, to test for differences in sodium azide sensitivity in *dbl-1* under- and over-expressing strains in our 90-minute assay. Similar to their

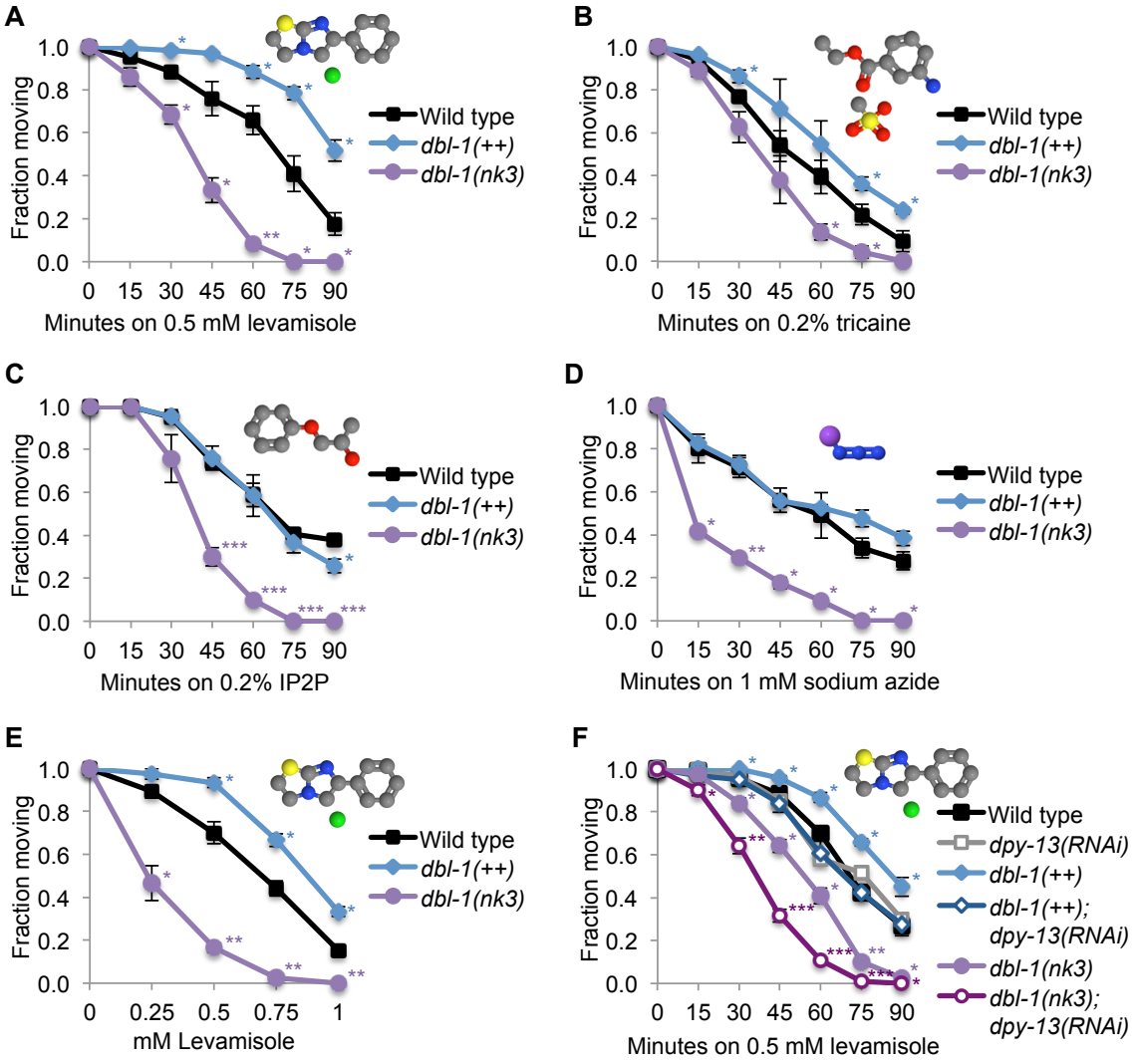

Figure 2.2 DBL-1 regulates cuticular permeability. (A-D) Sensitivity to levamisole (A), tricaine (B), IP2P (C), and sodium azide (D) was measured over time in animals with wild-type, reduced (*dbl-1(nk3)*), and increased (*dbl-1(++)*) DBL-1 pathway signaling. (E) Sensitivity to different levamisole doses by animals with wild-type, reduced (*dbl-1(nk3)*), and increased (*dbl-1(++)*) DBL-1 pathway signaling. (F) Sensitivity to levamisole in animals with different DBL-1 levels treated with *C06C3.5* (pseudogene control) or *dpy-13* RNAi was measured over time. (G–I) Hoechst 33342 staining in *dbl-1(++)* (G) or *dbl-1(nk3)* (H) animals. Faint intestinal autofluorescence is visible in (G). Scale bar = 10 μm. The fraction of animals that stain with Hoechst 33342 is shown in (I). Error bars indicate the mean ± SEM. P-values compare data to wild type (***P≤0.0001; **P≤0.001; *P≤0.05) using the unpaired t-test. Chemical structures were drawn using Jmol: an open-source Java viewer for chemical structures in 3D. http://www.jmol.org/. Molecule key: gray, carbon; blue, nitrogen; purple, sodium; green, chloride; yellow, sulfur; and red, oxygen.

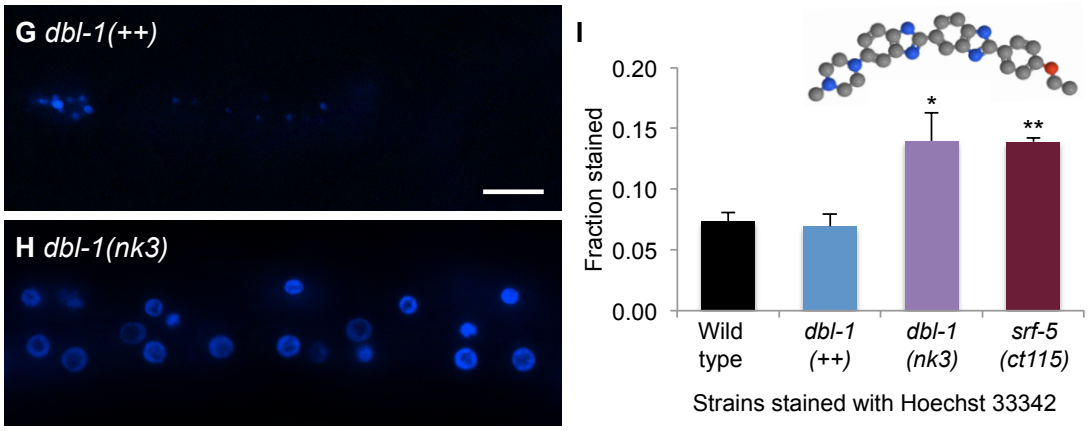

Figure 2.2 Continued.

behavior on the other tested anesthetics, small *dbl-1(nk3)* animals display a more sensitive response to sodium azide (Figure 2.2D). Similar to the result with IP2P, we discovered that long *dbl-1(++)* and *lon-2(e678)* animals are at least as sensitive to the paralyzing effects of sodium azide as wild-type animals (Figure 2.2D and data not shown). These results show that loss of DBL-1 results in hypersensitivity to multiple drugs of varied size and mode of action, while animals with enhanced DBL-1 signaling are resistant to the higher molecular weight drugs tested in this study, levamisole and tricaine. This data suggests that DBL-1 regulates the *C. elegans* permeability barrier, which provides a size exclusion barrier to compounds like levamisole and tricaine, but not lower molecular weight drugs like IP2P and sodium azide.

To quantify these differences in drug responsiveness, we determined the dose response of DBL-1 variant animals compared to wild type using a range of levamisole concentrations. We found that *dbl-1* mutants are more sensitive to levamisole, displaying

increased susceptibility ranging from 0.25 to 1 mM levamisole with a half-maximal effective concentration (EC_{50}) of 0.23, compared to an EC_{50} of 0.56 for wild-type animals (Figure 2.2E). *dbl-1(++)* animals are more resistant in higher concentrations of levamisole, with an EC_{50} of 0.83 (Figure 2.2E). These results indicate changes in DBL-1 signaling levels produce significant differences in sensitivity to a broad range of anesthetic concentrations.

DBL-1 is required for normal cuticular permeability

In nematodes, the cuticle and its underlying hypodermis form a permeability barrier that protects the animal from its environment. This environmental barrier is strong enough that nematodes submerged in 6% glutaraldehyde, a high concentration of fixative, continue to move even after 7 hours (Shepherd and Clark, 1976). However, this diffusion barrier can be breached by drugs and dyes, where molecule size and polarity are critical to dye entry or drug effectiveness (Ho et al., 1992; Ho et al., 1990; Ho et al., 1994; Moribe et al., 2004).

Drug sensitivity can be caused by altered surface permeability in *C. elegans* (Partridge et al., 2008; Ruiz-Lancheros et al., 2011). Because our drug assay results suggest a physical barrier is altered, we asked if altered drug responsiveness in the DBL-1 variant backgrounds is caused by changes in permeability barrier function specifically of the cuticle, not the hypodermal cell membrane. To further investigate the integrity of the cuticle, we took advantage of *dpy-13*, a cuticular collagen that is involved in covalently cross-linking cuticular proteins (von Mende et al., 1988). Reduction of DPY-

13 levels increases the permeability of the cuticle, thereby allowing more anesthetic to pass through the cuticle and reach receptors (Rand and Johnson, 1995). If the altered response to levamisole seen in DBL-1 variant animals is due to defects in cuticular permeability, reducing DPY-13 in the *dbl-1(++)* background should restore sensitivity to levamisole and possibly produce an even more sensitized response to levamisole in *dbl-1(nk3)* animals lacking DBL-1 activity. If, however, the resistance to levamisole in DBL-1 variant animals is caused by changes in the hypodermal membrane barrier, then increased permeability of the cuticle should not affect levamisole response in *dbl-1* overexpressing animals.

We tested the effect of DPY-13 depletion on cuticular permeability using gene-specific RNA interference (RNAi). While we found *dpy-13* RNAi depletion did not significantly sensitize wild-type animals to 0.5 mM levamisole, we did find that *dpy-13* RNAi significantly affected anesthetic response in animals with increased or decreased DBL-1 signaling (Figure 2.2F). We found that reducing DPY-13 levels in long *dbl-1(++)* animals restored sensitivity to levamisole to wild-type response levels, where levamisole response in *dbl-1(++); dpy-13(RNAi*) animals was significantly less compared to the response in *dbl-1(++)* animals (Figure 2.2F). Further, knockdown of DPY-13 in *dbl-1(nk3)* animals resulted in a significant increase in levamisole-induced paralysis over time compared to *dbl-1(nk3)* animals (Figure 2.2F). This result suggests that animals with abnormal levels of DBL-1 display defects in the barrier function of the cuticle, whereby further cuticle perturbation caused by loss of DPY-13 allows increased small molecule entry in DBL-1 variants. These genetic and pharmacological studies

suggest that DBL-1 affects permeability of the cuticle, and therefore drug response, in a dose-dependent manner.

Because the finding that knockdown of DPY-13 specifically affects drug response in animals with abnormal DBL-1 levels suggests DBL-1 variants display cuticle defects, we directly tested cuticular permeability using Hoechst 33342, a DNA-binding dye with a molecular weight of 616 that fails to transpass the cuticle in wild-type animals, but stains nuclei in animals with an impaired cuticular surface barrier (Kage-Nakadai et al., 2010). Wild-type control animals typically did not stain, nor did animals overexpressing DBL-1 (Figure 2.2G, I). However, animals lacking DBL-1 displayed increased staining within the population (Figure 2.2H, I), confirming a role for DBL-1 in cuticular barrier function. To support our results, we tested *srf-5*, a gene whose product is required for normal cuticular surface properties, and found that loss of this gene product also increases cuticular permeability to Hoechst 33342 (Figure 2.2I).

Loss of DBL-1 signaling causes worm-star aggregates in solution

In the course of these studies, we made a serendipitous discovery. Mutant *dbl-1(nk3)* populations suspended in buffer for three hours contained clumps of animals that were adhered to each other by their tail tips. These oriented aggregates have been previously described for multiple wild nematode species extracted from various sources (Table 2.2) (Barbercheck and Kaya, 1991; Croll, 1970; Haut, 1956; Hodgkin et al., 2013; Pye and Burman, 1981; Stock et al., 2005; Sudhaus and Hooper, 1994; Yoeli, 1957). Oriented clumps of animals were first described by Haut in 1956 as “spherical

nematode-aggregates," and have also been named "medusa-head formations," "sunflowers," or "rosettes." Nematode aggregates can be disrupted by the addition of sodium bicarbonate, indicating surface ionic interactions promote tail entanglement (Barbercheck and Kaya, 1991; Woodring and Kaya, 1988). A recent study showed these aggregates, called "worm-stars," are induced in wild-type *C. elegans* by the presence of pathogenic, cuticle-adhering bacteria (Hodgkin et al., 2013). These worm-stars occur within two minutes and animals are so strongly entangled that the few escapers often sever themselves in the process. To characterize the effect of decreased or increased DBL-1 signaling on aggregation between animals, we measured the formation of worm-stars by wild-type, *dbl-1(++)*, or *dbl-1(nk3)* animals suspended in buffer. We found that both wild-type and *dbl-1(++)* animals did not form aggregates in liquid media. However, *dbl-1(nk3)* animals form worm-stars under similar conditions, albeit at a low incidence, approximately 10% of animals in a population (Figure 2.3). Juvenile hermaphrodites also form clusters (Figure 2.3A). Worm-stars comprised as few as two animals with entwined tails (Figure 2.3A) to very densely populated aggregates (Figure 2.3B, C). Unlike the worm-stars that occur in the presence of pathogenic bacteria, *dbl-1(nk3)* worm-stars can be dissociated and typically do not cause the death of clumped animals (Figure 2.3 and data not shown). We confirmed that the worm-star phenotype is not specific to loss of DBL-1 function, but to DBL-1 pathway function. Animals lacking SMA-3, a transcription factor activated by DBL-1 receptor signaling, form worm-stars with about 5% incidence (Figure 2.4).

Table 2.2 Reports of aggregate formation in wild-type and mutant nematodes.

Species	Background	Parasitic	Reference
Caenorhabditis angaria	WT with cuticle adhering bacteria	No	(Hodgkin et al., 2013)
Caenorhabditis briggsae	WT with cuticle adhering bacteria	No	(Hodgkin et al., 2013)
Caenorhabditis elegans	WT with cuticle adhering bacteria	No	(Hodgkin et al., 2013)
Caenorhabditis elegans	WT with surface stripped	No	This work
Caenorhabditis elegans	*dbl-1(nk3)*	No	This work
Caenorhabditis elegans	*sma-3(wk30)*	No	This work
Caenorhabditis elegans	*srf-5(ct115)*	No	This work
Caenorhabditis n. sp. 11	WT with cuticle adhering bacteria	No	(Hodgkin et al., 2013)
Heterohabditis bacteriophora	WT	Yes	(Barbercheck and Kaya, 1991; Pye and Burman, 1981)
Oscheius colombiana	WT	Yes	(Stock et al., 2005)
Oscheius guentheri	WT	No	(Sudhaus and Hooper, 1994)
Oscheius tipulae	WT with cuticle adhering bacteria	No	(Hodgkin et al., 2013)
Rhabditid larvae	WT	Unknown	(Croll, 1970)
Rhabditis axei	WT	No	(Haut, 1956)
Rhabditis brassicae	WT with cuticle adhering bacteria	No	(Hodgkin et al., 2013)
Steinernema feltiae	WT	Yes	(Pye and Burman, 1981)
Wuchereria bancrofti	WT	Yes	(Yoeli, 1957)

WT indicates wild-type populations.

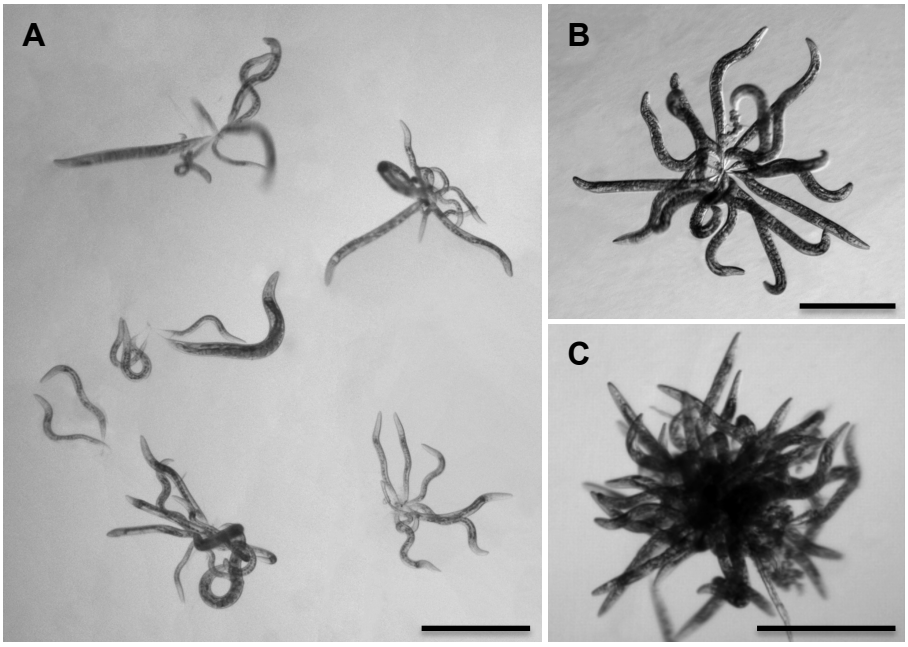

Figure 2.3 DBL-1 signaling affects surface adhesion. (A) Six worm-stars show larval and adult *dbl-1(nk3)* hermaphrodites knot by their tails. Scale bar = 0.5 mm. (B, C) *dbl-1(nk3)* adult animals become tangled by their tails, forming moderate (B) or dense (C) worm-star aggregates in liquid. Scale bars = 0.5 mm.

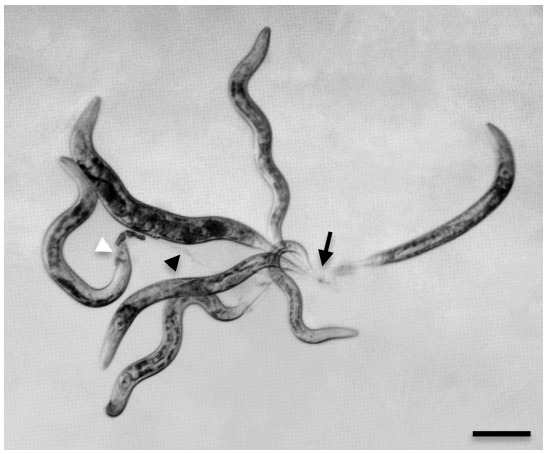

Figure 2.4 Unshed cuticle traps *sma-3* mutant adult male in a worm-star. A rare instance of a *sma-3(wk30); him-5(e1490)* adult male (tail is indicated with a white arrowhead) entangled by its unshed cuticle (black arrowhead) in a worm-star (point of entanglement is marked with an arrow). Scale bar = 0.1 mm.

Since animals lacking DBL-1 signaling display increased cuticular permeability and altered cuticular composition, we asked if loss of another gene known to regulate properties of the cuticular surface would also cause worm-star formation. To test this possibility, we used *srf-5(ct115)* mutant animals, which display altered surface antigenicity (Gravato-Nobre et al., 2005; Link et al., 1992), increased cuticular permeability (Figure 2.2I), altered immune defense (de Gives et al., 1999; Gravato-Nobre et al., 2005), and have altered patterns of surface lipids (Blaxter, 1993). A role for *srf-5* in susceptibility to infection is two-sided and dependent on the nature of the pathogen. For example, *srf-5(ct115)* mutant animals display increased resistance to a

nematode-specific bacterium due to an inability of the pathogen to adhere to the cuticular surface (Gravato-Nobre et al., 2005). However, *srf-5* mutant animals display increased susceptibility to nematophagous fungi (de Gives et al., 1999). Supporting the idea of altered surface properties causing aggregation, we found that adult hermaphrodites lacking functional SRF-5 formed worm-stars in liquid, with less than 5% of the hermaphrodites becoming entangled. Wild-type animals failed to aggregate in the same conditions (data not shown).

In populations of animals lacking DBL-1 pathway signaling or SRF-5, hermaphrodites of all stages were included in the oriented aggregates (Figure 2.3A and data not shown). To determine the requirement for the hermaphrodite and larval whip-like tail tip in worm-star aggregation, we used *sma-3(wk30)* and *srf-5(ct115)* strains that contain *him-5(e1490)*, which increases the incidence of males in the population. Interestingly, we found adult males, which display a specialized, blunt-ended tail structure instead of a tapered tail tip, were always excluded from these oriented aggregates. The one exception was a single *sma-3(wk30); him-5(e1490)* adult male that had not fully molted and was attached to a worm-star by its partially shed cuticle (Figure 2.4). The absence of adult males from these oriented aggregates suggests that tail whips contribute to worm-star formation in these mutant backgrounds.

Because worm-star formation is affected by altering the *C. elegans* surface coat (Himmelhoch and Zuckerman, 1983; Jansson et al., 1986; Zuckerman et al., 1979), we asked if loss of the cuticle's surface coat would affect aggregation in wild-type animals. Previous studies in *C. elegans* have shown that treating wild-type animals with ethanol

extracts surface lipids and removes their surface coat (Blaxter, 1993). Indeed, we recapitulated the worm-star formation phenotype in wild-type animals using a 30% ethanol extraction, though less than 1% of the population was affected. Taken together, these results suggest alteration of cuticular surface properties in *dbl-1* and *srf-5* mutant animals permit worm-star formation. This is the first report of worm-star formation in mutant nematode backgrounds and shows that endogenous surface coat properties can be altered in wild-type *C. elegans* to promote aggregation.

DBL-1 specifically affects ionic surface properties of the cuticle

Because our results indicate permeability of the cuticle and ionic surface properties are altered in DBL-1 variant strains, we asked if specific cuticular properties are altered in animals with decreased or increased DBL-1 signaling. The *C. elegans* cuticle is composed of different layers that entirely cover the animal's external surface in a flexible, resilient exoskeleton. This exoskeleton protects the animal from environmental insults and infection. A surface coat of charged glycoproteins, the glycocalyx, covers the epicuticle, a lipid-rich cuticular layer (Blaxter, 1993). Under the epicuticle are the cortical, medial, and basal cuticular layers. Wheat germ agglutinin (WGA) binds glycoproteins and stains the *C. elegans* cuticular surface when surface antigenicity is altered, as in *srf* mutant animals (Link et al., 1988; Link et al., 1992; Natsuka et al., 2005), while the red fluorescent lipophilic dye DiI stains phospholipids (Gullapalli et al., 2008; Schultz and Gumienny, 2012).

We first stained animals with reduced or overactive DBL-1 signaling relative to the wild type with fluorescently tagged WGA. DBL-1 variants were indistinguishable from the wild type, exhibiting limited staining, while positive control *srf-5* mutant animals stained extensively (Figure 2.5A-D). Abnormally exposed or accumulated mucin-type glycans bind WGA in *srf* mutants (Natsuka et al., 2005). We asked if WGA binding protein is affected in DBL-1 variants when the lectin-binding protein is revealed by loss of SRF-5. We stained *him-5(e1490); srf-5(ct115)* animals RNAi-depleted of *dbl-1*, the DBL-1 inhibitor *lon-2*, or a pseudogene control with rhodamine-labeled WGA. Males, generated by *him-5(e1490)*, stain with WGA more robustly than hermaphrodites. WGA staining was like the *srf-5* background, again indistinguishable in all three DBL-1 signaling conditions (Figure 2.5D-F). This result shows DBL-1 does not affect surface antigenicity of WGA in *srf-5* mutant animals.

We then asked if DBL-1 pathway signaling affected external cuticle morphology. A previous report that analyzed DBL-1 pathway genes *sma-2*, a Smad transcriptional regulator, and *lon-2* showed a relationship between body length and distance between annuli, ridges patterning the cortical layer that ring the animal from nose to tail (see Figure 2.5G) (Thein et al., 2003). Mild perturbations of annuli and longitudinal ridges called alae in *lon-2* mutant animals were noted (Thein et al., 2003). Other mutations that affect cuticle and body length show differences in annular ridge width (Page and Johnstone, 2007; Thein et al., 2003). Using DiI, a vital lipophilic dye that binds to lipids in the cuticular surface, to highlight annular furrows, we also found a direct correlation between annular width and body length in DBL-1 signaling variants (Figure 2.5G-I,

Table 2.1) (Schultz and Gumienny, 2012). We did not discern noticeable aberrations in annuli or alae in animals with decreased or increased DBL-1 signaling (Figure 2.5G-I and data not shown).

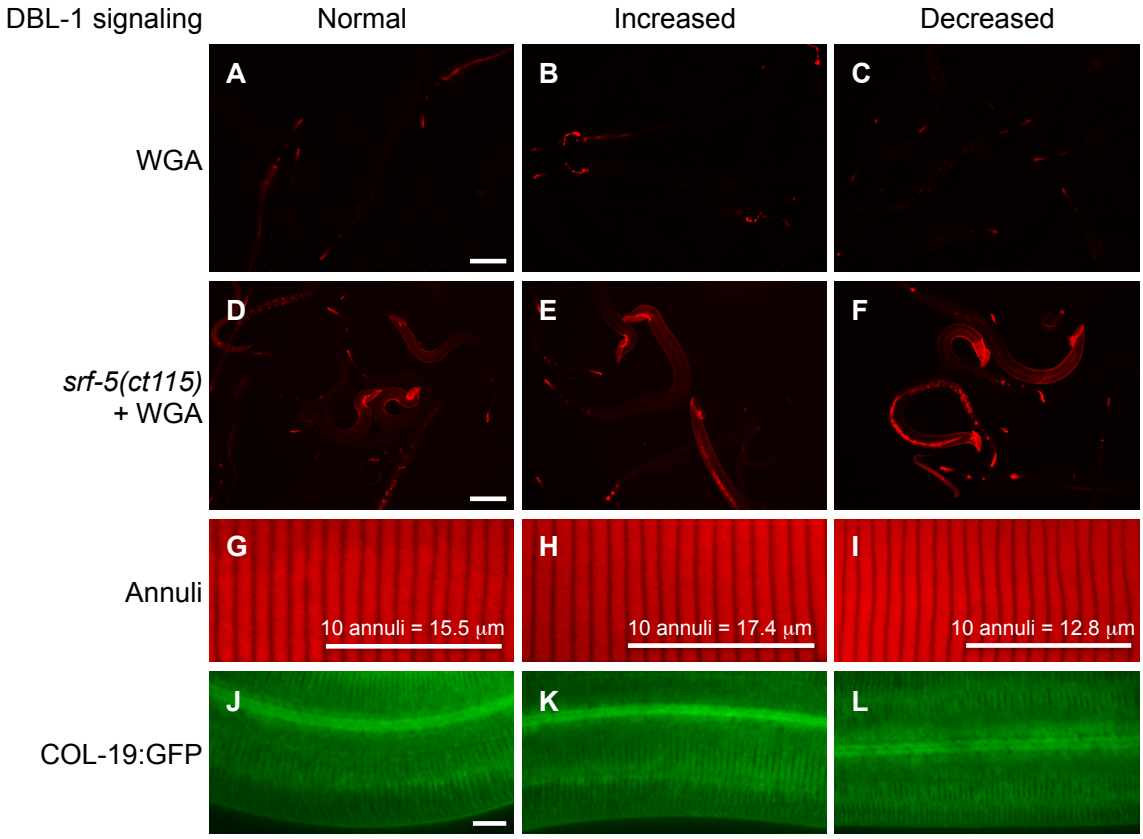

Figure 2.5 DBL-1 signaling affects specific cuticular surface properties. (A–C) Rhodamine-conjugated wheat germ agglutinin (WGA) staining in wild-type (A), *dbl-1(++)* (B), and *dbl-1(nk3)* (C) populations. Scale bar = 100 μm. (D–F) WGA staining in *him-5(e1490); srf-5(ct115)* animals with *C06C3.5(RNAi)* (pseudogene control RNAi) (D), *lon-2(RNAi)* (E), and *dbl-1(RNAi)* (F). Scale bar = 100 μm. (G–H) Staining of annuli in wild-type (G), *dbl-1(++)* (H), and *dbl-1(nk3)* (I) animals. Bars mark the length of 10 annuli and indicate the average length of 10 annuli for each strain. (J–L) COL-19:GFP expression in otherwise wild-type animals with *C06C3.5(RNAi)* (pseudogene control RNAi) (J), *lon-2(RNAi)* (K), and *dbl-1(RNAi)* (L). Scale bar = 10 μm.

Under the epicuticle lies the cortical layer of the cuticle. We asked if DBL-1 pathway signaling affected the distribution of a cortical cuticular component, COL-19 (Thein et al., 2003). We could discern no significant differences in COL-19 organization between the wild type and RNAi knockdown of DBL-1 pathway members *dbl-1* and *lon-2*. This result is supported by previous observations of normal GFP-tagged COL-19 patterning in *sma-2* and *lon-2* mutant strains (Figure 2.5J-L) (Thein et al., 2003). Together, these analyses suggest that the permeability and ionic surface defects of DBL-1 variants are not caused by gross defects in surface antigenicity or the patterning or organization of the cortical layer of the cuticle.

DBL-1 pathway signaling regulates composition and organization of the cuticle

To identify the physiological basis of the DBL-1 dose-dependent response to anesthetics and body length, we directly observed the cuticle of wild-type and DBL-1 signaling variant strains using transmission electron microscopy (TEM). We developed a microwave-assisted protocol that effectively and more quickly processes *C. elegans* specimens (see Materials and Methods) compared to traditional benchtop approaches. We also used malachite green, a classic dye used to preserve and stain lipids that would otherwise be extracted from samples during preparation (Teichman et al., 1972). This method differentiates the cuticular layers, which are thicker and readily distinguishable under the alae (Figure 2.6). We found that DBL-1 levels affect both the width and depth of the alae (Table 2.3). Further, phospholipids on the outer surface of the cuticle of wild-type animals are bound by malachite green (Figure 2.6A). This malachite green

preservation of lipid was sensitive enough to reveal differences in the external surface of the cuticle that DiI staining could not resolve (Figure 2.5G-I). Long animals overexpressing DBL-1 have a thicker layer of malachite green staining the surface, suggesting an increased surface lipid content in this strain (Figure 2.6B). Small animals lacking DBL-1 have very little bound malachite green, indicating lipids are depleted on the outer surface of the cuticle in this background (Figure 2.6C).

Further, malachite green preserves and differentially stains the inner layers of cuticle, clearly distinguishing the collagen and cuticlin-containing cortical, fluid-filled medial, and oriented collagen fiber-formed basal layers (Figure 2.6). We found that the cortical layer is largely indistinguishable in both size and organization in wild-type, *dbl-1(++)*, and *dbl-1(nk3)* animals (Figure 2.6 and Table 2.3). Ultrastructural analysis revealed that DBL-1 also affects both the medial and basal layers of the cuticle. *dbl-1(nk3)* animals (Figure 2.6C) have a strikingly denser medial layer compared to wild-type (Figure 2.6A) and *dbl-1* overexpressing animals (Figure 2.6B). DBL-1 levels also affect the dimensions of the medial layer, where increased or decreased DBL-1 signaling is associated with a significant decrease in the depth of the medial layer (Table 2.3). The composition of the topmost basal sublayer in some animals overexpressing DBL-1 (Figure 2.6B) is less organized compared to either wild-type (Figure 2.6A) or *dbl-1(nk3)* animals (Figure 2.6C).

Alteration of both the external lipids and underlying cuticular layers provides a physiological mechanism for the dose-dependent DBL-1-mediated drug responsiveness and body length phenotypes. These findings also suggest a mechanism for the Hoechst

33342 staining and worm-star formation phenotypes seen in animals lacking DBL-1. The reduced malachite green-stainable lipid layer may be important to prevent tail knotting. Reduction of this layer in *dbl-1* loss-of-function animals may increase surface adhesive properties by affecting surface ionic interactions.

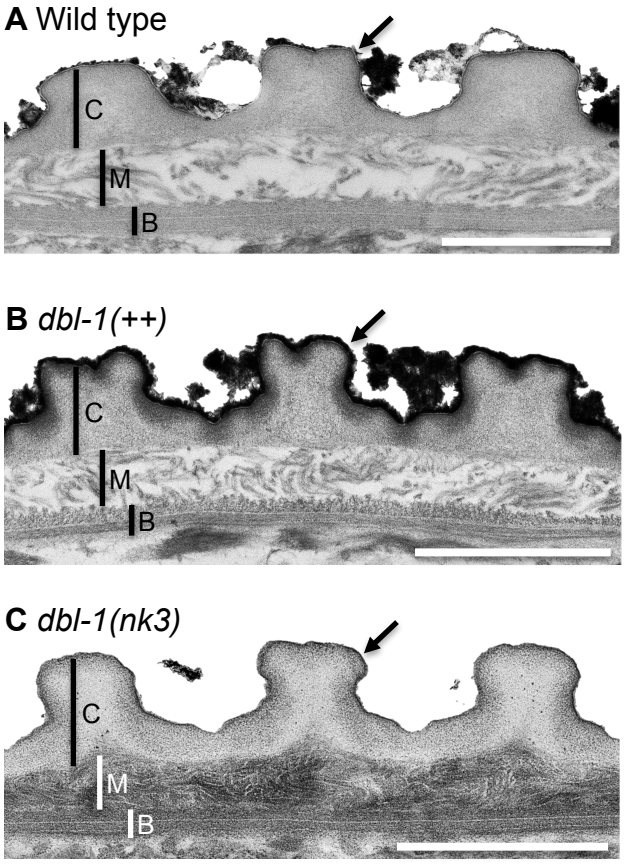

Figure 2.6 The DBL-1 pathway regulates cuticular organization and composition. Transmission electron microscopy (TEM) micrographs of wild-type (A), *dbl-1(++)* (B), and *dbl-1(nk3)* (C) animals. C indicates cortical layer; M indicates medial layer; B indicates basal layer; and the arrow marks the surface coat and epicuticular layer. Scale bars = 1 μm.

Table 2.3 DBL-1 levels affect the dimension of cuticular components.

Genotype	Alae width (μm)	Alae depth (μm)	Cortical layer depth (μm)	Medial layer depth (μm)
Wild type	3.06±0.06	1.15±0.07	0.55±0.05	0.39±0.04
dbl-1(++)	2.41±0.10***	0.84±0.07*	0.51±0.03	0.22±0.03*
dbl-1(nk3)	2.48±0.12*	0.99±0.03*	0.63±0.06	0.21±0.01**

Comparison of cuticular components in animals with varying levels of DBL-1 signaling. Values indicate the mean ± SEM. P-values compare data to wild type (***P≤0.0001; **P≤0.001; *P≤0.05) using the unpaired t-test. n=6 for each genotype.

Discussion

This work demonstrates that *C. elegans* DBL-1 shares a similar function with other BMPs in regulation of extracellular matrix. We provide a mechanism to largely explain some of the dose-dependent, seemingly disparate pleiotropic defects exhibited by DBL-1 pathway mutant animals (Gumienny and Savage-Dunn, 2013; Tuck, 2014). While previous work shows the hypodermis is a main DBL-1 target tissue, we confirm that DBL-1 signaling targets cuticle, a specialized extracellular matrix secreted, at least in part, by the hypodermis. Whether these cuticle phenotypes, especially the lipid layer differences, are strictly hypodermally derived or if DBL-1 signaling affects different tissues will help clarify the organismal context of this cellular signaling pathway. Using drug assays and a novel genetic analysis, we discovered that DBL-1 dose-dependent permeability alterations in the cuticle underlie the drug response phenotype. We assessed cuticular permeability directly with the dye Hoechst 33342 and found that *dbl-1* loss-of-function animals are more likely to stain with the nuclear dye Hoechst 33342 than the dye-impermeable wild-type and *dbl-1* over-expressing strains. DBL-1-mediated changes

in the cuticular surface facilitate tail entanglement and promote worm-star formation, another novel phenotype we identified for *dbl-1* loss-of-function populations in *C. elegans*. Ultrastructural composition of the cuticle is also affected in a DBL-1 dose-dependent manner, directly correlated with the DBL-1 body length and drug response phenotypes. However, body length is a multifactorial phenotype that has other contributing factors, including endoreduplication, environment quality, and other signaling pathways, that may ultimately affect body length independent of cuticle (Tuck, 2014).

The use of *C. elegans* as a tool for anthelmintic drug screening is a practical consideration, but the cuticle of *C. elegans* is more restrictive than some common parasitic nematodes (Lee et al., 2002; Ruiz-Lancheros et al., 2011). Using a *dbl-1* mutant background with its more permeable cuticle may prove useful for drug screening analyses.

Our studies also suggest a physiological mechanism for the increased susceptibility of DBL-1 pathway mutant animals to infection by bacteria and nematophagous fungus (Mallo et al., 2002; Portal-Celhay et al., 2013; So et al., 2011; Tenor and Aballay, 2008; Zugasti and Ewbank, 2009). Not only is DBL-1 highly up-regulated in innate immune responses, but genes involved in an effective innate immune response are significantly up-regulated by DBL-1 signaling without significant differences in immune challenge (Alper et al., 2007; Liang et al., 2007; Mallo et al., 2002; Mochii et al., 1999; Roberts et al., 2010). Infection of DBL-1-deficient animals

may be facilitated by the altered surface properties or compromised barrier function of the cuticle.

In addition, the male spicule, a rigid structure used to probe for and pry open the hermaphrodite vulva during mating, is crumpled in the *dbl-1* loss-of-function background (Baird and Ellazar, 1999; Krishna et al., 1999; Suzuki et al., 1999). Defective function of socket cells, which secrete the stiff cuticle that encases the spicule, is responsible for this phenotype (Jiang and Sternberg, 1999). While the *dbl-1* spicule defect is associated with mismigration of surrounding cells that mold the spicule cuticle, we propose that altered cuticle secreted by socket cells in *dbl-1* mutant animals contributes to the crumpled spicule defect.

We propose a model in which DBL-1 controls extracellular matrix organization and composition in a dose-dependent manner (Figure 2.7). In this model, decreased DBL-1 signal strength leads to changes in the cuticle that decrease body length and barrier function, leading to drug hypersensitivity, uptake of a normally cuticle-impermeable dye, and worm-star formation. Increased DBL-1 signaling causes cuticle changes that increase body length and barrier function, which results in drug insensitivity. The molecular tools we developed in the *in vivo* nematode model system may provide an attractive means to identify novel mechanisms and modulators of BMP signaling in extracellular matrix regulation.

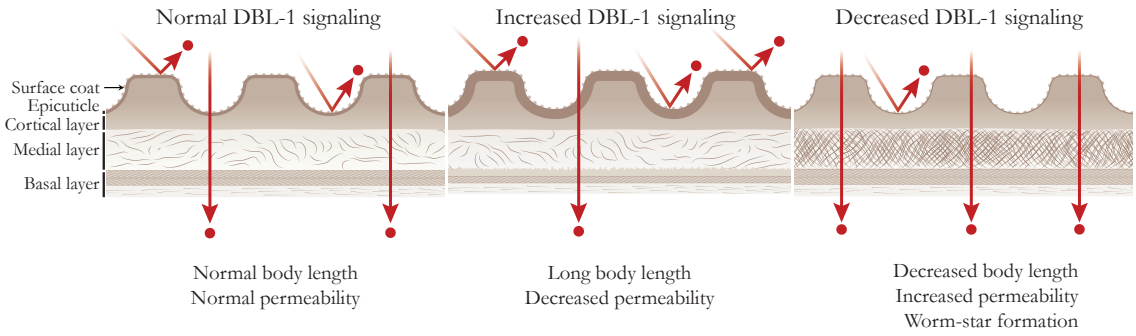

Figure 2.7 Model of DBL-1 pathway-mediated cuticular phenotypes. Model of how DBL-1 controls organization and composition of the cuticle, which affects body length, permeability barrier function, and worm-star formation in animals with normal (A), increased (B), and decreased (C) DBL-1 pathway signaling. Cuticle layers are indicated on the left.

3. MECHANISMS REGULATING BMP SECRETION IN *C. elegans*

Introduction

Bone morphogenetic proteins (BMPs) are cell-cell signaling molecules that are conserved from sea urchins to vertebrates (Wu and Hill, 2009). BMPs belong to the Transforming Growth Factor-β (TGF-β) superfamily of cell-cell signaling ligands and play important roles in development and diseases (Wu and Hill, 2009). Ligands belonging to the BMP are dose-dependent and undergo complex means of secretion, spatial regulation, and degradation. While the receptors and other signaling pathways members involved are well characterized, many of the mechanisms controlling BMP signal release remain to be explored (Ramel and Hill, 2012). To understand the spatial regulation of this pathway, others have used antibody staining and fluorescent tags to determine TGF-β ligand localization (Ramel and Hill, 2012). However, no study to date has directly analyzed the subcellular localization of a TGF-β and its regulation within the secreting cells. In vertebrates, there are over thirty TGF-β superfamily members (Wu and Hill, 2009), however, *C. elegans* have only five TGF-β ligands (Gumienny and Savage-Dunn, 2013). *C. elegans* is an ideal system to study regulation of BMP secretion as BMP pathway signaling is conserved and *C. elegans* has a simple, transparent body for visualizing fluorescently tagged transgenic proteins.

While DBL-1 is secreted from nervous tissue (Morita et al., 1999; Suzuki et al., 1999), it must be trafficked to the epidermis where it binds to receptors, activating a signaling pathway to regulate body size development (Krishna et al., 1999). How DBL-1

or any TGF-β member secretion is regulated to control its signaling ability is unknown. While some nerve-secreted proteins can be secreted constitutively, without the help of vesicle transport, others undergo regulated secretion to be transported from the Golgi to the cell's plasma membrane (Houy et al., 2013). Synaptic and dense core vesicles are common vehicles for methods of regulated secretion from nerve cells. While caveolin is best known for its role in endocytosis and signal transduction, caveolin also been shown to transport cargo from the Golgi to the plasma membrane (Parton and Simons, 2007).

In this chapter, we provide evidence that DBL-1 is regulated by a caveolin-mediated secretory process that includes transport to the cell's plasma membrane by motor proteins, and kiss-and-run fusion with the plasma membrane that suggests a mechanism of regulating DBL-1 secretion levels. Furthermore, this work shows that mouse BMP4 rescues loss of DBL-1 function in *C. elegans*, and suggests that the mechanism of DBL-1 regulation identified by this work may also be conserved in other systems.

Materials and methods

Strains and maintenance

C. elegans strains used in these studies were derived from the wild-type variety Bristol strain N2 and were cultured on nematode growth media (NGM) plates as previously described (Brenner, 1974). All strains were cultured on *E. coli* strain OP50 at 20˚C, except where noted. Strains used include: N2, TLG182 *texIs100 [dbl-1p::dbl-1:gfp + ttx-3p::rpf]* IV, TLG550 *texIs100 [dbl-1p::dbl-1:gfp + ttx-3p::rpf]* IV; *dbl-*

1(nk3) V; *texEx378 [dbl-1p::bmp4 + ttx-3p::gfp]*, TLG528 *texIs100 [dbl-1p::dbl-1:gfp + ttx-3p::rfp]* IV; *texEx361 [vha-5p::vha-5:mrfp + ttx-3p::gfp]*, and TLG447 *dbl-1(nk3)* V*; texEx306 [dbl-1p::bmp4 + ttx-3p::rfp]*.

PiMP super-resolution microscopy

Briefly, we acquired 50 images of a single plane over time using the spinning disk confocal microscope. We uploaded and processed these images using the PiMP plug-in (provided by Sebastian Munck and Wim Annaert) on FIJI to generate a final image at sub-diffraction resolution (Munck et al., 2012).

Immunocytochemical localization

As the nematode cuticle is relatively impermeable, we optimized methods for immunocytochemistry using the PELCO BioWave® microwave with ColdSpot® technology (Ted Pella, Redding, CA). This microwave-assisted whole-mount fixation and permeabilization protocol is adapted from the Finney-Ruvkun protocol (Finney and Ruvkun, 1990). Adult animals were washed in M9 buffer two times to remove residual bacteria and incubated in M9 buffer on ice for five minutes. Next, animals were suspended in fixative (3% paraformaldehyde and 2% (wt/vol) Triton X-100 in 0.1 M HEPES, pH 7.4) and were flash frozen in liquid nitrogen. The specimen tubes were then incubated in 60°C water until almost all the ice had melted. For all microwave steps for fixation and permeabilization, specimens were microwaved at 10°C on ice with a 25°C cut-out temperature and intermittent vacuum at 250 W unless otherwise noted. While

immersed in fixative, animals were microwaved for a 20-minute cycle (5 minutes on, 5 minutes off; repeat). Animals were then washed two times in 20 mM glycine in PBS, microwaving each wash for one minute to quench unreacted aldehydes. To reduce autofluorescence induced by aldehyde fixation, specimens were incubated in 1 mg/ml sodium borohydride in PBS and were microwaved for a 6-minute cycle (2 minutes on, 2 minutes off, 2 minutes on) two times. Samples were then washed in PBS, microwaving for one minute. Animals were washed two times in Tris-Triton buffer (100 mM Tris-HCl pH 7.4, 1% Triton X-100, 1 mM EDTA), microwaving each wash for one minute at 20°C. To permeabilize and reduce cross-linkages within the cuticle, animals were incubated in Tris-Triton buffer with 1% β-mercaptoethanol solution and were microwaved for a 6-minute cycle at 37°C four times. Animals were washed in borate buffer, microwaving one minute at 20°C. Animals were next incubated in 10 mM dithiothreitol (DTT) in borate buffer and were microwaved for a 6-minute cycle at 20°C. Specimens were then incubated in 0.3% H_2O_2 in borate buffer and were microwaved for a 6-minute cycle at 20°C to permeabilize and oxidize disulfides. Finally, animals were washed in borate buffer, microwaving one minute at 20°C.

For all microwave steps for immunolabeling, specimens were microwaved at 37°C with a 44°C cut-out temperature and constant vacuum at 250 W unless otherwise noted. Specimens were next incubated in blocker (0.1% (wt/vol) Triton X-100, 5% normal serum, 1% (vol/vol) glycerol, 1% (wt/vol) fish skin gelatin, 0.04% sodium azide in PBS) and microwaved for a 6-minute cycle. Then, animals were reacted with the primary antibody diluted in antibody wash buffer (0.1% (wt/vol) Triton X-100 in PBS)

for a 12-minute cycle (5 minutes on, 2 minutes off, 5 minutes on) two times. Animals were washed in antibody wash buffer three times, microwaving for one minute with each wash step. Specimens were incubated in secondary antibody diluted in antibody wash buffer for a 12-minute cycle. Animals were washed in antibody wash buffer four times, microwaving for one minute with each wash step. Immunolabeling steps were repeated for each group of primary and secondary antibodies as necessary.

Microscopy and imaging

For spinning disk and confocal microscopy, animals were immobilized in 2.5% (wt/vol) 0.1 μm diameter polystyrene beads (00876-15, Polysciences Inc., Warrington, PA) in 1 mM levamisole on 10% agarose pads (Fang-Yen et al., 2012). Spinning disk images were acquired on a Retiga-SRV CCD camera (Quantitative Imaging Corporation, Surrey, BC, Canada) mounted on a BD Carv II™ spinning disk confocal (BD Biosystems, San Jose, CA) on a Zeiss A1 compound microscope base (Carl Zeiss, Inc., Jena, Germany). A 63x/1.4 NA oil Plan-Apochromat objective (Carl Zeiss, Inc., Jena, Germany) and iVision-Mac™ software (BioVision Technologies, Exton, PA) were used for image acquisition. Confocal images were acquired on a Nikon A1R confocal laser microscope system (Nikon Instruments, Inc., Melville, NY, USA) using a 40x/1.15 NA water CFI Apo Lambda S LWD objective (Nikon Instruments, Inc., Melville, NY, USA) and NIS-Elements AR software (Nikon Instruments, Inc., Melville, NY, USA).

Pearson's correlation coefficient

The degree of overlap between red and green channels as reported by Pearson's correlation coefficient was quantified using the co-localization analysis tool in NIS-Elements AR software (Nikon Instruments, Inc., Melville, NY, USA). Multiple planes of 14 representative areas containing both red and green punctae were analyzed.

Results

DBL-1 localizes to neuronal puncta

To determine localization of DBL-1, we expressed a functional, GFP-tagged DBL-1 in otherwise wild-type animals. We imaged the GFP-tagged DBL-1 in immobilized, live animals using confocal microscopy and then enhanced the images using photobleaching microscopy with non-linear processing (PiMP) (Munck *et al*., 2012) to obtain a super-resolution image. We found that functional, GFP-tagged DBL-1 is expressed in a discrete punctate pattern along the ventral and dorsal nerve cords (Figure 3.1).

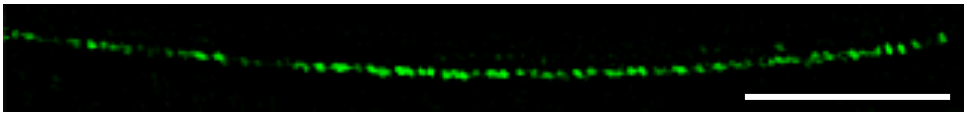

Figure 3.1 GFP-tagged DBL-1 localization. PiMP super-resolution image of GFP-tagged DBL-1 in live *C. elegans* in neuronal punctae along the dorsal and ventral nerve cords. Scale bar = 5 μm.

Secreted DBL-1 localization is juxtaposed to epidermal exosomes

While GFP-tagged DBL-1 localizes to punctae, the localization of these punctate structures was unknown. Because DBL-1 must bind to receptors in the hypodermis, we reasoned that GFP-tagged DBL-1 could be localized to vesicles in hypodermal tissue that cradles the DBL-1-secreting neurons. To investigate this possibility, we compared localization of GFP-tagged DBL-1 with mRFP-tagged VHA-5, which is expressed in the hypodermis and localizes to exosomes (Liegeois et al., 2006). We found that GFP-tagged DBL-1 localization is juxtaposed to mRFP-tagged VHA-5 (Figure 3.2). These results indicate that DBL-1 positive puncta are not localized within hypodermal tissue.

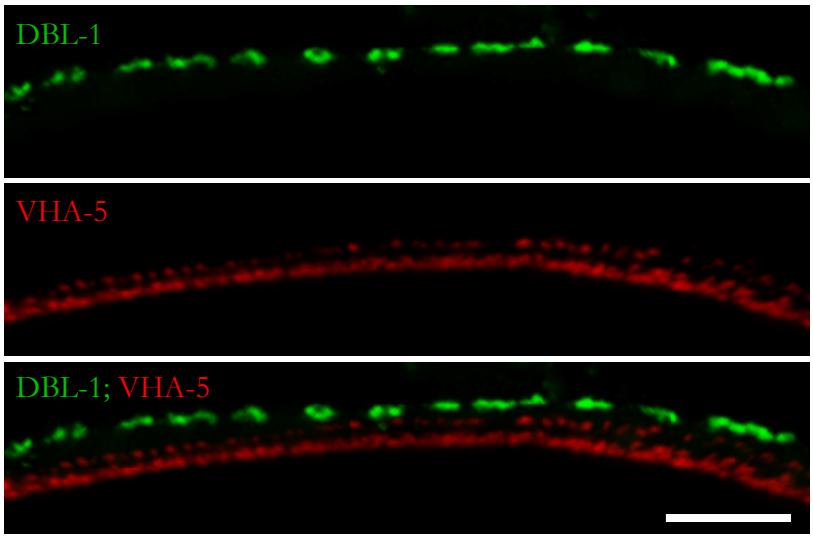

Figure 3.2 GFP-tagged does not localize to the hypodermis. Localization of GFP-tagged DBL-1 (green) with epidermal exosomes expressing mRFP-tagged VHA-5 (red). Scale bar = 5 μm.

BMP4 co-localizes with GFP-tagged DBL-1

To further probe localization of our DBL-1 BMP, we used whole mount immunofluorescent approaches in this transparent organism. For immunocytochemical studies, we engineered a plasmid containing the *dbl-1p* and cDNA of a mouse DBL-1 homolog, BMP4, and injected the construct into animals expressing GFP-tagged DBL-1. This DBL-1 homolog transgene is viable and functional, as it rescues body size defects in animals lacking functional *dbl-1* (data not shown). We optimized a microwave-assisted immunocytochemistry protocol to allow better preservation, increased infiltration of antibodies, and decreased fixation and staining time. Using this microwave-based whole mount immunofluorescence method we developed, we found that the BMP4 localizes to the nerve cord, in a punctate pattern similar to GFP-tagged DBL-1, and that mouse BMP4 co-localizes with GFP-tagged DBL-1 (Figure 3.3).

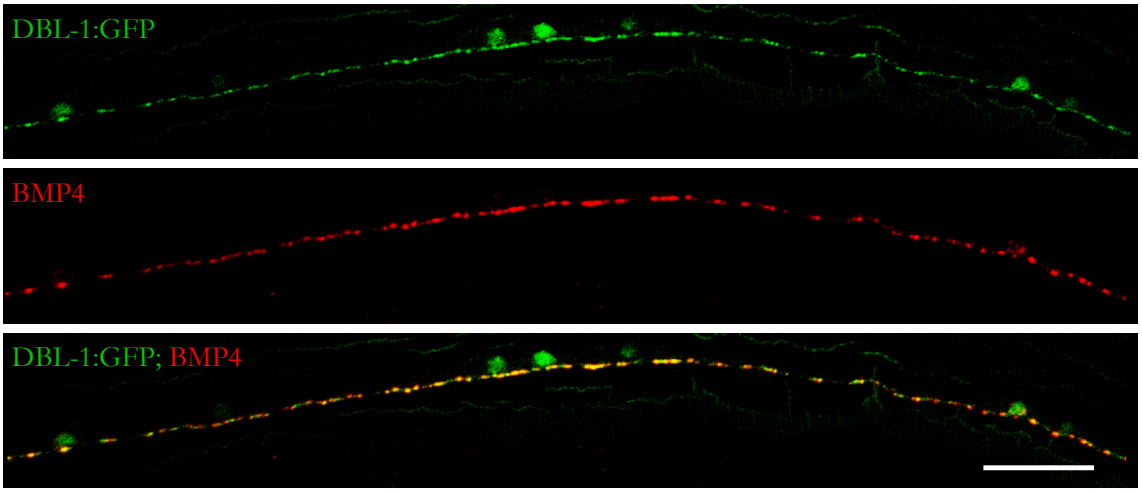

Figure 3.3 GFP-tagged DBL-1 co-localizes with BMP4. Localization of GFP-tagged DBL-1 (green) with BMP4 (red) in the ventral nerve cord upon immunofluorescent staining. Scale bar = 10 μm.

BMP4 localizes to neuronal vesicles

To further characterize localization of punctae expressing BMP4, we stained the transgenically expressed mammalian BMP4 along with proteins that localize within the nerve cord. We found that BMP4 co-localizes with SAX-7, an adhesion protein expressed at cell-cell contact sites in the nerve cord (Figure 3.4). These results suggest that BMP4 localizes to neuronal punctae at the plasma membrane.

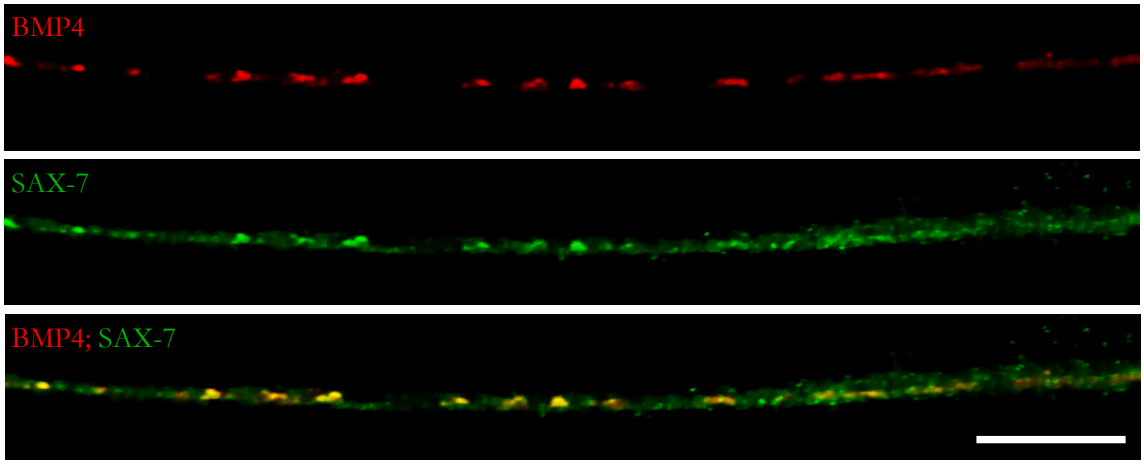

Figure 3.4 BMP4 localizes to neuronal cell contact sites. Localization of SAX-7 (green) at cell-cell adhesion sites with BMP4 (red) in nervous tissue upon whole mount immunofluorescent staining. Scale bar = 5 μm.

Based on its neuronal expression, we reasoned that BMP4 could be localized to secretory vesicles within the nerve cord. To test this possibility, we took advantage of DYN-1, a *C. elegans* dynamin homologue involved in vesicle scission. We found that BMP4 and DYN-1 partially co-localize (Figure 3.5). Consistent with partial co-localization between BMP4 and DYN-1, we calculated a Pearson correlation coefficient value of 0.52, a moderate positive correlation (Bolte and Cordelieres, 2006). These results indicate that BMP4 localizes to neuronal vesicles.

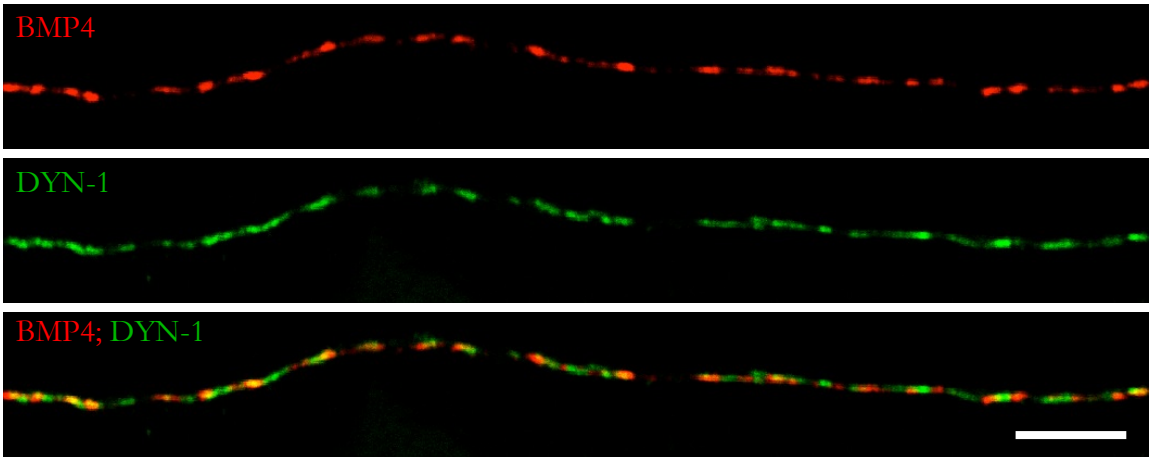

Figure 3.5 BMP4 localizes to neuronal vesicles. Localization of DYN-1 (green) with BMP4 (red) upon whole mount immunofluorescent staining. Scale bar = 5 μm.

BMP4 localizes to caveolar bodies

After realizing that BMP4 is localized to vesicles within neurons, we reasoned BMP4 could be transported from the Golgi to the plasma membrane to undergo secretion in synaptic, dense core, or caveolar vesicles. We found GFP-tagged DBL-1 is not secreted using synaptic or dense core vesicle machinery (Beifuss, Bageshwar, and Gumienny, unpublished). A *C. elegans* homologue of caveolin, CAV-1, localizes to lipid raft subdomains in caveolar structures. We found that BMP4 and CAV-1 co-localize (Figure 3.6), suggesting BMP4 is transported to the cell surface in caveolar bodies.

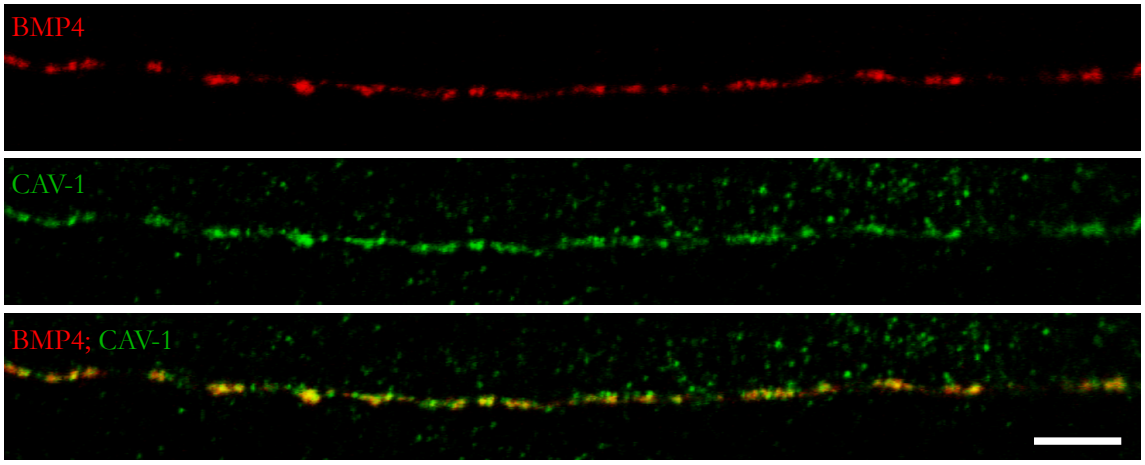

Figure 3.6 BMP4 localizes to caveolar bodies. Localization of CAV-1 (green) with BMP4 (red) in nervous tissue upon whole mount immunofluorescent staining. Scale bar = 5 μm.

DBL-1 undergoes bidirectional transport within neurons

In mammals caveolae can undergo microtubule-based transport (Pelkmans and Zerial, 2005). We analyzed movement of GFP-tagged DBL-1 using time lapse microscopy in live animals and found some puctae are actively transported within the neuronal cell, travelling either from dorsal to ventral or from ventral to dorsal areas within the nerve (Figure 3.7). Consistent with transport using kinesin and dynein motors, GFP-tagged DBL-1 vesicles undergo brief periods of rapid directed movement, stalls, and then continues with directed movement (data not shown).

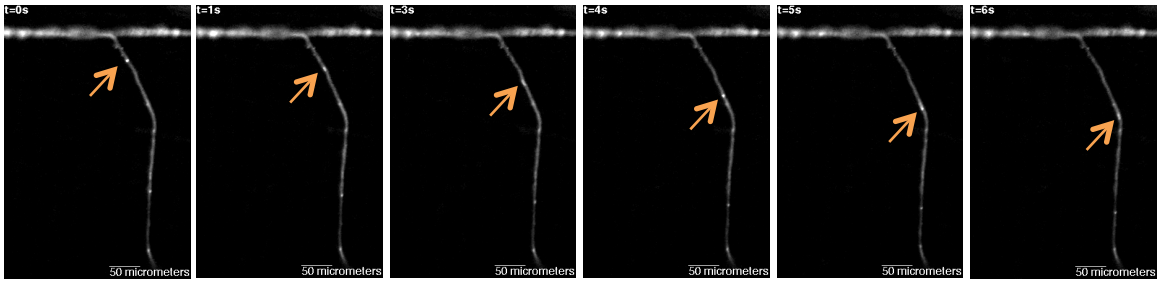

Figure 3.7 GFP-tagged DBL-1 undergoes transport. Time-lapse microscopy of GFP-tagged DBL-1 punctae transport within the nerve cord.

DBL-1 in punctae is exposed to the extracellular environment

In other systems, caveolin-scaffolded vesicles can briefly fuse with the plasma membrane, release some of their cargo, and then bud off again without releasing all of their contents, called "kiss-and-run" membrane dynamics (Pelkmans and Zerial, 2005). We asked if the GFP-tagged DBL-1 punctae were exposed to the extracellular environment by injecting anti-GFP antibody, tagged with a red fluorophore, into the pseudocoelom, which contacts the nerve cords. The anti-GFP antibody does not cross the cell membrane in intact, live animals. We found specific staining of GFP-tagged DBL-1-positive punctae by the anti-GFP antibody (Figure 3.8), indicating that some DBL-1 was accessible to the pseudocoelom.

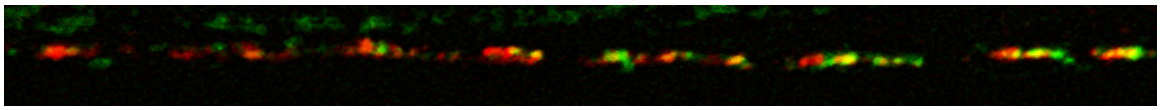

Figure 3.8 GFP-tagged DBL-1 is exposed to the extracellular environment. Localization of anti-GFP antibody, tagged with a red fluorophore (red), injected into the pseudocoelom of live animals with GFP-tagged DBL-1 (green).

Discussion

BMPs are signaling molecules that are critical for development and alteration in signaling is associated with multiple disease states (Wu and Hill, 2009). BMP molecules undergo complex processes of regulation, ranging from control of secretion from the Golgi to the plasma membrane to regulation of ligand availability in the extracellular matrix. Previous reports link caveolin to TGF-β and BMP signaling pathways, but the connection has remained unclear. This work shows that DBL-1 co-localizes with caveolin CAV-1 and is trafficked to the plasma membrane. While caveolin-mediated endocytosis is well described, caveolin-mediated secretion of nascent protein is understood by just two examples (Mao et al., 2009; Sato et al., 2006). We provide evidence that regulation of DBL-1 vesicle secretion may be provided through caveolin-based "kiss-and-run" dynamics, which could contribute to dose and spatial control of DBL-1 pathway signaling. This work also shows the conservation of BMP4 and DBL-1 functions, as mouse BMP4 rescues the mutant phenotype of DBL-1-deficient animals and localizes to the same subcellular compartments as DBL-1. We propose the nematode-expressed mouse BMP4 is regulated in *C. elegans* the same way as the endogenous DBL-1 to be active, and that this regulated secretion mechanism, which has

completely conserved machinery, is used to regulate TGF-β signaling in other systems. Based on these findings and other work, we propose that *C. elegans* DBL-1 BMP signaling is regulated by a novel caveolin-dependent secretion mechanism that controls the amount of BMP released from neurons.

4. ZONA PELLUCIDA-FAMILY MEMBER DYF-7 LOSS CREATES CELL ADHESION AND SENSORY DEPRIVATION SPECTRUM DEFECTS THROUGHOUT THE *C. elegans* LIFE CYCLE

Introduction

Cell adhesion is critical for all multicellular organisms. From the first touch of sperm to egg to maintenance of the aging organism, cells must adhere for proper cell migration and to maintain open communication lines and structural integrity. While mutations in canonical cell adhesion genes can have profound effects on organism viability, mild aberrations in cell adhesion can underlie rare, conserved disorders. Impaired cellular adhesion can contribute to disease, such as cancer metastasis, muscular dystrophy, and schizophrenia (Cohn and Campbell, 2000; Jeanes et al., 2008; Kanakry et al., 2007).

Zona pellucida-domain (ZP-domain) proteins (first identified in the zona pellucida, an extracellular matrix surrounding the mammalian egg) are a family of extracellular molecules defined by their ZP-domain, a self-assembling protein polymerization motif (Bork and Sander, 1992). The ZP-domain protein family has a diverse array of functions, ranging from cell-cell interactions, organization of extracellular matrices, establishment of cell shape, and sensory perception (Bokel et al., 2005; Plaza et al., 2010). One ZP-domain protein, α-tectorin, is a component of the tectorial membrane, an apical extracellular matrix of the inner ear. The tectorial membrane anchors the tip of stereocilia bundles of outer hair cells that transduce sound-

triggered mechanical forces into electrical signals. Mutation in the α-tectorin gene can result in detachment of the tectorial membrane from the sensory epithelium, defects in tectorial membrane formation, and loss of attachment of outer hair cells to the tectorial membrane, ultimately resulting in deafness in humans and mice (Liu et al., 2011; Richardson et al., 2011; Verhoeven et al., 1998).

In *C. elegans*, there are approximately 40 predicted ZP-domain proteins of largely unknown function (Sapio et al., 2005). One such tectorin-like ZP-domain protein is DYF-7, a transmembrane protein involved in shaping dendrites in the primary *C. elegans* sense organ, the amphid (Heiman and Shaham, 2009). Loss of DYF-7 prevents these sensory cells from being properly anchored to the basement membrane as they migrate, causing shortened neuronal dendrites that no longer sense poor environmental conditions that would normally signal entry into an alternative larval developmental stage called dauer (Heiman and Shaham, 2009; Starich et al., 1995).

Although cell adhesion has been recognized as a major player in muscular dystrophy and schizophrenia, the critical need for adhesion in viability has hindered studies in model systems. Indeed, many diseases associated with misregulated cell adhesion are caused by minor disruption of cell adhesion components, conferring pathology while retaining viability. It has become clearer even in this decade that accessory proteins are important for function and maintenance of core components in adhesive complexes, yet the molecular and cellular effects of altering these proteins remains largely unexplored.

In this work, we have identified a single gene, *dyf-7*, that plays important roles in cell adhesion and is required for a spectrum of environmental responses. We show here DYF-7 is a component of the basement membrane and controls epidermal adhesion and morphogenesis. We show an essential role for DYF-7-mediated neuronal anchoring in three environmentally mediated developmental stages, progression from the first larval (L1) stage, entry into a dauer stage in poor environments, and exit from dauer stage when favorable conditions resume. Finally, we show a continued requirement for DYF-7 in adult food-sensing behavior. These studies show a conserved role for ZP-proteins in extracellular matrix formation and epithelial organization, affecting both cell adhesion and sensory perception.

Materials and methods

Strains and maintenance

C. elegans strains were derived from the wild-type variety Bristol strain N2 and were cultured on nematode growth media (NGM) plates as previously described (Brenner, 1974). All strains were cultured on *E. coli* strain OP50 at 20˚C, except where noted. Strains used include:

N2, NL2099 *rrf-3(pk1426)* II, TLG552 *rrf-3(pk1426)* II; *dyf-7(m539)* X, DR40 *daf-1(m40)* IV, TLG478 *daf-1(m40)* IV; *dyf-7(m539)* X, JR667 *wIs51[scmp::gfp + unc-119(+)]* V, TLG496 *wIs51[scmp::gfp + unc-119(+)]* V; *dyf-7(m539)* X, SP1196 *dyf-7(m539)* X, SP1735 *dyf-7(m537)* X, TLG444 *dyf-7(m539)* X; *ncIs13[ajm-1::gfp]*, TLG474 *dyf-7(m537)* X; *texEx319[dyf-7p::dyf-7:gfp + ttx-3p::rfp]*, TLG475 *dyf-*

7(m537) X; *texEx320[dyf-7p::dyf-7:sfgfp + ttx-3p::rfp]*, ST65 *ncIs13[ajm-1::gfp]*, and TLG337 *texEx217[dyf-7p::gfp + ttx-3p::rfp]*.

L1 arrest assays

L1 arrest temperature assays were conducted as previously described (Ailion and Thomas, 2000). Briefly, animals were placed on plates seeded with food and allowed to lay embryos at room temperature. The embryos were then incubated at their respective test temperature for 100 hours at 15°C, 65 hours at 20°C, 48 hours at 25°C, or 44 hours at 27°C to allow wild-type animals to reach late larval or adult stages and to score populations before any F1 embryos were laid. The amount of time is shorter for higher temperatures, as animals develop faster. For animals incubated at 27 °C, the same animals were then incubated for an additional 44 hours at 20°C to measure for recovery to reproductive development. Assays were independently performed three times for each temperature tested, with at least 215 animals per genotype for each temperature.

Animals used in experiments requiring gene-specific RNAi were grown continuously and for multiple generations on the gene-specific RNAi bacteria. The RNAi-treated animals therefore had gene knockdown from L1 through adulthood with knockdown of any maternal contribution during embryogenesis prior to use in the assays. RNAi-treated gravid adults were then placed on plates seeded with food, either containing a gene-specific or the negative control (pseudogene C06C3.5) RNAi, and allowed to lay embryos at 15°C. The embryos were then incubated at the 27°C test temperature for 44 hours, which would allow wild-type animals to enter late larval or

early adult stages and permitted scoring of populations before any F1 embryos were laid. After the incubation period, the stage of each animal was scored. Assays were independently performed three times, with at least 275 animals per genotype.

Dauer formation assays

Dauer assays were conducted as previously described (Ailion and Thomas, 2000). Gravid adult animals were placed on plates and allowed to lay embryos at room temperature. The embryos were then incubated at their respective test temperature for 100 hours at 15°C (the permissive temperature) or 48 hours at 25°C (the restrictive temperature) to allow for scoring of transient dauers and to score populations before any F1 embryos were laid. The amount of time is shorter for higher temperatures, as animals develop faster. Assays were independently performed three times for each temperature tested, with at least 106 animals per genotype.

Roaming assays

Area roamed was assayed as previously described (Fujiwara et al., 2002). Briefly, an animal was placed onto an individual plate to track the area the animal traveled over time. After 18 hours, the animal was removed, the tracks of each animal were superimposed on a grid, and the number of squares the animal entered was counted. Assays were independently performed five times, with at least 61 animals per genotype.

Light touch response assay

Briefly, response to light touch was assay by scoring backing response to a gentle lateral stroke of an eyelash between the pharynx and intestine. At least 50 animals per genotype were assayed.

Microscopy and imaging

Dissecting scope images were acquired at 10x or 60x magnification using iVision-Mac™ software (BioVision Technologies, Exton, PA) and a Retiga-2000R CCD camera (QImaging Corporation, Surrey, BC, Canada) mounted on a Nikon SMZ1500 dissecting microscope (Nikon Instruments, Inc., Melville, NY).

For spinning disk and confocal microscopy, animals were immobilized in 2.5% (wt/vol) 0.1 μm diameter polystyrene beads (00876-15, Polysciences Inc., Warrington, PA) in 1 mM levamisole on 10% agarose pads (Fang-Yen et al., 2012). Spinning disk images were acquired on a Retiga-SRV CCD camera (Quantitative Imaging Corporation, Surrey, BC, Canada) mounted on a BD Carv II™ spinning disk confocal (BD Biosystems, San Jose, CA) on a Zeiss A1 compound microscope base (Carl Zeiss, Inc., Jena, Germany). A 63x/1.4 NA oil Plan-Apochromat objective (Carl Zeiss, Inc., Jena, Germany) and iVision-Mac™ software (BioVision Technologies, Exton, PA) were used for image acquisition. Confocal images were acquired on a Nikon A1R confocal laser microscope system (Nikon Instruments, Inc., Melville, NY, USA) using a 40x/1.15 NA water CFI Apo Lambda S LWD objective (Nikon Instruments, Inc., Melville, NY, USA) and NIS-Elements C software (Nikon Instruments, Inc., Melville, NY, USA).

Results

DYF-7 is a ZP-domain protein that is expressed post-embryonically

While embryonic *dyf-7* expression has been determined to be critical for the proper anchoring of some neurons during early development, other phenotypes displayed by animals lacking *dyf-7*, such as body size and male mating defects, suggested a postembryonic need for DYF-7. To determine post-embryonic expression of *dyf-7* transcriptional expression, we engineered a *dyf-7p::gfp* construct and found that *dyf-7p::gfp* localizes to neurons and neuronal support cells throughout larval and adult stages (Figure 4.1A-D). By staining environmentally exposed sensory neurons, we found *dyf-7p::gfp* is expressed in a subset of neurons, including ASJ amphid neurons, which have been shown to be critical for dauer entry and recovery, as well as other neuronal cells in the anterior ganglion (Figure 4.1A-C) (Bargmann and Horvitz, 1991; Tong and Burglin, 2010). We also discovered *dyf-7p::gfp* expression in epithelial cells, including specialized epidermal seam cells (Figure 4.1A) and the intestine (Figure 4.1D), and in PHA, PHB, PQR, and PLN neurons throughout post-embryonic development (Figure 4.1A, D).

Using a DYF-7 construct translationally fused with either GFP or a superfolder variant of GFP (sfGFP), we found DYF-7 is expressed post-embryonically in a subset of anterior neurons (Figure 4.1E, G), where sfGFP-tagged DYF-7 is restricted to the neuronal cell body and cilia (Figure 4.1G). Tagged DYF-7 also localizes to the intestine's apical extracellular matrix (Figure 4.1F, H) and basal extracellular matrix

(Figure 4.1F, H), where sfGFP-tagged DYF-7 assembles into a meshwork of filament-like structures at the basement membrane (Figure 4.1H).

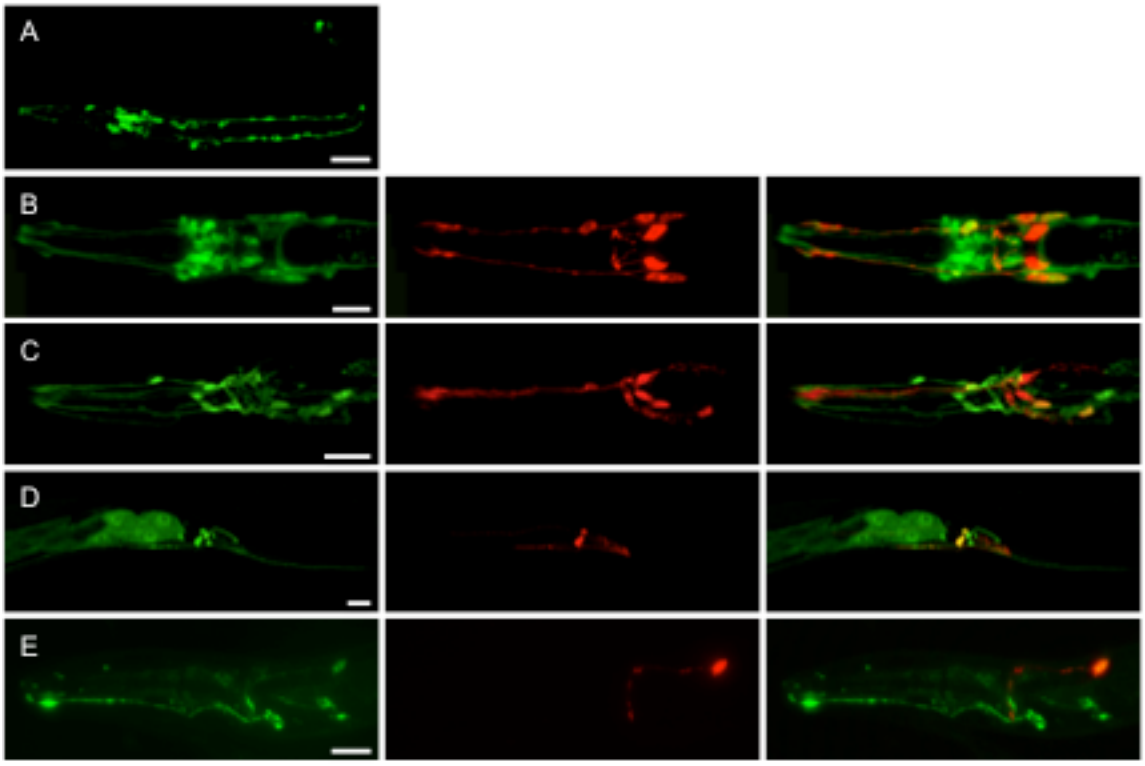

Figure 4.1 DYF-7 expression. (A) *dyf-7p::gfp* is expressed in head neurons and support cells, seam cells, and tail neurons in an L1. (B) *dyf-7p::gfp* is expressed in head neurons and support cells, co-localizing with a subset of DiI-stained and AIY neurons in red in an L2. (C) *dyf-7p::gfp* is visible in head neurons, including AIY and ASJ neurons, and support cells in an adult animal and co-localizes with a subset of DiI-stained and AIY neurons in red. (D) *dyf-7p::gfp* is expressed in PHA, PHB, PQR, and PLN neurons in an adult; PHA and PHB are also stained with DiI in red. (E) *dyf-7p::dyf-7:gfp* is visible in a restricted number of head neurons, co-localizing with AIY neurons in red in an L1. (F) *dyf-7p::dyf-7:gfp* localizes to the intestine's apical and basal extracellular matrices in an L2. Autofluorescence is shown in red. (G) *dyf-7p::dyf-7:sfgfp* localizes to neuronal cell bodies and cilia in an L3. (H) *dyf-7p:dyf-7:sfgfp* localizes to apical and basal extracellular matrices of the intestine, forming a meshwork of filaments in the basal lamina in a post-gravid adult. Scale bars = 10 μm.

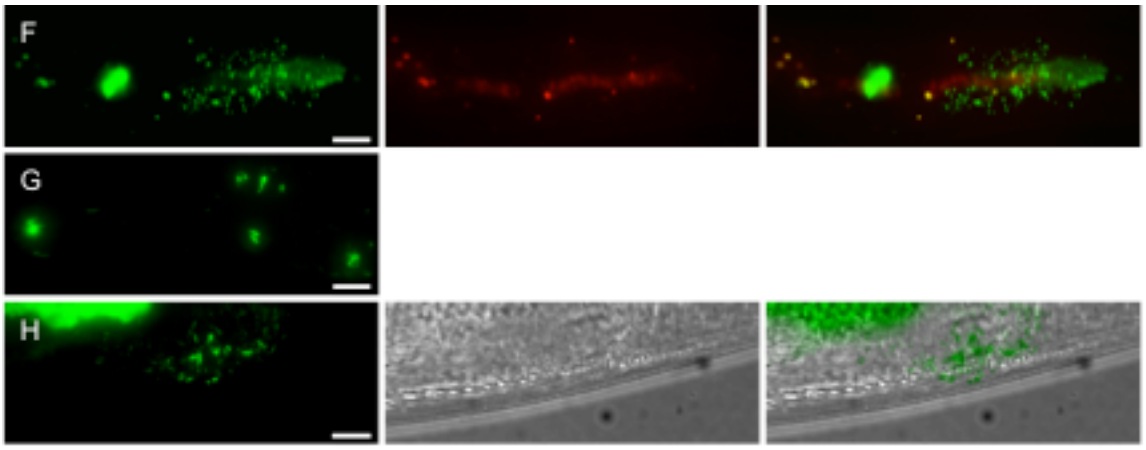

Figure 4.1 Continued.

DYF-7 is critical for maintenance of epithelial cellular adhesion

Modulation and assembly of adhesive complexes are conserved from *C. elegans* to humans (Cox and Hardin, 2004). Cell adhesion is accomplished through assembly, organization, and maintenance of junctional structures. While ZP-domain proteins have been shown to be involved in organization of apical structures in epithelial cells in *Drosophila*, the characterization of protein function in cell adhesion is an area of research that must be further studied (Bokel et al., 2005; Wilkin et al., 2000).

While foundational work has shown that DYF-7 is critical for anchoring sensory neurons to basement membrane during embryonic development (Heiman and Shaham, 2009), the post-embryonic expression of DYF-7 in non-neuronal tissue (Figure 4.1) inspired us to investigate a role for DYF-7 in maintaining proper cell contacts in epithelial tissues. The *C. elegans* epidermis can be divided into two broad groups: the hypodermis and specialized epithelial cells. The hypodermis is a multinucleated

syncytium that synthesizes and secretes cuticular components. Adherens junctions form transient links between the hypodermal cells of the head or of the tail. Upon fusion of these epidermal cells, their adjoining adherens junctions disassemble (Labouesse, 2006). Mild cell adhesion defects cause transient contacts between epidermal cells to be inappropriately maintained. When these transient contacts are not properly maintained, the resulting mutant animals display morphological defects in the head or tail, including Vab (Variably Abnormal) and split tail phenotypes (Ginzburg et al., 2002). To quantify the incidence of Vab and split tail in two canonical *dyf-7* mutant strains, *dyf-7(m537)* and *dyf-7(m539)*, containing insertions within the N- or C-terminal portions of the ZP-domain respectively, we took advantage of a staining procedure we developed that stains the cuticle using the vital lipophilic dye DiI (Heiman and Shaham, 2009; Schultz and Gumienny, 2012) (Max Heiman, personal communication). While wild-type and *dyf-7(m537)* animals never display a Vab phenotype, we found *dyf-7(m539)* animals are Vab at a low penetrance (Figure 4.2 A-C, E). Further, animals lacking *dyf-7* function display the split tail phenotype (Figure 4.2 D-E), where *dyf-7(m539)* populations display a more severe level of penetrance compared to levels in *dyf-7(m537)* populations. While Vab and split tail phenotypes seen in L1 animals indicate an embryonic requirement for DYF-7, Vab can be detected in all larval stages and adults, signifying a perduring, post-embryonic requirement for DYF-7 (Figure 4.2 A-C). These results indicate that *dyf-7* plays a mild role in embryonic and post-embryonic cellular adhesion between epidermal cells. The low-penetrance split tail phenotype is shared by only seven other genes, almost all of which have homologs involved in cell adhesion and are implicated in

schizophrenia (Ginzburg et al., 2002; Ikegami et al., 2004; Marcotte et al., 2001; Roy et al., 2000; Starich et al., 2003).

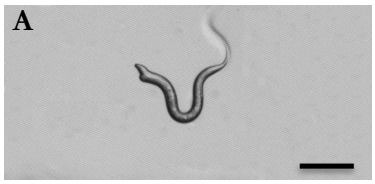

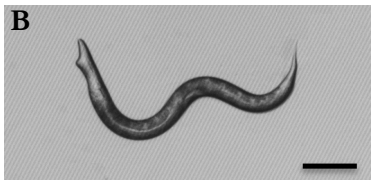

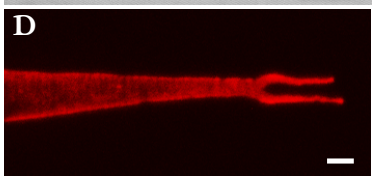

E

Strain	Vab	Split tail	n
Wild type	0%	5%	506
dyf-7(m539)	3%	11%	593
dyf-7(m537)	0%	8%	542

Figure 4.2 *dyf-7* mutants display Vab and split tail phenotypes. *dyf-7(m539)* animals display the Vab phenotype at all stages, including L2 (A), L4 (B), and adult (C) stages. *dyf-7(m539)* and *dyf-7(m537)* display split tail phenotypes at L1 (D). Incidence of Vab and split tail in wild-type and *dyf-7* mutant animals (E). A - C. Scale bars = 100 μm. D. Scale bar = 1 μm.

DYF-7 is required for proper apical junction organization in epithelia

We have shown that *dyf-7* plays a role in maintaining proper adhesion between epidermal cells (Figure 4.2). To better study the role of DYF-7 in cell adhesion in epithelia (which includes the epidermis, pharynx, intestine, and other cells), we directly compared epithelial apical junctions in wild-type and *dyf-7* mutant backgrounds. While we found DYF-7 is essential for maintaining proper dynamics at junctions between hypodermal cells, hypodermal apical contacts appear largely wild type (data not shown). However, consistent with a role for DYF-7 in regulating epithelial adhesion, we

observed that pharyngeal apical junction complexes are disorganized in *dyf-7(m539)* mutants (Figure 4.3 A-B). These results further confirm a role for *dyf-7* in regulating post-embryonic adhesion in epithelial tissue.

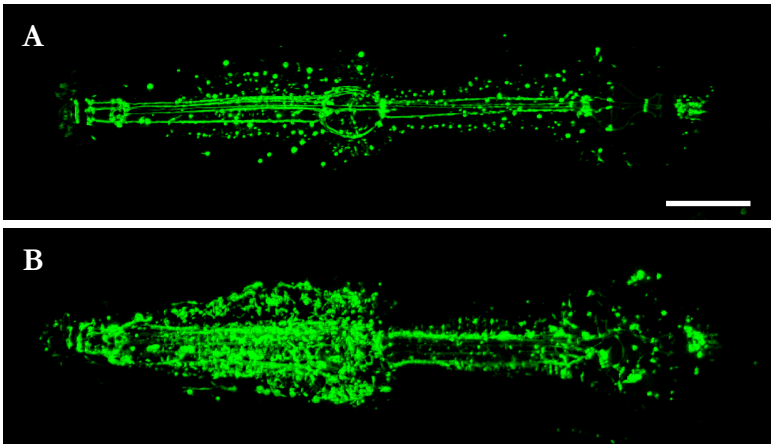

Figure 4.3 Epithelial adherens junctions are disorganized in *dyf-7* mutants. Adherens junctions in pharyngeal epithelia marked with AJM-1:GFP in wild type (A) and *dyf-7(m539)* (B) L1 animals. Scale bar = 10 μm.

DYF-7 does not influence seam cell development

We have shown that DYF-7 is critical for maintaining hypodermal cell contacts and for organization of epithelial apical junctions in the pharynx. Based on these roles in epithelial adhesion and the observation that *dyf-7p::*GFP is expressed in specialized epidermal seam cells, we investigated whether *dyf-7* plays a role in seam cell

development and morphology. We found that *dyf-7(m539)* animals display wild type seam cell number and arrangement at L1 (Figure 4.4).

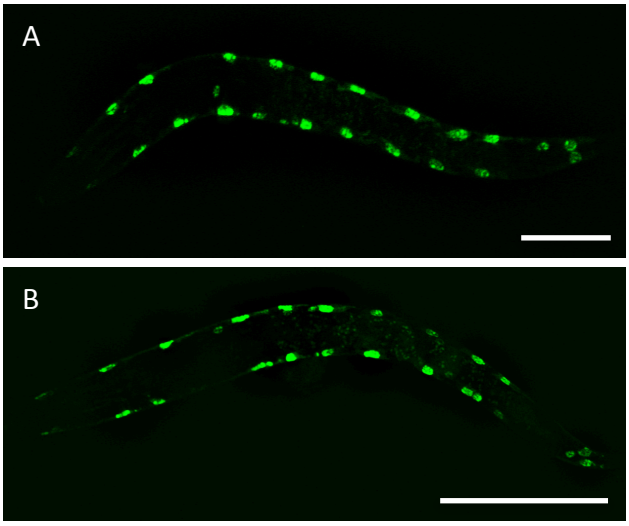

Figure 4.4 DYF-7 does not affect seam cell morphology. Seam cells marked with a fluorescent GFP tag in wild type (A) and *dyf-7(m539)* (B) L1 animals. Scale bars = 10 μm.

DYF-7 is required for progression from L1 arrest

The ability to sense and appropriately interpret environmental cues is an important survival skill for all organisms. *C. elegans* first responds to environmental cues upon hatching, where the nematode's default state is to pause at the first larval stage and post-embryonic development is only initiated upon feeding. L1 arrest, or diapause, unlike the later dauer arrest, occurs without any type of morphological

modification. Environmental factors including nutrient availability and temperature contribute to the decision to exit L1 arrest (Baugh and Sternberg, 2006; Fukuyama et al., 2006; Hong et al., 1998).

To characterize the role of *dyf-7* in sensory perception, we assayed how *dyf-7* affects environmental response at L1 arrest. When wild-type animals are grown at 15°C to 25°C in the presence of food, the vast majority of animals continue with normal development and enter late larval or adult stages in our assay (Figure 4.5A). However, we found that 17% of *dyf-7(m539)* mutant animals constitutively arrest at L1 even in the presence of food at normal growth temperatures (Figure 4.5A). We found wild-type animals grown at high temperature, 27°C, will either arrest in dauer development or continue to reproductive development (Figure 4.5A-B). No wild-type animals fail to exit L1 arrest (Figure 4.5A-B). However, when *dyf-7* mutants were hatched and grown at high temperature, we discovered that nearly all (95%) *dyf-7(m539)* and to a lesser extent (28%) *dyf-7(m537)* mutant animals failed to progress past L1 arrest (Figure 4.5A-B). In the less severe *dyf-7(m537)* animals, incubation at high temperature also caused a large fraction of animals to arrest in dauer, a more typical response to high temperature for sensory perception mutants (Ailion and Thomas, 2000) (Figure 4.5B). These results show that penetrance of the L1 arrest phenotype of *dyf-7* mutants increases with temperature, suggesting that animals with loss of *dyf-7* signaling display a starved nutritional state at high temperature even in the presence of food.

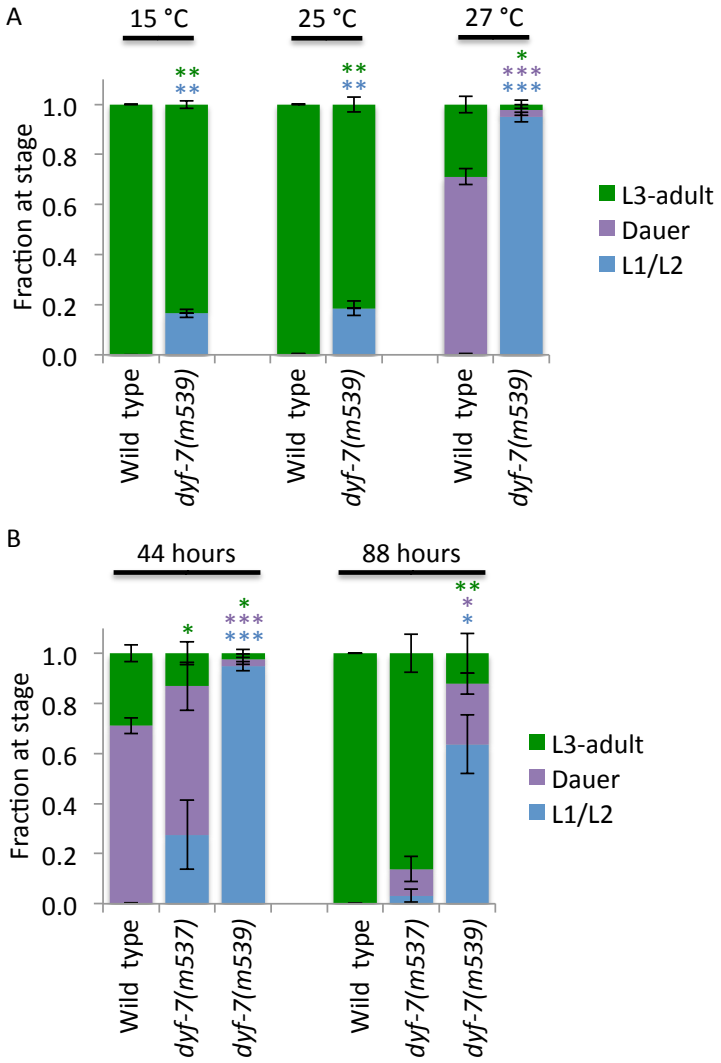

Figure 4.5 DYF-7 is required for progression from L1 arrest. (A) The stage of each animal was measured after being grown at 15, 25, or 27°C. (B) Developmental progress was measured for animals that were grown for 44 hours at high temperature, 27°C (left), and then allowed to continue to grow for an additional 44 hours at 20°C (right). Error bars indicate the mean ± SEM. P-values compare data to wild type (***P≤0.0001; **P≤0.001; *P≤0.05) using the unpaired t-test.

Animals typically exit L1 arrest after eating food. To determine if high temperature-induced L1 arrest is a reversible condition, we took animals that were initially grown at high temperature and incubated them for a 44-hour recovery period at 20°C. While all wild-type animals continued with reproductive development (Figure 4.5B), only a fraction of *dyf-7* mutants exited L1 diapause and some of these animals that had recovered from L1 arrest entered dauer by the end of the recovery period (Figure 4.5B), showing that if *dyf-7* sensory mutant animals progress past L1 arrest at high temperature, then animals often also arrest in dauer. These results indicate that *dyf-7* mutant animals are so severely sensory deprived they maintain a physiological condition mimicking starvation even in the absence of thermosensory cues.

DYF-7 and synMuv B genes act independently to regulate recovery from L1 arrest

Misregulated recovery from L1 arrest at high temperature has been described for animals lacking function in specific synMuv B genes (Petrella et al., 2011). synMuv B genes are involved in regulation of chromatin structure and have no known effect on sensory perception. We have shown that *dyf-7* plays a role in L1 arrest, with an increased penetrance at high temperature (Figure 4.5).

In order to determine whether *dyf-7* acts in the same pathway as synMuv B members to regulate high temperature arrest, we assayed *dyf-7* with *lin-35*, a synMuv B gene involved in high temperature L1 arrest phenotype; *mes-6*, a suppressor of the synMuv B mutant L1 arrest; and *isw-1,* a suppressor of the synMuv B mutant L1 arrest phenotype (Petrella et al., 2011). If *dyf-7(m539); lin-35(RNAi)* animals have an additive

increase in the fraction of animals displaying L1 arrest as compared to either single mutant alone, we can conclude that *dyf-7* and *lin-35* act in parallel pathways to regulate L1 arrest. However, if the percentage of arrested L1 animals in the *dyf-7(m539); lin-35(RNAi)* population masks the phenotypic effects of loss of *dyf-7* or *lin-35*, we can infer that these regulators of L1 arrest are acting in the same pathway. Knockdown of either *mes-6* or *isw-1* by RNAi inhibits high temperature arrest in *lin-35* defective animals (Petrella et al., 2011). If knockdown of either *mes-6* or *isw-1* synMuv B mutant suppressor in *dyf-7(m539)* mutant animals results in suppression of the L1 arrest phenotype, we can conclude that *dyf-7* acts in the same pathway as synMuv B genes to regulate L1 diapause at high temperature (or alternatively the two pathways are regulated in a similar manner). However, if *dyf-7(m539); mes-6(RNAi)* or *dyf-7(m539); isw-1(RNAi)* animals display a high temperature arrest phenotype similar to that of *dyf-7(m539)*, then we can conclude that *dyf-7* acts in an independent manner to regulate high temperature L1 arrest.

For these studies, we took advantage of the *rrf-3(pk1426)* mutation, which has been shown to make animals more susceptible to RNAi (Simmer *et al*., 2002). In a wild-type (*rrf-3(pk1426)* fed the pseudogene*)* population, a small fraction of the population undergo high temperature arrest (Figure 4.6). As expected, *rrf-3(pk1426); dyf-7(m539)* mutants displayed a higher fraction of animals in L1 arrest at high temperature as compared to *rrf-3(pk1426)* RNAi-sensitized control animals (Figure 4.6). Similar to previous studies, RNAi of the synMuv B gene *lin-35* had no apparent effect on high temperature arrest in an *rrf-3(pk1426)* background (Figure 4.6) (Petrella et al., 2011).

We found an additive effect on the L1 high temperature arrest phenotype by *lin-35(RNAi)* in *rrf-3(pk1426); dyf-7(m539)* animals (Figure 4.6). As RNAi of *isw-1* and *mes-6* inhibit the high temperature arrest phenotype of a *lin-35* genetic mutant (Petrella et al., 2011), we examined whether RNAi of *isw-1* and *mes-6* inhibit the high temperature arrest phenotype of a *dyf-7* genetic mutant. RNAi of *isw*-1 or *mes-6* failed to inhibit high temperature arrest in *rrf-3(pk1426); dyf-7(m539)* mutant animals (Figure 4.6). Further, the additive effect of *lin-35(RNAi)* in *rrf-3(pk1426); dyf-7(m539)* animals was abolished in these animals when RNAi of *mes-6* or *isw-1* was additionally applied (Figure 4.6). We conclude that RNAi of *lin-35* incompletely removes LIN-35 and the threshold to arrest in L1 is not breached, but animals with loss of DYF-7 display a more sensitized background for L1 arrest, revealing the effect of *lin-35(RNAi)* on L1 arrest. Based on these results, we conclude *dyf-7* regulates high temperature arrest independently of the synMuv B members.

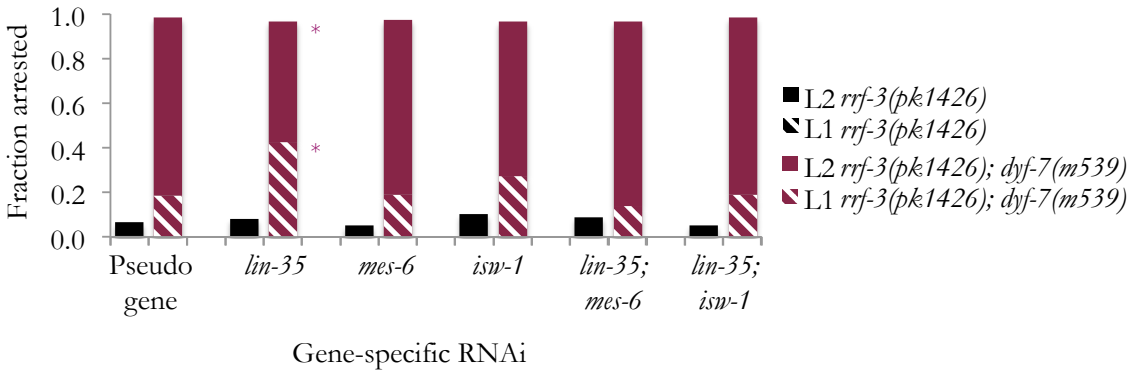

Figure 4.6 DYF-7 regulates L1 arrest independent of synMuv B members. The fraction of RNAi-treated animals at L1 or L2 was measured. P-values compare data to *rrf-3(-); dyf-7(-)* (fed pseudo gene) (*P≤0.05) using the unpaired t-test.

DYF-7 is required for sensing dauer entry cues

Perception of environmental cues is crucial at specific points during larval development. One of those critical points is at the transition to the second larval stage. If the animal senses that the environment is favorable enough for larval survival but not reproductive fitness, it enters an alternative, environment-resistant stage called dauer ("enduring" in German) (Hu, 2007). Unlike animals in L1 arrest, which display no morphological modifications, dauer animals survive harsh environmental conditions by altering their anatomy and physiology. Environmental conditions including food supply, temperature, and population density contribute to the decision to enter dauer (Golden and Riddle, 1984). Both extrinsic and intrinsic cues mediate pathways that regulate dauer formation. Key regulators that mediate dauer developmental are neural signaling (Vowels and Thomas, 1992) and hormone signaling pathways, including Transforming

Growth Factor-β (TGF-β), insulin, and guanylyl cyclase signaling (Birnby et al., 2000; Kimura et al., 1997; Ren et al., 1996). Mutations in dauer development genes can cause animals to inappropriately and constitutively enter the dauer state under non-inducing conditions (dauer constitutive) or to fail to enter the dauer state under inducing conditions (dauer defective). Sensory perception mutant animals are typically dauer defective because they fail to sense environmental stimuli that signal for an animal to enter the dauer pathway (Starich et al., 1995).

Environmental cues are transformed into neuroendocrine signals by environmentally exposed neurons in the head. Signaling from hormonal pathways act to regulate dauer formation by inhibiting dauer development under favorable conditions. When environmental conditions are favorable, the DAF-7 TGF-β ligand is produced in ASI amphid neurons and acts on the DAF-1 type I, and DAF-4 type II receptors, allowing the animal to continue with reproductive development. However, if cues indicate an unfavorable environment, DAF-7 is no longer produced and, in the lack of DAF-7 pathway signaling, the animal will arrest in dauer (Gumienny and Savage-Dunn, 2013).

To determine how *dyf-7* affects dauer development, we analyzed the genetic relationship between *dyf-7* and the DAF-7 type I receptor gene *daf-1*. Wild-type or dauer defective *dyf-7(m539)* animals do not enter dauer at 15°C to 25°C in the presence of food (Figure 4.7), while dauer constitutive *daf-1(m40)* temperature sensitive mutants enter dauer with increased penetrance at higher temperature.

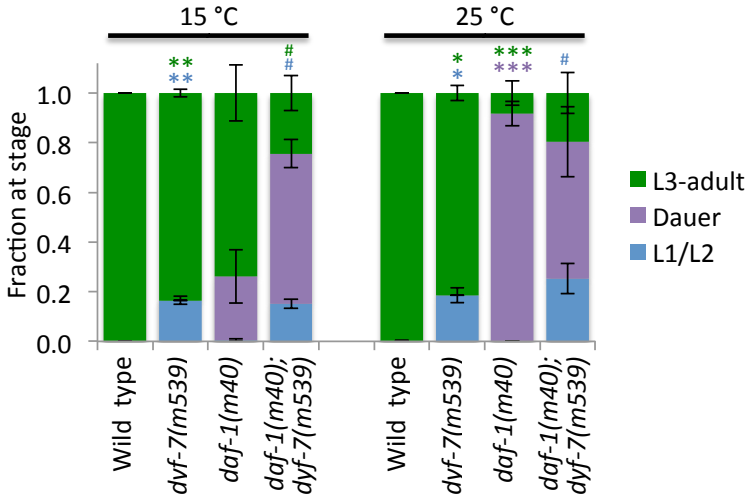

Figure 4.7 *dyf-7* requires *daf-1* activity to prevent dauer development. Mean incidence of dauer arrest at 15 and 25°C. Error bars indicate the mean ± SEM. P-values compare data to wild type (***P≤0.0001; **P≤0.001; *P≤0.05) or *daf-1(m40)* (#P≤0.05) using the unpaired t-test.

At the 15°C permissive temperature, the incidence of dauer formation is increased in *daf-1(m40)* mutant animals lacking *dyf-7* function as compared to *daf-1(m40)* single mutants (Figure 4.7). At the 25°C restrictive temperature, the rate of dauer formation in double mutant animals is less than that of the *daf-1(m40)* mutant animals (Figure 4.7). However, this result is compounded by the high incidence of L1 arrest in strains carrying the *dyf-7* mutant background, where this high incidence of arrested L1 animals is maintained in *dyf-7(m539)* mutant animals that are defective in *daf-1* signaling (Figure 4.7). The high incidence of L1/L2 animals indicates that a significant portion of the population failed to progress to the dauer stage of development, and therefore potentially causes the fraction of the population that could arrest in dauer

development to be underestimated. These results show that the dauer constitutive phenotype of *daf-1(m40)* mutants at the permissive temperature is enhanced by loss of anchoring in amphid neurons due to loss of *dyf-7* function. We therefore conclude that *dyf-7* requires *daf-1* signaling to prevent dauer arrest and continue with reproductive development.

DYF-7 is required for recovery from dauer arrest

Despite being resistant to the external insults of detergents, dehydration, low oxygen, and some of the internal insults of aging, animals in the dauer stage are still highly sensitive to changes in their environment that signal them to resume reproductive development and exit dauer. While dauer entry has been widely studied, little is known about dauer maintenance and recovery (Ouellet et al., 2008).

Examination of a GFP-tagged DYF-7 transcriptional fusion indicates that *dyf-7* is expressed in environmentally exposed neurons, including the ASJ, which is involved in dauer recovery (Figure 4.1B-C) (Bargmann and Horvitz, 1991). Because animals lacking functional *dyf-7* do not enter dauer, the effect of *dyf-7* on dauer exit has not been measured.

To examine *dyf-7*'s role in this environmental response, we examined *dyf-7* mutant dauers induced by high temperature, eliminating any confounding results of a background dauer constitutive mutation. For this assay, we induced dauer formation at 27°C and then allow the dauered animals to recover at 20°C over time. We found that at day 3, all wild-type dauers had recovered and resumed reproductive development

(Figure 4.8). However, 8% of *dyf-7(m537)* and 23% of *dyf-7(m539)* dauers had failed to recover (Figure 4.8). Even after 14 days, 1% of *dyf-7(m537)* and 8% of *dyf-7(m539)* dauers failed to properly sense environmental cues and remained arrested (Figure 4.8). Based on these results, we conclude that *dyf-7* is critical for progression from dauer arrest.

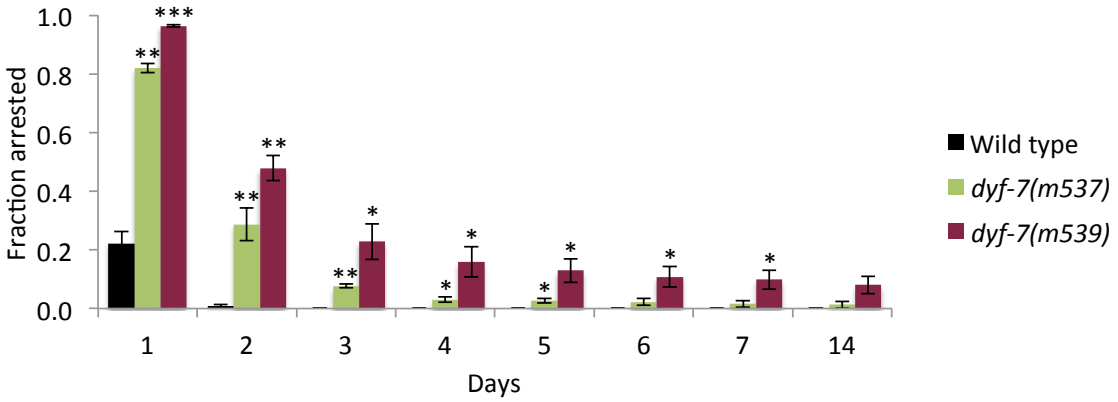

Figure 4.8 DYF-7 is required for dauer recovery. Mean number of animals recovered from dauer. Recovery was measured for as many as 14 days. Error bars indicate the mean ± SEM. P-values compare data to wild type (***P≤0.0001; **P≤0.001; *P≤0.05) using the unpaired t-test.

DYF-7 is required for proper roaming behavior and sensing food

Mature *C. elegans* animals continue to sample and respond to environmental cues. Adult behaviors that require proper environmental perception include locomotory and food-searching behavior. *C. elegans* exhibits characteristic behaviors on standard food, including roaming (rapid, longer distance movements) and dwelling (shorter

distance movements punctuated by frequent reversals and turns). Wild-type animals typically roam 25% of the time and dwell 75% of the time when on standard food (Fujiwara et al., 2002).

dyf-7 mutant animals are severely sensory deprived and, as we and others have shown, display a plethora of environmental sensing defects. We found that *dyf-7* mutant animals are much less active than wild-type animals (Figure 4.9). After an overnight incubation, *dyf-7(m537)* and *dyf-7(m539)* animals only covered 42% and 16% respectively of the area wild-type animals covered (Figure 4.9). We also found a large fraction of *dyf-7* mutants failed to recognize food cues. While only 8% of wild-type animals crawled off the plate over a period of six days, 92% of the more active *dyf-7(m537*) and 58% of the less active *dyf-7(m539)* populations failed to recognize chemosensory food cues and crawled off the plate. These results suggest DYF-7, by altering the ability to sense an area with desirable environmental conditions such as the presence of food, affects the locomotion activity in which an animal engages.

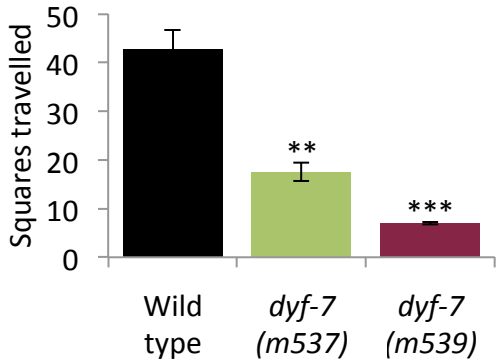

Figure 4.9 *dyf-7* mutants display roaming defects. The average number of squares an animal crawled into after an 18-hour incubation was used to measure activity in wild-type and *dyf-7* mutant animals. Error bars indicate the mean ± SEM. P-values compare data to wild type (***P≤0.0001; **P≤0.001) using the unpaired t-test.

DYF-7 does not influence light touch response.

Because *dyf-7(m539)* mutant animals are profoundly sensory deprived, we wondered if these animals would have any difficulty in perceiving gentle mechanical stimuli. Light touch response is received by non-ciliated neurons. We found that *dyf-7(m539)* mutant animals displayed a wild-type light touch response (Table 4.1). These results indicate that while *dyf-7* mutant animals are severely unaware of environmental stimuli, they have wild-type perception of mechanical stimuli.

Table 4.1 DYF-7 does not affect light touch response.

Genotype	WT light touch response
Wild type	100%
dyf-7(m539)	98%

Discussion

We have shown that the ZP-domain containing protein DYF-7 is required embryonically and post-embryonically to regulate multiple processes, including maintenance and organization of cell contacts in epithelia and perception of environmental cues. We found DYF-7 is expressed in neurons and neuronal support cells as well as the pharyngeal epithelia. We further show that DYF-7 localizes to epithelial apical and basal extracellular matrix, where DYF-7 appears to form a filamentous matrix within the basement membrane. Supporting a role for DYF-7 in epithelial cell adhesion, DYF-7 is important for proper maintenance of hypodermal cell contacts in the head and the tail. Further, DYF-7 is required for proper organization of apical adhesion complexes in pharyngeal epithelial cells. The animal's requirement for DYF-7 function in regulating epidermal cell adhesion continues throughout larval development and adulthood, as animals lacking DYF-7 display a low penetrance split tail phenotype at L1, but the Vab phenotype, which usually is restored to wild type at the L2 molt in other Vab backgrounds, is displayed even in adults. While DYF-7 is required for extension of multiple sensory neurons, we have shown that loss of DYF-7 results in a spectrum of sensory defects more profound than has been described for any other nematode

ciliopathy to date. Loss of perception of environmental cues in *dyf-7* mutant animals affects L1 and dauer diapauses and recovery from these developmentally arrested stages. We have shown *dyf-7* plays a role in regulating L1 arrest under normal growing conditions, with an increasing importance at high temperature. L1 arrest is a perduring state without functional DYF-7 even in the absence of harsh environmental cues, indicating loss of DYF-7 mimics a physiological stressed condition even in the presence of food. Loss of DYF-7 function also increases dauer formation in animals lacking DAF-7 pathway signaling, indicating DYF-7 acts upstream of DAF-7 signaling in dauer response. Consistent with DYF-7's expression from multiple neurons within the anterior ganglion, including the dauer recovery neuron, ASJ, DYF-7 is required for proper exit from developmental arrest in L1 or dauer.

Mechanisms of epithelial adhesion are often found to also establish dendrite shape (McLachlan and Heiman, 2013). Consistent with this idea of shared machineries, we show DYF-7, previously shown to establish dendrite shape, plays a broader, heretofore unappreciated, role in epithelial cell adhesion. Misregulation of DYF-7-mediated adhesion affects a variety of developmental processes ranging from proper epithelial cell morphology, organization of epithelial adhesion complexes, perception of environmental cues, and recovery from developmental arrest. These studies expand our understanding of the role of a ZP protein in adhesion and how its loss, though not lethal, can result in a spectrum of consequences.

5. ZONA PELLUCIDA-DOMAIN PROTEIN DYF-7 ORGANIZES EXTRACELLULAR MATRIX IN *C. elegans*

Introduction

Body size determination is a process that is precisely controlled by regulating either cell size and/or cell number. Body height in mammals is precisely controlled by multiple molecular mechanisms, including bone morphogenetic protein (BMP), insulin, and hormone signaling, which in turn control cellular processes, including cell size, long bone growth, and response to environmental cues including nutritional status (Le Goff and Cormier-Daire, 2012; Visser et al., 2009). Some of these factors also govern body size regulation in *C. elegans*. As *C. elegans* has an invariant cell lineage, the factors that determine body size are strictly regulated by cell size, not cell number (Sulston and Horvitz, 1977). The three most relevant of these mechanisms affecting body size include BMP signaling, environmental sensation, and cuticular organization.

The best studied of these body size regulators is BMP signaling, which belongs to the transforming growth factor-β (TGF-β) superfamily of proteins. The invariant, transparent *C. elegans* has conserved BMP pathways and well-developed genetic tools for studying BMP trafficking. Analyses of BMP signaling in vertebrates is often complicated by either a critical early requirement for BMP or redundancy in function among the 30+ TGF-β family members (Wu and Hill, 2009). In comparison, *C. elegans* has only five TGF-β ligands with non-redundant, non-lethal functions (Gumienny and Savage-Dunn, 2013). One BMP is DBL-1, a dose dependent regulator of body size

where animals with increased signaling display a long body length and animals with decreased signaling display a small body length, providing a sensitive *in vivo* readout of ligand activity. Extracellular proteins are involved in regulation of the *dbl-1* pathway, including LON-2, a negative regulator of DBL-1 signaling (Gumienny et al., 2007). The DBL-1 ligand acts on the DAF-4 type II and the SMA-6 type I receptor complex. The receptors then act on receptor Smads, SMA-2 and SMA-3, which complex with the co-SMAD, SMA-4. The SMAD complex can then translocate into the nucleus to regulate expression of genes involved in body size determination (Krishna et al., 1999; Morita et al., 1999).

Genetic analyses have mapped a pathway for body size regulation where EGL-4, a cGMP dependent protein kinase, acts downstream of sensory perception genes (Fujiwara et al., 2002) and upstream of DBL-1 BMP signaling to control body size development (Fujiwara et al., 2002; Hirose et al., 2003). *egl-4* promotes a reduced body size through inhibition of the DBL-1 BMP pathway (Fujiwara et al., 2002; Hirose et al., 2003), where loss-of-function mutations in *egl-4* produce an animal with a large body size (Daniels et al., 2000) and gain-of-function mutations result in an animal that is smaller than wild-type (Raizen et al., 2006).

Another mechanism of regulation of *C. elegans* body size development is through environmental sensation. Animals that cannot sense their environment are typically smaller than wild type (Fujiwara et al., 2002). While the role of sensory perception genes in body size regulation is not well understood, studies have shown that while these animals cannot properly sense their environment, the small body size of

these mutant animals is not caused by an inability of locate food (Fujiwara et al., 2002). These results suggest that sensory perception may regulate neuroendocrine function to determine body size. Epistasis analyses have collectively placed genes involved in sensory perception upstream of *egl-4* and *dbl-1* BMP signaling (Fujiwara et al., 2002).

C. elegans body shape can also be influenced through organization of the cuticle. The cuticle is a secreted extracellular matrix comparable to bone, which serves as an exoskeleton, provides protection from and interaction with the environment, and allows the animal to move (Kramer et al., 1988; Page and Johnstone, 2007). Genes involved in cuticular organization influence body shape by affecting the structure of the cuticle (Fernando et al., 2011; Sapio et al., 2005). The cuticle, which is secreted by underlying hypodermal tissue, is composed of multiple layers, which can be distinguished using transmission electron microscopy techniques. The composition of the cuticle includes primarily collagens and various heavily cross-linked collagen-like proteins called cuticulins (Cox et al., 1981a).

As our understanding of the various modes of body size regulation deepen, we realize that there is extensive overlap in many of the mechanisms that govern body size. BMP signaling in mammals and *C. elegans* has been shown to regulate extracellular matrix organization (Brazil et al., 2015; Schultz et al., 2014). In *C. elegans* defects in body length as well as permeability in BMP variants are associated with changes in composition and organization of the cuticle (Schultz et al., 2014). Further, the ADAMTS-like protease ADT-2*,* a positive regulator of DBL-1 BMP pathway signaling

is also involved in modification of the cuticle. Animals lacking *adt-2* function display defects in annuli organization and are small (Fernando et al., 2011).

In this paper, we describe the role of a protein belonging to the zona pellucida-domain (ZP-domain) family of proteins, in regulation of body size. Founding members of the ZP family have been shown to play a role in composition and function of another secreted extracellular matrix, the zona pellucida (Wassarman, 1988). The ZP-domain is a polymerization motif that allows self-assembly of these extracellular proteins into fibrils and even matrices (Bork and Sander, 1992). ZP-domain protein functions are diverse, ranging from organization of extracellular matrices, establishment of cell shape, and sensory perception (Bokel et al., 2005; Plaza et al., 2010). ZP-proteins are often expressed in epithelial cells, where they are involved in organization of apical extracellular matrix structures (Plaza et al., 2010). In *C. elegans*, the ZP-protein DYF-7 is critical for establishing shape and adherence of neurons involved in sensory perception during embryonic development (Heiman and Shaham, 2009). DYF-7 plays a role in body size development and drug response, as *dyf-7* mutant animals are small and resistant to ivermectin, through unknown mechanisms (Starich et al., 1995; Urdaneta-Marquez et al., 2014).

We show that DYF-7 is required for proper body length and *dyf-7* mutant animals only display defects in body size post-embryonically. Loss of *dyf-7* affects permeability to exogenously supplied drugs and dye, indicating permeability of the cuticle is altered in *dyf-7* mutants. We show that by genetically reducing cross-linkages within the cuticle, permeability of the cuticle is restored, potentially indicating a role for

DYF-7 in organization of cross-linkages. We found cuticular structures are less regular and organized in animals deficient in DYF-7, suggesting DYF-7 is critical for proper organization of the cuticle. Finally, we show *dyf-7* acts partially independent of *egl-4* and *dbl-1* pathway signaling to regulate body size, suggesting *dyf-7* and *dbl-1* are partially dependent on one another for establishing body length. Consistent with this idea, we found *dyf-7* positively affects *dbl-1* pathway transcriptional activity. Our findings reveal a critical role for DYF-7 in regulating organization of the cuticle, showing a conserved role for a ZP protein in regulating extracellular matrix in *C. elegans*.

Materials and methods

Strains and maintenance

C. elegans strains used in these studies were derived from the wild-type variety Bristol strain N2 and were cultured on nematode growth media (NGM) plates as previously described (Brenner, 1974). All strains were cultured on *E. coli* strain OP50 at 20˚C, except where noted. Strains used include:

N2, LT186 *sma-6(wk7)* II, TLG384 *sma-6(wk7)* II*; dyf-7(m539)* X, DA521 *egl-4(ad450)* IV, MT1073 *egl-4(n478)* IV, TLG182 *texIs100 [dbl-1p::dbl-1:gfp + ttx-3p::rpf]* IV (referred to as *dbl-1(++)* in this paper), TLG361 *texIs100 [dbl-1p::dbl-1:gfp + ttx-3p::rpf]* IV; *dyf-7(m539)* X, TLG436 *egl-4(ad450)* IV*; dyf-7(m539)* X, TLG459 *egl-4(n478)* IV*; dyf-7(m539)* X, CHB84 *oyIs44 [odrp::rfp + lin-15(+)]* V; *dyf-7(ns88)* X, CHB91 *oyIs44 [odrp::rfp + lin-15(+)]* V; *dyf-7(ns116)* X, CHB94 *oyIs44 [odrp::rfp*

+ lin-15(+)] V; *dyf-7(ns120)* X, CHB95 *oyIs44 [odrp::rfp + lin-15(+)]* V; *dyf-7(ns119)* X, CL261 *him-5(e1940)* V; *srf-5(ct115)* X, LT121 *dbl-1(wk70)* V, NU3 *dbl-1(nk3)* V, TLG119 *dbl-1(wk70)* V*; dyf-7(m539)* X, TLG383 *dbl-1(nk3)* V*; dyf-7(m539)* X, CB678 *lon-2(e678)* X, SP1196 *dyf-7(m539)* X, SP1735 *dyf-7(m537)* X, TLG112 *dyf-7(m539)* X; *lon-2(e678)* X, TLG331 *dyf-7(m537)* X; *texEx202 [sma-6p::sma-6:mCherry + ttx-3p::gfp]*, TLG381 *dyf-7(m539)* X; *kaIs12 [col-19p::col-19:gfp],* TLG443 *dyf-7(m539)* X; *wkEx52 [spp-9p::gfp],* TLG445 *dyf-7(m539)* X; *texEx304[dyf-7p::dyf-7:gfp + ttx-3p::rfp]*, TLG446 *dyf-7(m539)* X; *texEx305[dyf-7p::dyf-7:gfp + ttx-3p::rfp]*, TLG473 *dyf-7(m537)* X; *texEx318[dyf-7p::dyf-7:gfp + ttx-3p::rfp]*, TLG474 *dyf-7(m537)* X; *texEx319[dyf-7p::dyf-7:gfp + ttx-3p::rfp]*, TP12 *kaIs12 [col-19p::col-19:gfp]*, LT620 *wkEx52 [spp-9p::gfp],* and TLG316 *texEx202 [sma-6p::sma-6:mCherry + ttx-3p::gfp]* (referred to as *sma-6(++)* in this paper).

Body length measurements

Body measurements of animals were performed as previously described (Taneja-Bageshwar and Gumienny, 2012). Specifically, about 30 staged young adult animals were transferred to 2% agar pads on glass slides and were imaged when moving forward at 60x magnification using iVision-Mac™ software (BioVision Technologies, Exton, PA) and a Retiga-2000R CCD camera (QImaging Corporation, Surrey, BC, Canada) mounted on a Nikon SMZ1500 dissecting microscope (Nikon Instruments, Inc., Melville, NY). Body size for the *dyf-7* rescue experiments were performed at 48 hours after L4 and epistasis analyses were performed at 16 hours after L4.

Lengths of animals were determined using the length measurement image tool within iVision-Mac™ software (BioVision Technologies, Exton, PA). Average body length values of strain populations were converted to percent wild-type average body lengths using staged wild-type control populations that were imaged the same day as the experimental strain(s). 95% confidence intervals were calculated using Prism (GraphPad Software, Inc., La Jolla, CA). P-values (using the unpaired t-test) were determined using Excel (Microsoft Corporation, Redmond, WA).

Growth curve measurements

Body lengths were measured and imaged as described above except animals were staged at 0, 24, 48, 72, and 96 hours after L1 arrest.

Brood size analysis

L4 animals were moved to individual 60 mm seeded NGM agar plates and the number of viable progeny was counted daily for 4 days total. 60 mm plates were used to prevent matricide and only animals that had not crawled off the plate and were still alive at the end of the four-day period were assayed for progeny number. At least 20 animals for each genotype were assayed.

Drug sensitivity assays

Sensitivity to drugs was assayed as previous described (Gottschalk et al., 2005). Briefly, about 40 staged young adult animals were transferred to NGM plates containing

1 mM levamisole HCl, 31 mM nicotine, or 1 mM sodium azide. For standard drug sensitivity assays, the number of animals moving was scored by visual inspection every 15 minutes and was defined as response (movement) to prodding. At least three independent trials were performed and the results were pooled, with at least 116 animals total for each genotype at each time point. The average fraction of animals moving, standard error of the mean (SEM), and p-values (using the unpaired t-test) were determined using Excel (Microsoft Corporation, Redmond, WA).

RNA interference

RNA interference (RNAi) was performed as previously described (Beifuss and Gumienny, 2012), with the exception that generations of animals were continuously grown on IPTG-containing NGM plates that were seeded with bacteria expressing gene-specific double stranded RNA. Briefly, single colonies of HT115 bacteria containing relevant plasmids (Thermo Fisher Scientific, Waltham, MA) were selected, isolated, and grown overnight in carbenicillin, then induced for 4 to 5 hours with IPTG to express double stranded RNA from the plasmid. Each bacterial growth was spotted onto NGM plates containing carbenicillin and IPTG and dried. Animals were then transferred to and continuously cultured on NGM plates seeded with RNAi bacterial lawns at 15°C for use in the drug sensitivity assays. Drug sensitivity scoring was performed as described above.

Hoechst 33342 staining and quantification

To provide more consistent staining, L3 animals were staged by allowing gravid adults to lay embryos for about 16 hours on a plate. These animals that had never been starved or bleached were then washed in M9 buffer three times to remove residual bacteria. Next, animals were stained with the cuticle impermeable dye, Hoechst 33342 (2'-[4-ethoxyphenyl]-5-[4-methyl-1-piperazinyl]-2,5'-bi-1H-benzimidazole trihydrochloride trihydrate, Life Technologies, Grand Island, NY) by microwave irradiation treatment. Using the PELCO BioWave® microwave (Ted Pella, Redding, CA), live animals were stained by microwaving at 20°C with intermittent vacuum at 250 watts (W) for a 12-minute cycle (5 minutes on, 2 minutes off, 5 minutes on) in 1 μg/ml Hoechst 33342 in M9 buffer. Prior to imaging, animals were washed four times in M9 buffer. Imaging was performed as described below.

The number of animals displaying fluorescently stained hypodermal nuclei was scored by visual inspection. Three independent trials were performed and the results were pooled, with at least 390 animals per trial for each genotype. The average fraction of stained animals, SEM, and p-values (using the unpaired t-test) were determined using Excel (Microsoft Corporation, Redmond, WA).

Cuticular structure staining

The cuticle of staged adult animals was stained with DiI (1,1'-dioctadecyl-3,3,3',3'-tetramethylindocarbocyanine perchlorate, Biotium Inc., Hayward, CA) as previously described (Schultz and Gumienny, 2012). Specifically, staged young adult

animals were washed once with M9 buffer with 0.5% (vol/vol) Triton X-100, then two times in M9 buffer. Next, animals were stained in 30 μg/ml DiI in M9 for approximately three hours while shaking at high speed at 20°C. Prior to imaging, animals were washed in M9 buffer to remove residual DiI. Confocal imaging was performed as described below.

Wheat germ agglutinin staining

Lectin staining was performed as previous described (Link et al., 1988). Briefly, populations of staged adult animals were washed three times in M9 buffer to remove any residual bacteria. To further remove any residual bacteria from the cuticular surface, animals were incubated in M9 buffer for an hour while gently shaking at 20°C. Animals were then stained in 200 μg/ml rhodamine-conjugated wheat germ agglutinin (WGA) (Vector Laboratories, Inc., Burlingame, CA) in M9 buffer for one hour while gently shaking at 20°C. Prior to imaging, animals were washed four times in M9 buffer. Imaging was performed as described below.

Microscopy and imaging

For spinning disk and confocal microscopy, animals were immobilized in 2.5% (wt/vol) 0.1 μm diameter polystyrene beads (00876-15, Polysciences Inc., Warrington, PA) in 1 mM levamisole on 10% agarose pads (Fang-Yen et al., 2012). Spinning disk images were acquired on a Retiga-SRV CCD camera (Quantitative Imaging Corporation, Surrey, BC, Canada) mounted on a BD Carv II™ spinning disk confocal (BD

Biosystems, San Jose, CA) on a Zeiss A1 compound microscope base (Carl Zeiss, Inc., Jena, Germany). A 63x/1.4 NA oil Plan-Apochromat objective (Carl Zeiss, Inc., Jena, Germany) and iVision-Mac™ software (BioVision Technologies, Exton, PA) were used for image acquisition. Confocal images were acquired on a Nikon A1R confocal laser microscope system (Nikon Instruments, Inc., Melville, NY, USA) using a 40x/1.15 NA water CFI Apo Lambda S LWD objective (Nikon Instruments, Inc., Melville, NY, USA) and NIS-Elements C software (Nikon Instruments, Inc., Melville, NY, USA).

For scanning electron microscopy, adult animals were fixed with acrolein, then imaged at 7000x magnification using a Hitachi Tabletop TM3000 scanning electron microscope.

Results

Body length defects are specific to loss of dyf-7 function in dyf-7 mutant animals

Animals defective in *dyf-7* signaling are smaller than wild-type animals. When comparing the two canonical *dyf-7* mutant strains, *dyf-7(m539)* and *dyf-7(m537)* which contain an insertion within the N- or C-terminal portion of the ZP-domain respectively (Figure 5.1A), we found *dyf-7(m537)* and *dyf-7(m539)* animals are small, with *dyf-7(m539)* animals displaying a more severe phenotype than *dyf-7(m537)* animals (Figure 5.1B). In order to determine whether body size defects seen in *dyf-7* mutant animals are due to loss of *dyf-7* signaling, we measured body length in *dyf-7* mutant animals expressing GFP-tagged DYF-7. We found that GFP-tagged DYF-7 expression rescues body size defects in *dyf-7* mutant animals (Figure 5.1B). These results indicate that

mutations in the *dyf-7* gene are responsible for the body length defects observed in *dyf-7* mutant animals.

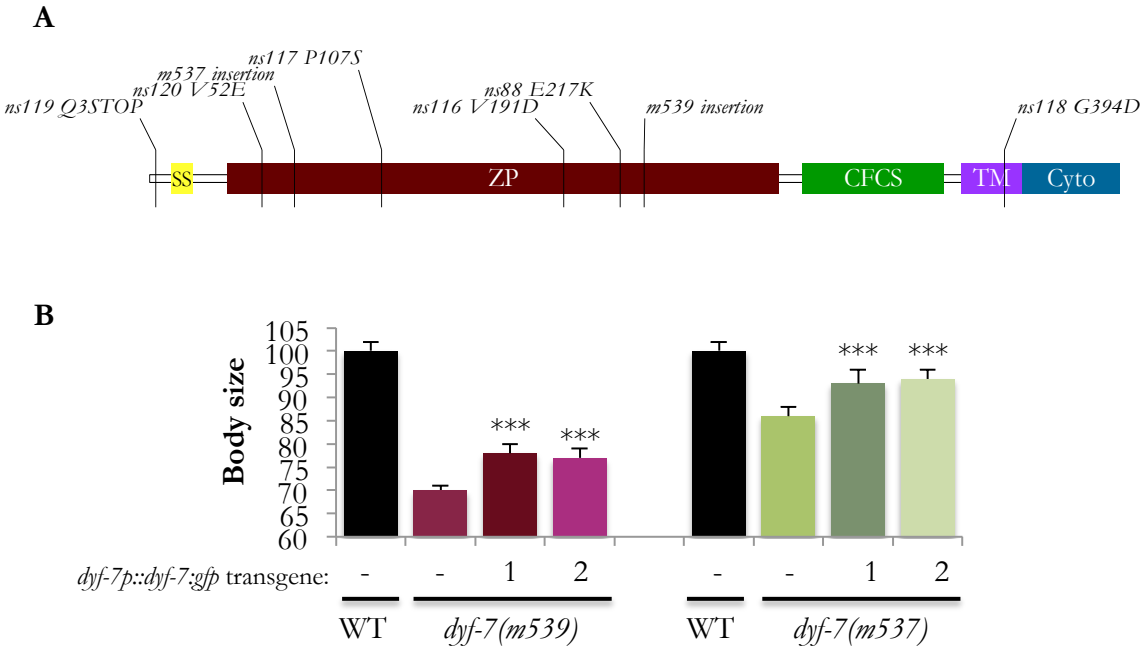

Figure 5.1 ZP-domain protein DYF-7 regulates body size development. (A) Schematic of DYF-7, a ZP-domain containing protein that contains an N-terminal signal sequence (SS), a conserved furin cleavage sequence (CFCS), transmembrane domain (TM), and a short cytoplasmic region (Cyto). The genetic mutation for each *dyf-7* allele is indicated. (B) Relative body lengths of wild type animals and *dyf-7* mutants with or without expression of a *dyf-7p::dyf-7:gfp* transgene. Two independent lines were measured in each *dyf-7* strain. Error bars indicate the mean ± the 95% confidence interval. P-values compare data to wild type (***P≤0.0001) using the unpaired t-test.

dyf-7 is required post-embryonically to regulate body size development

Regulators of body size in *C. elegans* have been shown to act through multiple mechanisms. For example, SMA-1, a β spectrin involved in embryonic elongation and cell adhesion, establishes body size during embryonic development (Praitis et al., 2005). The BMP DBL-1 pathway, which acts through cell signaling to regulate body size development, acts post-embryonically (Savage-Dunn et al., 2000). To characterize when *dyf-7* acts to regulate body size, we examined the length of *dyf-7* mutants throughout larval and adult development as compared to both wild-type animals and *dbl-1* mutants. We found that, similar to *dbl-1*, both *dyf-7* mutant strains exhibit a normal body size at hatching and only exhibited a smaller body size than wild type beginning at 24 hours after L1 arrest and continuing through adult development (Figure 5.2A). This growth curve analysis reveals that *dyf-7* is required post-embryonically to regulate body size.

dyf-7 is critical for normal brood size

Small body size is often correlated with decreased brood size (Knight et al., 2001; Roff, 2000). To determine the ability of *dyf-7* mutants to produce viable embryos, we counted the number of viable embryos that were laid over a period of four days. We found *dyf-7(m539)* and *dyf-7(m537)* mutant strains produced fewer progeny as compared to wild-type animals (Figure 5.2B). Consistent with the idea that reduced body size could act as a physical limitation to brood size, *dyf-7(m539)* animals display a smaller brood than *dyf-7(m537)* mutants (Figure 5.2B). These results indicate that DYF-7 is required for proper fecundity.

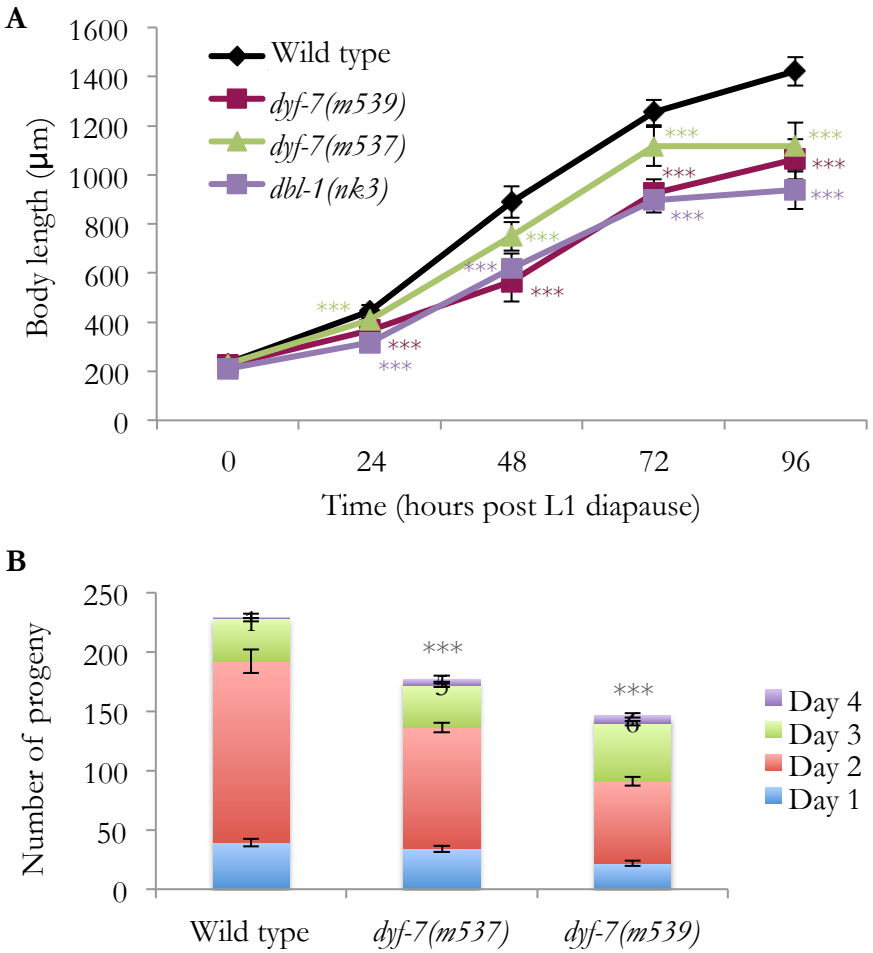

Figure 5.2 *dyf-7* is required for proper post-embryonic body length and brood size. (A) Body lengths of animals at L1 and continuing throughout adult development. Error bars indicate the mean ± the standard deviation. P-values compare data to wild type (***P≤0.0001) using the unpaired t-test. (B) Brood size was measured over a period of 4 days. Error bars indicate the mean ± SEM. P-values compare data to wild type (***P≤0.0001) using the unpaired t-test.

dyf-7 is required for normal cuticular permeability

Defects in *dyf-7* signaling confer resistance to ivermectin (Urdaneta-Marquez et al., 2014). Ivermectin belongs to the macrocyclic lactone family and acts as a nematode

anesthetic by inhibiting activity of neurons involved in locomotion (Wolstenholme and Rogers, 2005). We wondered if this drug resistance phenotype was specific to the anesthetic ivermectin or if *dyf-7* mutants displayed resistance to other drugs. To test this possibility, we measured drug sensitivity to multiple anesthetics with varied sizes and modes of action in *dyf-7* mutant strains. The first drug we tested was levamisole, a cholinergic agonist that acts as an anesthetic by causing hypercontraction of muscles (Almedom et al., 2009; Vashlishan et al., 2008). The fraction of wild-type animals that retain the ability to move decreases with time after being placed on levamisole (Figure 5.3A). We found *dyf-7(m539), dyf-7(ns119)*, and *dyf-7(ns120)* animals are resistant to paralyzing effects of levamisole, with *dyf-7(m539)* showing a striking level of resistance and *dyf-7(ns119)* and *dyf-7(ns120)* displaying a less severe phenotype (Figure 5.3A). Less severe *dyf-7* mutant strains displayed wild-type levels of sensitivity to levamisole (Figure 5.3A). Overexpression of a GFP-tagged DYF-7 restores levamisole sensitivity in *dyf-7(m539)* mutant animals (Figure 5.3A). Next, we quantitated response to another anesthetic, nicotine. While levamisole has a relative molecular mass (M_r) of $2.41x10^3$, the M_r of nicotine is lower, at $1.62x10^3$. Nicotine, similar to levamisole, is an acetylcholine agonist that causes hypercontracted paralysis. We found *dyf-7(m539)* animals were significantly resistant to the effects of nicotine and *dyf-7(m537)* animals displayed a mild resistance, while sensitivity in all other *dyf-7* mutant strains was similar to wild type (Figure 5.3B). Based on the results that *dyf-7(m539)* animals show a significant resistance to levamisole and nicotine, which have higher M_r values, we wondered how *dyf-7(m539)* animals would respond to another anesthetic, sodium azide,

which has a lower M_r of $0.065x10^3$. Sodium azide is thought to induce paralysis by inhibiting the electron transport chain (Duncan and Mackler, 1966; Herweijer et al., 1985; Van der Bend et al., 1985). We found sensitivity to this lower mass molecule was normal or mildly increased in *dyf-7(m539)* and *dyf-7(m537)* mutant animals (Figure 5.3C). Resistance to multiple drugs in animals with defective DYF-7 suggests DYF-7 regulates permeability of the diffusion barrier.

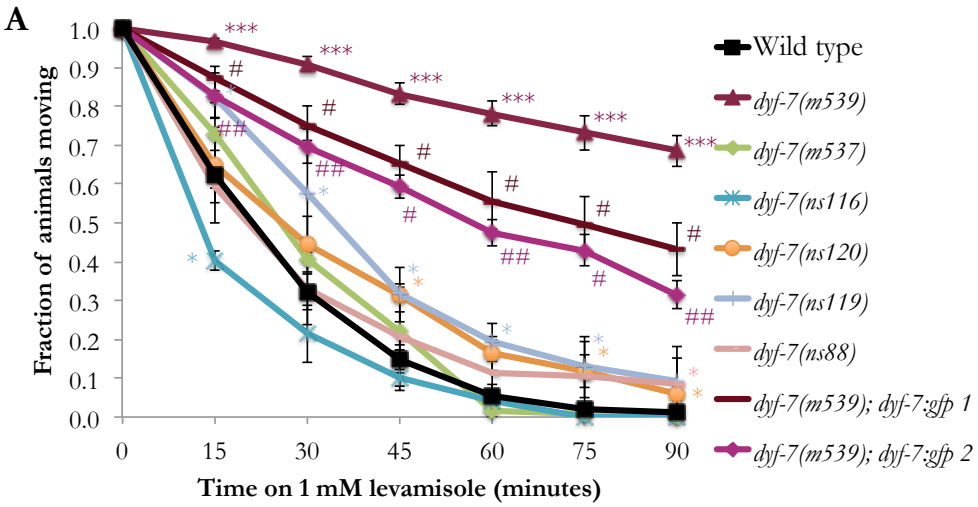

Figure 5.3 DYF-7 is required for normal permeability. Sensitivity to levamisole (A), nicotine (B), and sodium azide (C) was measured over time in wild-type and *dyf-7* mutant animals. Error bars indicate the mean ± SEM. P-values compare data to wild type (***P≤0.0001; **P≤0.001; *P≤0.05) or *dyf-7(m539)* (##P≤0.001; #P≤0.05) using the unpaired t-test.

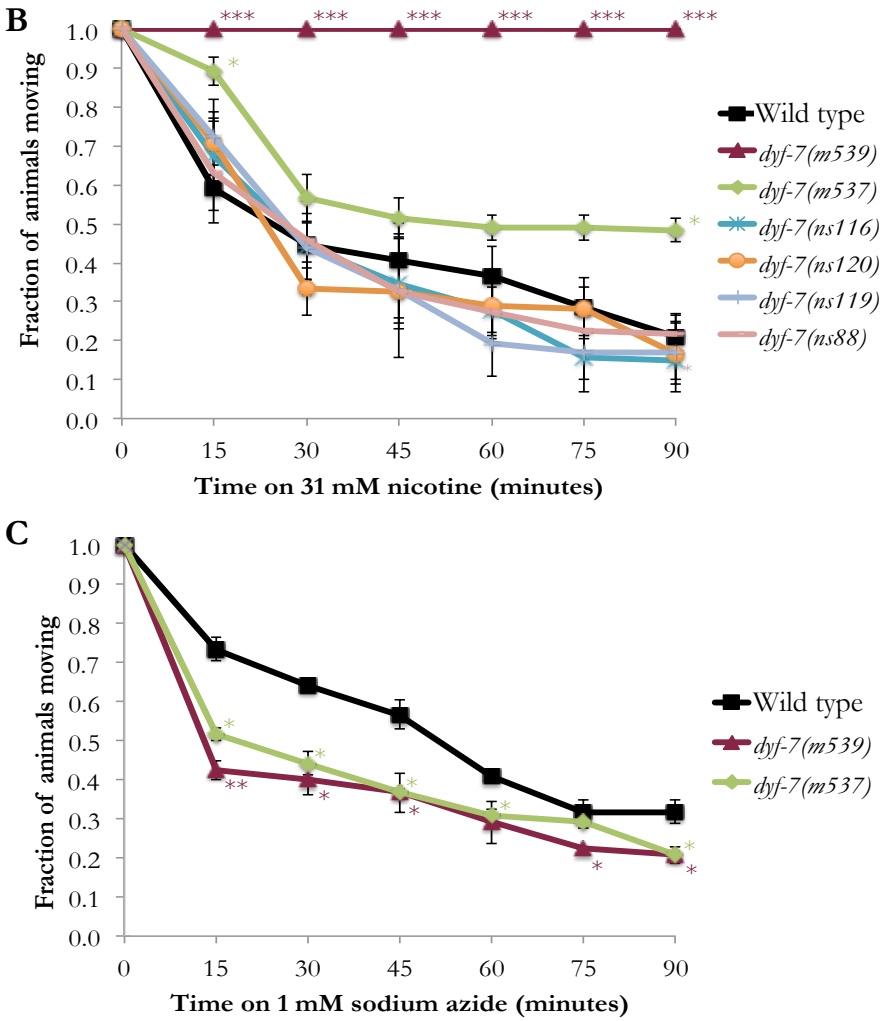

Figure 5.3 Continued.

The diffusion barrier in *C. elegans* is composed of two parts, the epidermal membrane and the cuticle. The ability of a molecule, including exogenous drugs or dyes, to cross this diffusion barrier is dependent on both molecule size and polarity (Ho et al., 1992; Ho et al., 1990; Ho et al., 1994; Moribe et al., 2004). To investigate if the altered drug response in *dyf-7* mutants is associated with defects in permeability of the cuticle,

we took advantage of *dpy-13*, a cuticle collagen involved in forming cross-linkages in the cuticle (von Mende et al., 1988). By reducing DPY-13 levels, we genetically increased the permeability of the cuticle and access of an environmentally supplied drug to reach its target (Rand and Johnson, 1995). If the altered drug sensitivity in *dyf-7(m539)* mutant animals is due to decreased cuticular permeability, reducing DPY-13 in the *dyf-7(m539)* background should establish a more wild-type response. We found that reduction of DPY-13 did not significantly affect levamisole sensitivity in wild-type animals (Figure 5.4A). However, DPY-13 knockdown in *dyf-7(m539)* animals restored drug sensitivity to more normal levels (Figure 5.4A). This result suggests that animals with loss of DYF-7 display defects in the barrier function of the cuticle, whereby further cuticle perturbation caused by loss of DPY-13 allows increased small molecule entry in DYF-7 mutants.

Another method to test permeability of the cuticle is to measure the ability of an environmentally supplied nuclear dye to transverse the cuticle and stain nuclei in the underlying epidermal tissue (Kage-Nakadai et al., 2010). Hoechst 33342, which has an M_r value of $0.616x10^3$, typically fails to transpass the cuticle in wild-type animals. Using a microwave procedure we developed to increase basal levels of Hoechst 33342 staining in live animals, we found 9% of wild-type animals stain, whereas only 4% or 2% of *dyf-7(m537)* or *dyf-7(m539)* stain respectively (Figure 5.4B). Similar to our findings for drug response, *dyf-7* mutant animals are less permeable and therefore more resistant to staining by exogenously supplied Hoechst 33342. Taken together these results suggest that DYF-7 is critical for normal cuticular permeability.

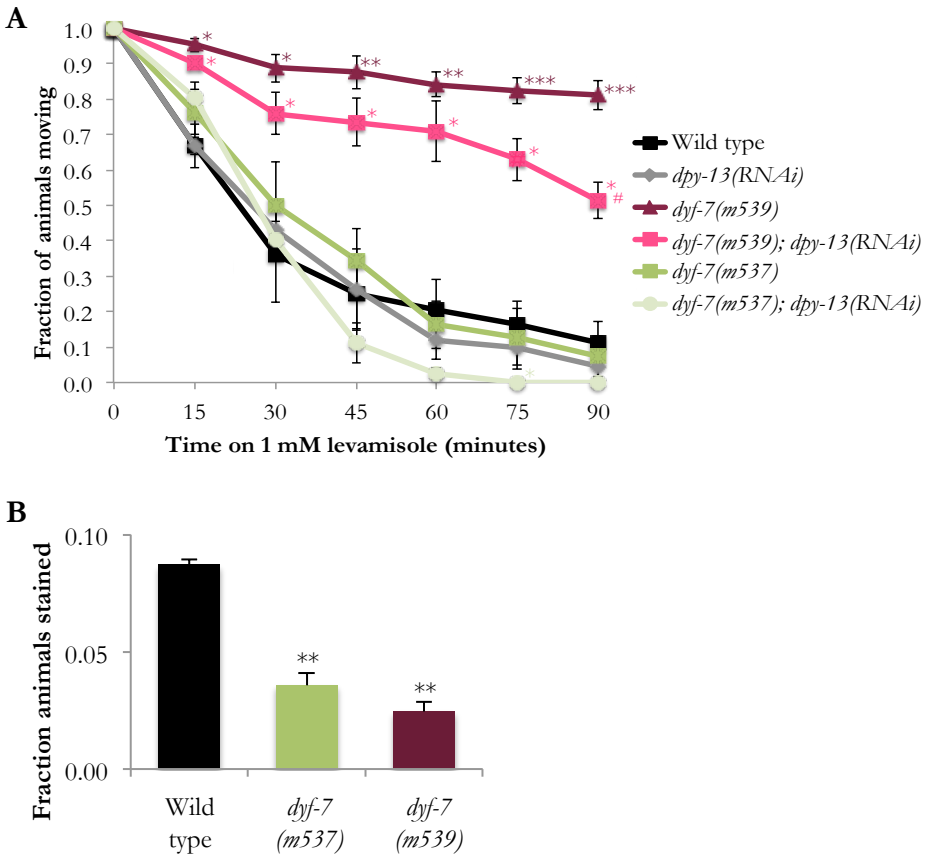

Figure 5.4 DYF-7 regulates cuticular permeability. (A) Sensitivity to levamisole in wild type or *dyf-7* animals treated with *C06C3.5* (pseudogene control) or *dpy-13* RNAi was measured over time. (B) The fraction of animals that stain with Hoechst 33342. Error bars indicate the mean ± SEM. P-values compare data to wild type (***P≤0.0001; **P≤0.001; *P≤0.05) or *dyf-7(m539)* (#P≤0.05) using the unpaired t-test.

DYF-7 is required for normal cuticular organization and shape

The cuticle is primarily composed of collagen and collagen-like proteins, called cuticulins. Genes involved in collagen organization can affect both the size and shape of the animal (Fernando et al., 2011; Sapio et al., 2005; von Mende et al., 1988). Disruption

of cuticular cuticulin components, including ZP-domain proteins CUT-1, CUT-3, and CUT-5, affects both body shape and alae formation (Sapio et al., 2005). As body length and cuticular permeability are affected in *dyf-7* mutants (Figures 5.1, 5.3-5.4), we reasoned that loss of *dyf-7* alters organization of cuticular structure. Adult animals are patterned by circumferential ridges called annuli and stage specific lateral ridges called alae (Cox et al., 1981b). Alar components are secreted by specialized epidermal cells called seam cells (Singh and Sulston, 1978), which we have shown express *dyf-7* (Figure 4.1A). To examine morphology of both alae and annuli, we stained the cuticle using the vital dye DiI to highlight cuticular structures and mild defects that are otherwise difficult to distinguish using standard DIC microscopy (see Appendix) (Schultz and Gumienny, 2012). In wild-type animals, alae are regular in appearance (Figure 5.5A). *dyf-7(m539)* adults display subtle differences in alar morphology, including fusions and bifurcations in these cuticular structures (Figure 5.5B). Scanning electron microscopy studies corroborate these results and reveal extranumerary alae (Figure 5.5C). Annuli are regular in spacing and appearance in wild type animals (Figure 5.5D). Annular structures in adult *dyf-7(m539)* mutant animals are irregular, containing fusions as well as bifurcations (Figure 5.5E). These results indicate DYF-7 is required for proper organization of cuticular structures.

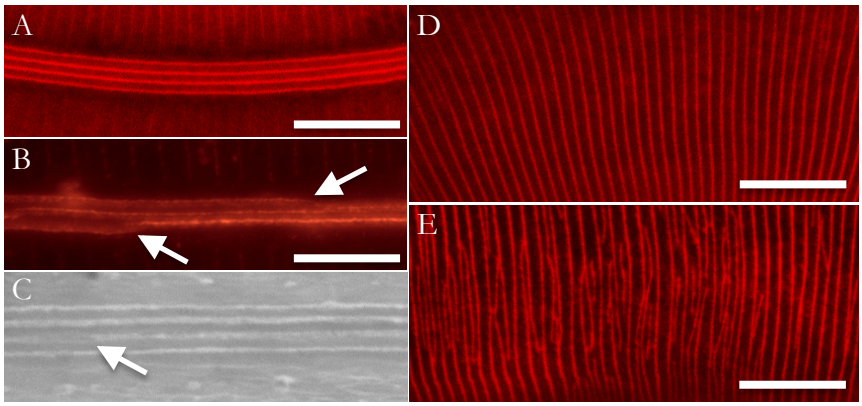

Figure 5.5 DYF-7 affects cuticular morphology. DiI stained alae in wild-type (A) and *dyf-7(m539)* (B) adult animals. SEM of alae in *dyf-7(m539)* adults (C). DiI stained annuli in wild-type (D) and *dyf-7(m539)* (E) adults. Scale bars = 10 μm.

The nematode cuticle is composed of multiple layers. The outmost layer is the surface coat, a negatively charged, glycoprotein rich non-structural component of the cuticle that overlies the epicuticle (Blaxter, 1993; Spiegel and McClure, 1995). The epicuticle is a non-structural component of the cuticle composed of lipids and glycolipids (Blaxter, 1993). The inner cuticular layers include the cortical, medial, and basal layers, which are composed of cuticulins and collagens (Cox et al., 1981a). To determine if composition of the cuticle is altered in *dyf-7* mutants, we examined the surface coat using wheat germ agglutinin (WGA), which binds glycoproteins on the cuticle's surface when surface antigenicity is altered (Link et al., 1988; Link et al., 1992; Natsuka et al., 2005). Wild-type and *dyf-7* mutant animals did not stain with WGA (Figure 5.6A-B), indicating proper surface antigenicity in *dyf-7* mutants. *srf-5* mutants stain with WGA, indicating the presence of abnormally exposed or accumulated glycans

(Natsuka et al., 2005) (Figure 5.6C). We next asked if depletion of DYF-7 in a *srf-5* mutant background would affect localization or accumulation of WGA-stained glycans. We found that knockdown of DYF-7 does not affect WGA staining in the *srf-5* mutant background (Figure 5.6D). These results show DYF-7 does not affect surface antigenicity.

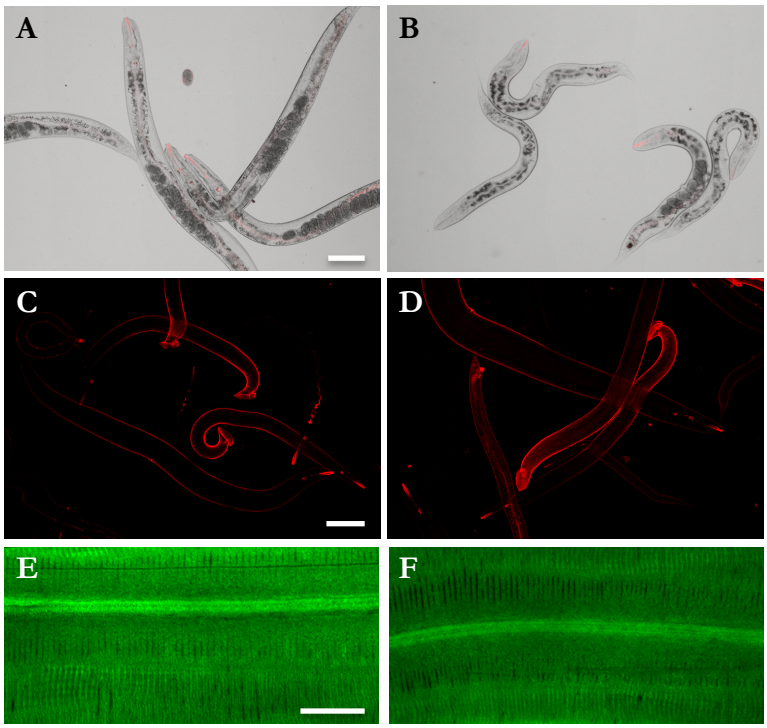

Figure 5.6 Loss of DYF-7 does not affect surface antigenicity and COL-19. (A-B) Rhodamine-conjugated wheat germ agglutinin (WGA) staining in wild-type (A) and *dyf-7(m539)* (B) populations. Scale bar = 100 μm. (C–D) WGA staining in *him-5(e1490); srf-5(ct115)* animals with *C06C3.5(RNAi)* (pseudogene control RNAi) (C) and *dyf-7(RNAi)* (D). Scale bar = 100 μm. (E–F) COL-19:GFP expression in otherwise wild-type animals with *C06C3.5(RNAi)* (pseudogene control RNAi) (E) and *dyf-7(RNAi)* (F). Scale bar = 10 μm.

As collagen is a major component of the cuticle, we asked if localization of the adult-specific cuticle collagen COL-19 would be altered in *dyf-7* mutants. We examined expression of COL-19:GFP, which localizes to the cortical layer of the cuticle (Liu *et al*., 1995; Thein *et al*., 2003). We found COL-19:GFP expression to be similar in wild-type and *dyf-7(RNAi)* backgrounds (Figure 5.6E-F). From these findings we conclude DYF-7 is not required for localization of COL-19 collagen.

dyf-7 requires egl-4 and dbl-1 pathway activity to regulate body length

egl-4 is a cGMP dependent protein kinase that is involved in both regulation of body size development and sensory perception. *egl-4* acts downstream of sensory perception genes, but upstream of the *dbl-1* BMP pathway to regulate body size (Fujiwara et al., 2002; Hirose et al., 2003). Increasing or decreasing levels of EGL-4 causes reciprocal changes in body length, where a loss-of-function mutation, *egl-4(n478)*, produces a longer than wild-type animal and a gain-of-function mutation, *egl-4(ad450)*, produces a smaller than wild-type animal (Daniels et al., 2000; Raizen et al., 2006). Similar to *egl-4*, loss of *dyf-7* function also affects body size and environmental sensation, so we reasoned that *egl-4* could function with *dyf-7* to regulate body size development. To test this possibility, we examined for a genetic relationship between *egl-4* and *dyf-7* using epistatic analyses with loss- or gain-of-function mutations in *egl-4* and loss-of-function mutation in *dyf-7*. An epistasis analysis compares phenotypes of genetic mutants to examine for an interaction between two genes. If two genes act in the same pathway, mutation in one of the genes will completely mask the phenotypic effects

of the other gene. However, if the two genes act in an independent fashion, then a double mutant will show an intermediate or an additive phenotype compared to animals with mutation in either single gene. Results show that removing *dyf-7* function in the *egl-4(n478)* loss-of-function or *egl-4(ad450)* gain-of-function backgrounds significantly decreased body length (Figure 5.7). Suppression of the long phenotype or the additive decrease in length indicates that *dyf-7* acts independent of *egl-4* to regulate body size development.

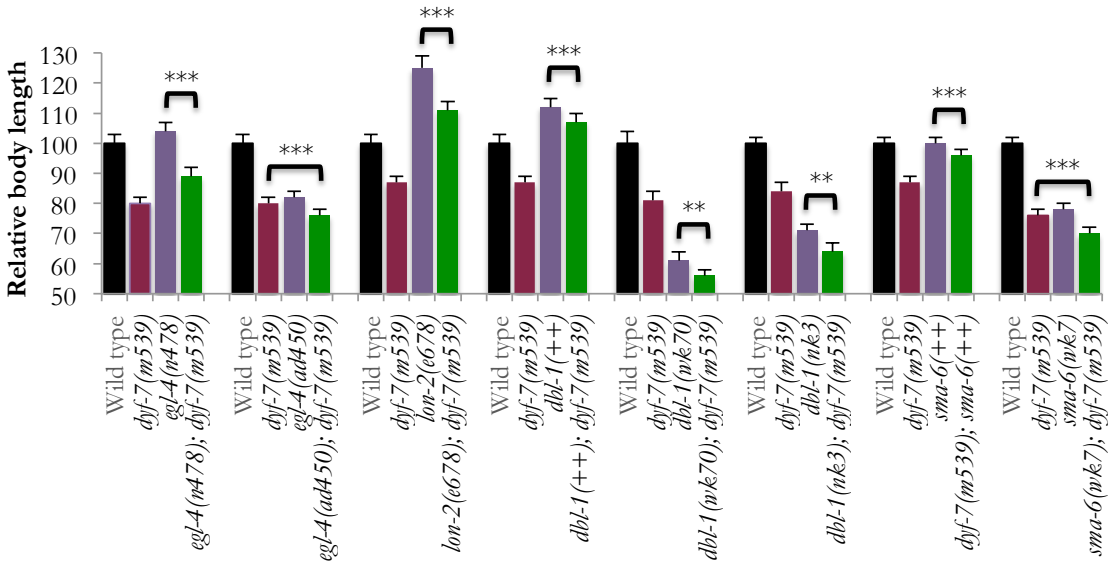

Figure 5.7 *dyf-7* requires *egl-4* and *dbl-1* pathway signaling for normal body length. Error bars indicate the mean relative length ± 95% confidence interval. P-values compare indicated data (***P≤0.0001; **P≤0.001) using the unpaired t-test.

Next we investigated whether DYF-7 functions as part of the DBL-1 core pathway. Genetic analyses place the *dbl-1* ligand upstream of the type I receptor, *sma-6*

and type II receptor, *daf-4* (Suzuki et al., 1999). Animals with loss of *dbl-1* or *sma-6* that also lack *dyf-7* function are significantly smaller than either respective single mutant (Figure 5.7). To further investigate genetic interaction between *dyf-7* and the *dbl-1* BMP pathway, we performed epistasis analyses of *dyf*-7 and animals with an overexpression of *dbl-1* pathway signaling. DBL-1 overexpression was accomplished by knocking down function of *lon-2*, a negative regulator of *dbl-1* signaling, or through overexpression of the *dbl-1* ligand, using an integrated transgene; overexpression of *dbl-1* in both cases creates a long animal (Gumienny et al., 2007; Schultz et al., 2014). Loss of *dyf-7* activity in animals with increased ligand signaling through loss of *lon-2* or overexpression of *dbl-1* results in partial suppression of the long phenotype (Figure 5.7). Another potential way to increase *dbl-1* pathway signaling is through overexpression of the *sma-6*, type I receptor. With the goal of amplifying *dbl-1* signaling, we created a translational fusion of *sma-6* and injected it into wild-type animals. This overexpressing line of *sma-6* produces an animal that is the same length as wild type, suggesting the type I receptor is in excess as compared to the ligand (Figure 5.7). When *dyf-7* function is removed from this *sma-6(++)* overexpressing background, an animal with an intermediate length is produced (Figure 5.7). Based on these findings, we conclude *dyf-7* acts independently of the *dbl-1* pathway in regulation of body length.

We noticed a trend of partial suppression of the long phenotype or an additive decrease in body length in the double mutants described (Figure 5.7). While these results indicate independent effects on body size, we wondered if these results could be used to evaluate a partial genetic interaction between *dyf-7* and the various *dbl-1* pathway

members. To test for any genetic interaction, we calculated the expected lengths of these double mutant animals assuming a simple additive independent relationship of effects for each mutation (Table 5.1). In the case of the small animals (*egl-4(ad450), dbl-1(wk70), dbl-1(nk3),* or *sma-6(wk7)* along with *dyf-7(m539))*, we found the double mutant animals were smaller than would be expected if *dyf-7* and *egl-4* or *dbl-1* pathway members acted totally independent from one another (Table 5.1). In the case of long animals, including *egl-4(n478), dbl-1(++),* and *sma-6(++)* along with *dyf-7(m539)*, the mean length of double mutant animals was smaller than would be expected if *dyf-7* and *egl-4* or *dbl-1* pathway members were regulating body length in complete independence (Table 5.1). Interestingly, in the case of *lon-2(e678); dyf-7(m539)*, the observed length of the double mutant animals was the same as the expected length of the animals if they were acting independently of one another, indicating a completely independent relationship between *dyf-7* and *lon-2* (Table 5.1). These genetic analyses show a partial genetic interaction between *dyf-7* and *egl-4* or *dbl-1* BMP pathway genes in regulating body length.

Table 5.1 *dyf-7*'s regulation of body length is partially dependent on *egl-4* and *dbl-1* pathway genes.

Genotype	Length[A]	Expected length if no interaction[B]	P-value[C]
egl-4(n478); dyf-7(m539)	89	84	≤ 0.001
egl-4(ad450); dyf-7(m539)	76	62	≤ 0.0001
lon-2(e678); dyf-7(m539)	111	112	0.36
dbl-1(++); dyf-7(m539)	107	99	≤ 0.0001
dbl-1(wk70); dyf-7(m539)	56	42	≤ 0.0001
dbl-1(nk3); dyf-7(m539)	64	55	≤ 0.0001
dyf-7(m539); sma-6(++)	96	87	≤ 0.0001
sma-6(wk7); dyf-7(m539)	70	54	≤ 0.0001

1. The observed mean length of double mutant animals shown in Figure 5.7.
2. The expected mean length if there is no genetic interaction between *dyf-7* and *egl-4* or *dbl-1* pathway genes assuming a simple additive relationship.
3. P-values were calculated using the one-way t-test to compare observed and expected means.

DYF-7 positively affects DBL-1 pathway activity

The DBL-1 BMP pathway regulates transcription of multiple genetic targets (Roberts et al., 2010). One target that was found to be highly regulated by DBL-1 pathway activity is *spp-9*, a saposin involved in innate immune response (Nicholas and Hodgkin, 2004; Roberts et al., 2010). Our epistasis analyses indicate a partial interaction between *dyf-7* and *dbl-1* pathway members in body size development. To further investigate the nature of the genetic relationship between *dyf-7* and *dbl-1,* we took advantage of a *gfp*-tagged *spp-9* transcriptional fusion that acts as a reporter of *dbl-1* pathway signaling. Animals lacking *dbl-1* pathway signaling display increased levels of this intestinally expressed fluorescent reporter (Roberts et al., 2010). In order to determine whether *dyf-7* regulates *dbl-1* pathway signaling, we measured fluorescent

intensity levels per area of this *dbl-1* reporter in the intestines of wild-type and *dyf-7(m539)* animals. We found that *dyf-7* mutant animals, like animals lacking *dbl-1* function, display upregulated *spp-9p::gfp* expression (Figure 5.8A-C). Consistent with our previous finding that *dyf-7* and *dbl-1* are partially dependent on one another for establishing body length, these results suggest that *dyf-7* positively affects *dbl-1* pathway transcriptional activity.

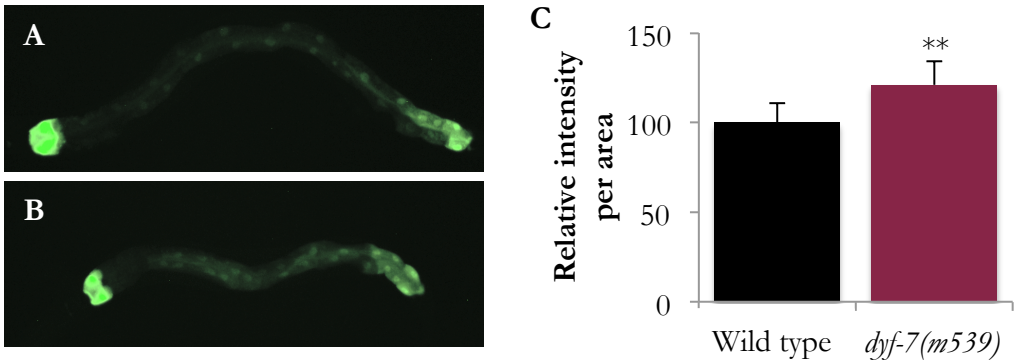

Figure 5.8 DYF-7 positively affects DBL-1 pathway reporter signaling. *Spp-9p::*GFP expression in wild-type (A) and *dyf-7(m539)* (B) animals. (C) Relative expression of *spp-9p::*GFP expression. Error bars indicate the mean ± 95% confidence interval. P-values compare data to wild type (***P≤0.0001) using the unpaired t-test.

DISCUSSION

Determination of body size is a process that is regulated by both genes and environment. Many of the mechanisms that regulate body size in mammals are conserved in *C. elegans*. Like bones in vertebrates, the nematode's cuticle, a secreted

extracellular matrix, can influence body shape and size. The BMP pathway signaling also determines body size in many animals. In this paper, we characterize the role of ZP-domain protein DYF-7 in establishing body size.

ZP-domain proteins are a family of extracellular molecules that display a diverse range of functions. ZP-domain proteins are found in all epithelia and they are often involved in organization and structure of apical epithelial extracellular matrix (Plaza et al., 2010). We have shown the *C. elegans* ZP-domain protein DYF-7 plays a critical role in organization of the cuticle, an extracellular matrix secreted by underlying epithelia. While *dyf-7* mutant animals are best known for their profound sensory deprivation, they also display a plethora of other defects. We have shown that the dwarfism displayed in animals lacking *dyf-7* function is a post-embryonic phenotype that is only partially dependent on the DBL-1 BMP pathway. We have also shown that the severe impenetrability to environmentally supplied drugs and dye seen in *dyf-7* mutant animals is associated with defects in cuticular organization. Our findings suggest a unique role for ZP-domain containing protein DYF-7 in regulation of body size and permeability through DBL-1 pathway signaling and organization of the cuticle. Taken together, our results show a conserved role for regulation of extracellular matrix organization by a ZP-domain protein in *C. elegans*.

We have shown a partial interaction between *dyf-7* and *dbl-1* in regulating body length and that loss of DYF-7 affects activity of the DBL-1 pathway. In these studies, the transcriptional regulation of the DBL-1 signaling target *spp-9* was used to measure DBL-1 pathway activity. While indeed *spp-9* is highly regulated by the DBL-1 pathway,

it is possible that changes in activity of this innate immunity gene are due to other, non-DBL-1 dependent factors. It would be interesting to further characterize the relationship between *dyf-7* and *dbl-1* in governing body size and if *dyf-7* plays a direct or indirect role in regulating *dbl-1* pathway activity. Another area to further investigate would be the mechanisms and regulation of *dyf-7* and its role in body length that are independent of the *dbl-1* pathway.

Previous studies have found DYF-7 is involved in shaping dendrites in the primary *C. elegans* sense organ (Heiman and Shaham, 2009). We have shown DYF-7 is critical for establishing epithelial cell adhesion and shape. In this study, we have expanded DYF-7's role to organization of extracellular matrix secreted by epithelia. Based on previous studies and the research presented here, we propose a model whereby DYF-7 continues to play postembryonic roles in epithelial cell shape, organization, and interactions that affect body size and permeability. We suspect that by interfering with epithelial cell shape and organization, cuticle components are not properly secreted or assembled, thus affecting both secretion and organization of cuticular components leading to defects in body size and permeability in animals with defects in *dyf-7* function.

6. CONCLUSIONS AND FUTURE DIRECTIONS

In these studies we show how extracellular matrix is regulated through activity of a cell-signaling molecule and elucidate the functions of a structural component of the extracellular matrix. Further, we establish the *C. elegans* DBL-1 signaling pathway as a tractable genetic system to study regulation of extracellular matrix by BMPs. Finally, we propose the ZP-domain protein DYF-7 functions as an extracellular matrix component that is critical for epithelial cell adhesion and loss of this adhesion underlies a spectrum of morphological, sensory, and cuticular defects.

Future studies are needed to further describe and compare the molecular machinery that is affected in the cuticle when body size and permeability are altered in various genetic backgrounds. More research is also required to examine regulation of DBL-1 signaling to determine ultrastructural localization and mechanisms regulating intercellular trafficking of DBL-1. Finally, it would be of interest to examine DYF-7 localization in TEM sections and further characterize DYF-7's role in extracellular matrix and cell adhesion using electron microscopy.

REFERENCES

Ailion, M. and Thomas, J. H. (2000). Dauer formation induced by high temperatures in *Caenorhabditis elegans*. *Genetics* **156**, 1047-1067.

Almedom, R. B., Liewald, J. F., Hernando, G., Schultheis, C., Rayes, D., Pan, J., Schedletzky, T., Hutter, H., Bouzat, C. and Gottschalk, A. (2009). An ER-resident membrane protein complex regulates nicotinic acetylcholine receptor subunit composition at the synapse. *Embo J* **28**, 2636-2649.

Alper, S., McBride, S. J., Lackford, B., Freedman, J. H. and Schwartz, D. A. (2007). Specificity and complexity of the *Caenorhabditis elegans* innate immune response. *Mol Cell Biol* **27**, 5544-5553.

Baird, S. E. and Ellazar, S. A. (1999). TGFβ-like signaling and spicule development in *Caenorhabditis elegans*. *Dev Biol* **212**, 93-100.

Bandyopadhyay, A., Tsuji, K., Cox, K., Harfe, B. D., Rosen, V. and Tabin, C. J. (2006). Genetic analysis of the roles of BMP2, BMP4, and BMP7 in limb patterning and skeletogenesis. *PLoS Genet* **2**, e216.

Barbercheck, M. E. and Kaya, H. K. (1991). Effect of host condition and soil texture on host finding by the entomogenous nematodes *Heterorhabditis bacteriophora* (Rhabditida: Heterorhabditidae) and *Steinernema carpocapsae* (Rhabditida: Steinernematidae). *Environ Entomol* **20**, 582-589.

Bargmann, C. I. and Horvitz, H. R. (1991). Control of larval development by chemosensory neurons in *Caenorhabditis elegans*. *Science* **251**, 1243-1246.

Baugh, L. R. and Sternberg, P. W. (2006). DAF-16/FOXO regulates transcription of *cki-1*/Cip/Kip and repression of *lin-4* during *C. elegans* L1 arrest. *Curr Biol* **16**, 780-785.

Beifuss, K. K. and Gumienny, T. L. (2012). RNAi Screening to Identify Postembryonic Phenotypes in *C. elegans*. *J Vis Exp*, e3442.

Birnby, D. A., Link, E. M., Vowels, J. J., Tian, H., Colacurcio, P. L. and Thomas, J. H. (2000). A transmembrane guanylyl cyclase (DAF-11) and Hsp90 (DAF-21) regulate a common set of chemosensory behaviors in *Caenorhabditis elegans*. *Genetics* **155**, 85-104.

Blaxter, M. L. (1993). Cuticle surface proteins of wild type and mutant *Caenorhabditis elegans*. *J Biol Chem* **268**, 6600-6609.

Bokel, C., Prokop, A. and Brown, N. H. (2005). Papillote and Piopio: *Drosophila* ZP-domain proteins required for cell adhesion to the apical extracellular matrix and microtubule organization. *J Cell Sci* **118**, 633-642.

Bolte, S. and Cordelieres, F. P. (2006). A guided tour into subcellular colocalization analysis in light microscopy. *J Microsc* **224**, 213-232.

Bork, P. and Sander, C. (1992). A large domain common to sperm receptors (Zp2 and Zp3) and TGF-β type III receptor. *FEBS Lett* **300**, 237-240.

Brazil, D. P., Church, R. H., Surae, S., Godson, C. and Martin, F. (2015). BMP signalling: agony and antagony in the family. *Trends in cell biology*.

Brenner, S. (1974). The genetics of *Caenorhabditis elegans*. *Genetics* **77**, 71-94.

Carmichael, F. J. (1985). General anaesthetics and local anaesthetics. In *Principles of medical pharmacology* (ed. H. Kalant, W. H. E. Roschlau & E. M. Sellers), pp. 265-289. Toronto, Ontario: Department of Pharmacology, University of Toronto Press.

Cassada, R. C. and Russell, R. L. (1975). The dauerlarva, a post-embryonic developmental variant of the nematode *Caenorhabditis elegans*. *Dev Biol* **46**, 326-342.

Cohn, R. D. and Campbell, K. P. (2000). Molecular basis of muscular dystrophies. *Muscle Nerve* **23**, 1456-1471.

Collet, J., Spike, C. A., Lundquist, E. A., Shaw, J. E. and Herman, R. K. (1998). Analysis of *osm-6*, a gene that affects sensory cilium structure and sensory neuron function in *Caenorhabditis elegans*. *Genetics* **148**, 187-200.

Costa, M., Draper, B. W. and Priess, J. R. (1997). The role of actin filaments in patterning the Caenorhabditis elegans cuticle. *Dev Biol* **184**, 373-384.

Cox, E. A. and Hardin, J. (2004). Sticky worms: adhesion complexes in *C. elegans*. *Journal of cell science* **117**, 1885-1897.

Cox, G. N., Kusch, M. and Edgar, R. S. (1981a). Cuticle of *Caenorhabditis elegans*: its isolation and partial characterization. *J Cell Biol* **90**, 7-17.

Cox, G. N., Staprans, S. and Edgar, R. S. (1981b). The cuticle of *Caenorhabditis elegans*. II. Stage-specific changes in ultrastructure and protein composition during postembryonic development. *Dev Biol* **86**, 456-470.

Croll, N. A. (1970). *The behaviour of nematodes: their activity, senses and responses*. London: Edward Arnold.

Daniels, S. A., Ailion, M., Thomas, J. H. and Sengupta, P. (2000). *egl-4* acts through a transforming growth factor-β/SMAD pathway in *Caenorhabditis elegans* to regulate multiple neuronal circuits in response to sensory cues. *Genetics* **156**, 123-141.

de Gives, P. M., Davies, K., Clark, S. and Behnke, J. (1999). Predatory behaviour of trapping fungi against *srf* mutants of *Caenorhabditis elegans* and different plant and animal parasitic nematodes. *Parasitology* **119**, 95-104.

Dean, J. (1992). Biology of mammalian fertilization: role of the zona pellucida. *J Clin Invest* **89**, 1055-1059.

Duncan, H. M. and Mackler, B. (1966). Electron Transport Systems of Yeast: III. Preparation and Properties of Cytochrome Oxidase. *J Biol Chem* **241**, 1694-1697.

Ellis, E. A. (2006). Corrected Formulation for Spurr Low Viscosity Embedding Medium Using The Replacement Epoxide ERL 4221. *Microsc Microanal* **12**, 288-289.

Fang-Yen, C., Gabel, C. V., Samuel, A. D., Bargmann, C. I. and Avery, L. (2012). Laser microsurgery in *Caenorhabditis elegans*. *Methods in cell biology* **107**, 177-206.

Fay, D. S. and Yochem, J. (2007). The SynMuv genes of Caenorhabditis elegans in vulval development and beyond. *Dev Biol* **306**, 1-9.

Feinbaum, R. and Ambros, V. (1999). The timing of *lin-4* RNA accumulation controls the timing of postembryonic developmental events in *Caenorhabditis elegans*. *Dev Biol* **210**, 87-95.

Fernando, T., Flibotte, S., Xiong, S., Yin, J., Yzeiraj, E., Moerman, D. G., Melendez, A. and Savage-Dunn, C. (2011). *C. elegans* ADAMTS ADT-2 regulates body size by modulating TGFβ signaling and cuticle collagen organization. *Dev Biol* **352**, 92-103.

Ferreira, A. R., Felgueiras, J. and Fardilha, M. (2015). Signaling pathways in anchoring junctions of epithelial cells: cell-to-cell and cell-to-extracellular matrix interactions. *Journal of receptor and signal transduction research*, **35**, 67-75.

Finney, M. and Ruvkun, G. (1990). The *unc-86* gene product couples cell lineage and cell identity in *C. elegans*. *Cell* **63**, 895-905.

Flemming, A. J., Shen, Z. Z., Cunha, A., Emmons, S. W. and Leroi, A. M. (2000). Somatic polyploidization and cellular proliferation drive body size evolution in nematodes. *Proc Natl Acad Sci U S A* **97**, 5285-5290.

Fujiwara, M., Sengupta, P. and McIntire, S. L. (2002). Regulation of body size and behavioral state of *C. elegans* by sensory perception and the EGL-4 cGMP-dependent protein kinase. *Neuron* **36**, 1091-1102.

Fukuyama, M., Rougvie, A. E. and Rothman, J. H. (2006). *C. elegans* DAF-18/PTEN mediates nutrient-dependent arrest of cell cycle and growth in the germline. *Curr Biol* **16**, 773-779.

Fung, W. Y., Fat, K. F., Eng, C. K. and Lau, C. K. (2007). *crm-1* facilitates BMP signaling to control body size in *Caenorhabditis elegans*. *Dev Biol* **311**, 95-105.

Ginzburg, V. E., Roy, P. J. and Culotti, J. G. (2002). Semaphorin 1a and semaphorin 1b are required for correct epidermal cell positioning and adhesion during morphogenesis in *C. elegans*. *Development* **129**, 2065-2078.

Golden, J. W. and Riddle, D. L. (1984). The *Caenorhabditis elegans* dauer larva: developmental effects of pheromone, food, and temperature. *Dev Biol* **102**, 368-378.

Gottlieb, S. and Ruvkun, G. (1994). *daf-2*, *daf-16* and *daf-23*: genetically interacting genes controlling Dauer formation in *Caenorhabditis elegans*. *Genetics* **137**, 107-120.

Gottschalk, A., Almedom, R. B., Schedletzky, T., Anderson, S. D., Yates, J. R., III and Schafer, W. R. (2005). Identification and characterization of novel nicotinic receptor-associated proteins in *Caenorhabditis elegans*. *Embo J* **24**, 2566-2578.

Gravato-Nobre, M. J., Nicholas, H. R., Nijland, R., O'Rourke, D., Whittington, D. E., Yook, K. J. and Hodgkin, J. (2005). Multiple genes affect sensitivity of *Caenorhabditis elegans* to the bacterial pathogen *Microbacterium nematophilum*. *Genetics* **171**, 1033-1045.

Gullapalli, R. R., Demirel, M. C. and Butler, P. J. (2008). Molecular dynamics simulations of DiI-C18(3) in a DPPC lipid bilayer. *Phys Chem Chem Phys* **10**, 3548-3560.

Gumienny, T. L., MacNeil, L. T., Wang, H., de Bono, M., Wrana, J. L. and Padgett, R. W. (2007). Glypican LON-2 is a conserved negative regulator of BMP-like signaling in *Caenorhabditis elegans*. *Curr Biol* **17**, 159-164.

Gumienny, T. L. and Savage-Dunn, C. (2013). TGF-β signaling in *C. elegans*. In *WormBook, The C. elegans Research Community, ed.*

Hall, D. and Altun, Z. (2008). *C. elegans Atlas*. Cold Spring Harbor: Cold Spring Harbor Laboratory Press.

Hall, D. H., Hartwieg, E. and Nguyen, K. C. (2012). Modern electron microscopy methods for *C. elegans*. *Methods in cell biology* **107**, 93-149.

Haut, H. V. (1956). Das Champignon-Myzel Als Indikator Für Die Wirkung Saprober Nematoden in Komposten. *Nematologica* **1**, 165-173.

Heiman, M. G. and Shaham, S. (2009). DEX-1 and DYF-7 establish sensory dendrite length by anchoring dendritic tips during cell migration. *Cell* **137**, 344-355.

Herweijer, M., Berden, J., Kemp, A. and Slater, E. (1985). Inhibition of energy-transducing reactions by 8-nitreno-ATP covalently bound to bovine heart submitochondrial particles: direct interaction between ATPase and redox enzymes. *Biochim Biophys Acta* **809**, 81-89.

Himmelhoch, S. and Zuckerman, B. M. (1983). *Caenorhabditis elegans*: characters of negatively charged groups on the cuticle and intestine. *Exp Parasitol* **55**, 299-305.

Hirose, T., Nakano, Y., Nagamatsu, Y., Misumi, T., Ohta, H. and Ohshima, Y. (2003). Cyclic GMP-dependent protein kinase EGL-4 controls body size and lifespan in *C. elegans*. *Development* **130**, 1089-1099.

Ho, N. F., Geary, T. G., Barsuhn, C. L., Sims, S. and Thompson, D. P. (1992). Mechanistic studies in the transcuticular delivery of antiparasitic drugs II: ex vivo/in vitro correlation of solute transport by *Ascaris suum*. *Mol Biochem Parasitol* **52**, 1-13.

Ho, N. F., Geary, T. G., Raub, T. J., Barsuhn, C. L. and Thompson, D. P. (1990). Biophysical transport properties of the cuticle of *Ascaris suum*. *Mol Biochem Parasitol* **41**, 153-165.

Ho, N. F., Sims, S. M., Vidmar, T. J., Day, J. S., Barsuhn, C. L., Thomas, E. M., Geary, T. G. and Thompson, D. P. (1994). Theoretical perspectives on anthelmintic drug discovery: interplay of transport kinetics, physicochemical properties, and in vitro activity of anthelmintic drugs. *J Pharm Sci* **83**, 1052-1059.

Hodgkin, J., Felix, M. A., Clark, L. C., Stroud, D. and Gravato-Nobre, M. J. (2013). Two *Leucobacter* strains exert complementary virulence on *Caenorhabditis* including death by worm-star formation. *Curr Biol* **23**, 2157-2161.

Hong, Y., Roy, R. and Ambros, V. (1998). Developmental regulation of a cyclin-dependent kinase inhibitor controls postembryonic cell cycle progression in *Caenorhabditis elegans*. *Development* **125**, 3585-3597.

Hope, I. A., Stevens, J., Garner, A., Hayes, J., Cheo, D. L., Brasch, M. A. and Vidal, M. (2004). Feasibility of genome-scale construction of promoter::reporter gene fusions for expression in *Caenorhabditis elegans* using a multisite gateway recombination system. *Genome Res* **14**, 2070-2075.

Horton, R. M., Cai, Z. L., Ho, S. N. and Pease, L. R. (1990). Gene splicing by overlap extension: tailor-made genes using the polymerase chain reaction. *Biotechniques* **8**, 528-535.

Houy, S., Croise, P., Gubar, O., Chasserot-Golaz, S., Tryoen-Toth, P., Bailly, Y., Ory, S., Bader, M. F. and Gasman, S. (2013). Exocytosis and endocytosis in neuroendocrine cells: inseparable membranes! *Frontiers in endocrinology* **4**, 135.

Hu, P. J. (2007). Dauer. In *WormBook, The C. elegans Research Community, ed.*

Hutter, H., Vogel, B. E., Plenefisch, J. D., Norris, C. R., Proenca, R. B., Spieth, J., Guo, C., Mastwal, S., Zhu, X., Scheel, J., et al. (2000). Conservation and novelty in the evolution of cell adhesion and extracellular matrix genes. *Science* **287**, 989-994.

Ikegami, R., Zheng, H., Ong, S. H. and Culotti, J. (2004). Integration of semaphorin-2A/MAB-20, ephrin-4, and UNC-129 TGF-β signaling pathways regulates sorting of distinct sensory rays in *C. elegans*. *Developmental cell* **6**, 383-395.

Jansson, H.-B. r., Jeyaprakash, A., Coles, G. C., Marban-Mendoza, N. and Zuckerman, B. M. (1986). Fluorescent and ferritin labelling of cuticle surface carbohydrates of *Caenorhabditis elegans* and *Panagrellus redivivus*. *J Nematol* **18**, 570.

Jeanes, A., Gottardi, C. J. and Yap, A. S. (2008). Cadherins and cancer: how does cadherin dysfunction promote tumor progression? *Oncogene* **27**, 6920-6929.

Jiang, L. I. and Sternberg, P. W. (1999). Socket cells mediate spicule morphogenesis in *Caenorhabditis elegans* males. *Dev Biol* **211**, 88-99.

Johnstone, I. L. (2000). Cuticle collagen genes. Expression in *Caenorhabditis elegans*. *Trends Genet* **16**, 21-27.

Jones, J. T. and Gwynn, I. A. (1991). A method for rapid fixation and dehydration of nematode tissue for transmission electron microscopy. *J Microsc* **164**, 43-51.

Kage-Nakadai, E., Kobuna, H., Kimura, M., Gengyo-Ando, K., Inoue, T., Arai, H. and Mitani, S. (2010). Two very long chain fatty acid acyl-CoA synthetase genes, *acs-20* and *acs-22*, have roles in the cuticle surface barrier in *Caenorhabditis elegans*. *PLoS One* **5**, e8857.

Kanakry, C. G., Li, Z., Nakai, Y., Sei, Y. and Weinberger, D. R. (2007). Neuregulin-1 regulates cell adhesion via an ErbB2/phosphoinositide-3 kinase/Akt-dependent pathway: potential implications for schizophrenia and cancer. *PLoS One* **2**, e1369.

Kimura, K. D., Tissenbaum, H. A., Liu, Y. and Ruvkun, G. (1997). *daf-2*, an insulin receptor-like gene that regulates longevity and diapause in *Caenorhabditis elegans*. *Science* **277**, 942-946.

Knight, C. G., Azevedo, R. B. and Leroi, A. M. (2001). Testing life-history pleiotropy in *Caenorhabditis elegans*. *Evolution; international journal of organic evolution* **55**, 1795-1804.

Kramer, J. M., French, R. P., Park, E. C. and Johnson, J. J. (1990). The Caenorhabditis elegans rol-6 gene, which interacts with the sqt-1 collagen gene to determine organismal morphology, encodes a collagen. *Mol Cell Biol* **10**, 2081-2089.

Kramer, J. M., Johnson, J. J., Edgar, R. S., Basch, C. and Roberts, S. (1988). The *sqt-1* gene of *C. elegans* encodes a collagen critical for organismal morphogenesis. *Cell* **55**, 555-565.

Krishna, S., Maduzia, L. L. and Padgett, R. W. (1999). Specificity of TGFβ signaling is conferred by distinct type I receptors and their associated SMAD proteins in *Caenorhabditis elegans*. *Development* **126**, 251-260.

Labouesse, M. (2006). Epithelial junctions and attachments. In *WormBook, The C. elegans Research Community, ed.*

Le Goff, C. and Cormier-Daire, V. (2012). From tall to short: the role of TGFβ signaling in growth and its disorders. *Am J Med Genet C Semin Med Genet* **160C**, 145-153.

Lee, B. H., Clothier, M. F., Dutton, F. E., Nelson, S. J., Johnson, S. S., Thompson, D. P., Geary, T. G., Whaley, H. D., Haber, C. L., Marshall, V. P., et al. (2002). Marcfortine and paraherquamide class of anthelmintics: discovery of PNU-141962. *Current topics in medicinal chemistry* **2**, 779-793.

Liang, J., Yu, L., Yin, J. and Savage-Dunn, C. (2007). Transcriptional repressor and activator activities of SMA-9 contribute differentially to BMP-related signaling outputs. *Dev Biol* **305**, 714-725.

Liegeois, S., Benedetto, A., Garnier, J. M., Schwab, Y. and Labouesse, M. (2006). The V0-ATPase mediates apical secretion of exosomes containing Hedgehog-related proteins in *Caenorhabditis elegans*. *The Journal of cell biology* **173**, 949-961.

Link, C. D., Ehrenfels, C. W. and Wood, W. B. (1988). Mutant expression of male copulatory bursa surface markers in *Caenorhabditis elegans*. *Development* **103**, 485-495.

Link, C. D., Silverman, M. A., Breen, M., Watt, K. E. and Dames, S. A. (1992). Characterization of *Caenorhabditis elegans* lectin-binding mutants. *Genetics* **131**, 867-881.

Liu, C. C., Gao, S. S., Yuan, T., Steele, C., Puria, S. and Oghalai, J. S. (2011). Biophysical mechanisms underlying outer hair cell loss associated with a shortened tectorial membrane. *Journal of the Association for Research in Otolaryngology : JARO* **12**, 577-594.

Lo, R. S., Chen, Y. G., Shi, Y., Pavletich, N. P. and Massague, J. (1998). The L3 loop: a structural motif determining specific interactions between SMAD proteins and TGF-β receptors. *Embo J* **17**, 996-1005.

Lozano, E., Saez, A. G., Flemming, A. J., Cunha, A. and Leroi, A. M. (2006). Regulation of growth by ploidy in *Caenorhabditis elegans*. *Curr Biol* **16**, 493-498.

Mallo, G. V., Kurz, C. L., Couillault, C., Pujol, N., Granjeaud, S., Kohara, Y. and Ewbank, J. J. (2002). Inducible antibacterial defense system in *C. elegans*. *Curr Biol* **12**, 1209-1214.

Mao, H., Diehl, A. M. and Li, Y. X. (2009). Sonic hedgehog ligand partners with caveolin-1 for intracellular transport. *Laboratory investigation; a journal of technical methods and pathology* **89**, 290-300.

Marcotte, E. R., Pearson, D. M. and Srivastava, L. K. (2001). Animal models of schizophrenia: a critical review. *J Psychiatry Neurosci* **26**, 395-410.

McAllister, K. A., Grogg, K. M., Johnson, D. W., Gallione, C. J., Baldwin, M. A., Jackson, C. E., Helmbold, E. A., Markel, D. S., McKinnon, W. C., Murrell, J., et al. (1994). Endoglin, a TGF-β binding protein of endothelial cells, is the gene for hereditary haemorrhagic telangiectasia type 1. *Nature genetics* **8**, 345-351.

McLachlan, I. G. and Heiman, M. G. (2013). Shaping dendrites with machinery borrowed from epithelia. *Current opinion in neurobiology* **23**, 1005-1010.

McMahon, L., Muriel, J. M., Roberts, B., Quinn, M. and Johnstone, I. L. (2003). Two sets of interacting collagens form functionally distinct substructures within a *Caenorhabditis elegans* extracellular matrix. *Mol Biol Cell* **14**, 1366-1378.

Mello, C. and Fire, A. (1995). DNA transformation. *Methods in cell biology* **48**, 451-482.

Miyazono, K., Kamiya, Y. and Morikawa, M. (2010). Bone morphogenetic protein receptors and signal transduction. *J Biochem* **147**, 35-51.

Mochii, M., Yoshida, S., Morita, K., Kohara, Y. and Ueno, N. (1999). Identification of transforming growth factor-β-regulated genes in *Caenorhabditis elegans* by differential hybridization of arrayed cDNAs. *Proc Natl Acad Sci U S A* **96**, 15020-15025.

Moribe, H., Yochem, J., Yamada, H., Tabuse, Y., Fujimoto, T. and Mekada, E. (2004). Tetraspanin protein (TSP-15) is required for epidermal integrity in *Caenorhabditis elegans*. *J Cell Sci* **117**, 5209-5220.

Morita, K., Chow, K. L. and Ueno, N. (1999). Regulation of body length and male tail ray pattern formation of *Caenorhabditis elegans* by a member of TGF-β family. *Development* **126**, 1337-1347.

Morita, K., Flemming, A. J., Sugihara, Y., Mochii, M., Suzuki, Y., Yoshida, S., Wood, W. B., Kohara, Y., Leroi, A. M. and Ueno, N. (2002). A *Caenorhabditis elegans* TGF-β, DBL-1, controls the expression of LON-1, a PR-related protein, that regulates polyploidization and body length. *Embo J* **21**, 1063-1073.

Munck, S., Miskiewicz, K., Sannerud, R., Menchon, S. A., Jose, L., Heintzmann, R., Verstreken, P. and Annaert, W. (2012). Sub-diffraction imaging on standard microscopes through photobleaching microscopy with non-linear processing. *Journal of cell science* **125**, 2257-2266.

Nagamatsu, Y. and Ohshima, Y. (2004). Mechanisms for the control of body size by a G-kinase and a downstream TGFβ signal pathway in *Caenorhabditis elegans*. *Genes to cells : devoted to molecular & cellular mechanisms* **9**, 39-47.

Natsuka, S., Kawaguchi, M., Wada, Y., Ichikawa, A., Ikura, K. and Hase, S. (2005). Characterization of wheat germ agglutinin ligand on soluble glycoproteins in *Caenorhabditis elegans*. *J Biochem* **138**, 209-213.

Nicholas, H. R. and Hodgkin, J. (2004). Responses to infection and possible recognition strategies in the innate immune system of *Caenorhabditis elegans*. *Molecular immunology* **41**, 479-493.

Nyström, J., Shen, Z. Z., Aili, M., Flemming, A. J., Leroi, A. and Tuck, S. (2002). Increased or decreased levels of *Caenorhabditis elegans lon-3*, a gene encoding a collagen, cause reciprocal changes in body length. *Genetics* **161**, 83-97.

Olsen, P. H. and Ambros, V. (1999). The *lin-4* regulatory RNA controls developmental timing in *Caenorhabditis elegans* by blocking LIN-14 protein synthesis after the initiation of translation. *Dev Biol* **216**, 671-680.

Ouellet, J., Li, S. and Roy, R. (2008). Notch signalling is required for both dauer maintenance and recovery in *C. elegans*. *Development* **135**, 2583-2592.

Padua, D. and Massague, J. (2009). Roles of TGFβ in metastasis. *Cell research* **19**, 89-102.

Page, A. P. and Johnstone, I. L. (2007). The cuticle. In *WormBook, The C. elegans Research Community, ed.*

Parton, R. G. and Simons, K. (2007). The multiple faces of caveolae. *Nature reviews. Molecular cell biology* **8**, 185-194.

Partridge, F. A., Tearle, A. W., Gravato-Nobre, M. J., Schafer, W. R. and Hodgkin, J. (2008). The *C. elegans* glycosyltransferase BUS-8 has two distinct and essential roles in epidermal morphogenesis. *Dev Biol* **317**, 549-559.

Pelkmans, L. and Zerial, M. (2005). Kinase-regulated quantal assemblies and kiss-and-run recycling of caveolae. *Nature* **436**, 128-133.

Petrella, L. N., Wang, W., Spike, C. A., Rechtsteiner, A., Reinke, V. and Strome, S. (2011). synMuv B proteins antagonize germline fate in the intestine and ensure *C. elegans* survival. *Development* **138**, 1069-1079.

Plaza, S., Chanut-Delalande, H., Fernandes, I., Wassarman, P. M. and Payre, F. (2010). From A to Z: apical structures and zona pellucida-domain proteins. *Trends in cell biology* **20**, 524-532.

Portal-Celhay, C., Nehrke, K. and Blaser, M. J. (2013). Effect of *Caenorhabditis elegans* age and genotype on horizontal gene transfer in intestinal bacteria. *Faseb J* **27**, 760-768.

Praitis, V., Ciccone, E. and Austin, J. (2005). SMA-1 spectrin has essential roles in epithelial cell sheet morphogenesis in *C. elegans*. *Dev Biol* **283**, 157-170.

Pye, A. E. and Burman, M. (1981). Rosette formation by *Heterorhabditis bacteriophora*. *Nematologica* **27**, 117-119.

Raizen, D. M., Cullison, K. M., Pack, A. I. and Sundaram, M. V. (2006). A novel gain-of-function mutant of the cyclic GMP-dependent protein kinase *egl-4* affects multiple physiological processes in *Caenorhabditis elegans*. *Genetics* **173**, 177-187.

Ramel, M. C. and Hill, C. S. (2012). Spatial regulation of BMP activity. *FEBS Lett* **586**, 1929-1941.

Rand, J. B. and Johnson, C. D. (1995). Genetic pharmacology: interactions between drugs and gene products in *Caenorhabditis elegans*. *Methods in cell biology* **48**, 187-204.

Ren, P., Lim, C. S., Johnsen, R., Albert, P. S., Pilgrim, D. and Riddle, D. L. (1996). Control of *C. elegans* larval development by neuronal expression of a TGF-β homolog. *Science* **274**, 1389-1391.

Reynolds, E. S. (1963). The use of lead citrate at high pH as an electron-opaque stain in electron microscopy. *J Cell Biol* **17**, 208-212.

Richardson, G. P., de Monvel, J. B. and Petit, C. (2011). How the genetics of deafness illuminates auditory physiology. *Annual review of physiology* **73**, 311-334.

Roberts, A. F., Gumienny, T. L., Gleason, R. J., Wang, H. and Padgett, R. W. (2010). Regulation of genes affecting body size and innate immunity by the DBL-1/BMP-like pathway in *Caenorhabditis elegans*. *BMC Dev Biol* **10**, 61.

Roff (2000). Trade-offs between growth and reproduction: an analysis of the quantitative genetic evidence. *Journal of Evolutionary Biology* **13**, 434-445.

Roy, P. J., Zheng, H., Warren, C. E. and Culotti, J. G. (2000). *mab-20* encodes Semaphorin-2a and is required to prevent ectopic cell contacts during epidermal morphogenesis in *Caenorhabditis elegans*. *Development* **127**, 755-767.

Ruiz-Lancheros, E., Viau, C., Walter, T. N., Francis, A. and Geary, T. G. (2011). Activity of novel nicotinic anthelmintics in cut preparations of *Caenorhabditis elegans*. *Int J Parasitol* **41**, 455-461.

Sapio, M. R., Hilliard, M. A., Cermola, M., Favre, R. and Bazzicalupo, P. (2005). The Zona Pellucida domain containing proteins, CUT-1, CUT-3 and CUT-5, play essential roles in the development of the larval alae in *Caenorhabditis elegans*. *Dev Biol* **282**, 231-245.

Sato, K., Sato, M., Audhya, A., Oegema, K., Schweinsberg, P. and Grant, B. D. (2006). Dynamic regulation of caveolin-1 trafficking in the germ line and embryo of *Caenorhabditis elegans*. *Mol Biol Cell* **17**, 3085-3094.

Savage, C., Das, P., Finelli, A. L., Townsend, S. R., Sun, C. Y., Baird, S. E. and Padgett, R. W. (1996). *Caenorhabditis elegans* genes *sma-2*, *sma-3*, and *sma-4* define a conserved family of transforming growth factor β pathway components. *Proc Natl Acad Sci U S A* **93**, 790-794.

Savage-Dunn, C., Tokarz, R., Wang, H., Cohen, S., Giannikas, C. and Padgett, R. W. (2000). SMA-3 smad has specific and critical functions in DBL-1/SMA-6 TGFβ-related signaling. *Dev Biol* **223**, 70-76.

Schackwitz, W. S., Inoue, T. and Thomas, J. H. (1996). Chemosensory neurons function in parallel to mediate a pheromone response in *C. elegans*. *Neuron* **17**, 719-728.

Schulenburg, H., Kurz, C. L. and Ewbank, J. J. (2004). Evolution of the innate immune system: the worm perspective. *Immunol Rev* **198**, 36-58.

Schultz, R. D., Bennett, E. E., Ellis, E. A. and Gumienny, T. L. (2014). Regulation of extracellular matrix organization by BMP signaling in *Caenorhabditis elegans*. *PLoS One* **9**, e101929.

Schultz, R. D. and Gumienny, T. L. (2012). Visualization of *Caenorhabditis elegans* cuticular structures using the lipophilic vital dye DiI. *J Vis Exp*, e3362.

Shaham (ed.), S. (2006). Methods in cell biology. In *WormBook, The C. elegans Research Community, ed.*

Shepherd, A. M. and Clark, S. A. (1976). Structure of the anterior alimentary tract of the passively feeding nematode *Hexatylus viviparus* (Neotylenchidae: Tylenchida). *Nematologica* **22**, 332-342.

Simmer, F., Tijsterman, M., Parrish, S., Koushika, S. P., Nonet, M. L., Fire, A., Ahringer, J. and Plasterk, R. H. (2002). Loss of the putative RNA-directed RNA polymerase RRF-3 makes C. elegans hypersensitive to RNAi. *Curr Biol* **12**, 1317-1319.

Singh, R. N. and Sulston, J. E. (1978). Some observations on moulting in *Caenorhabditis elegans*. *Nematologica* **24**, 63-71.

So, S., Tokumaru, T., Miyahara, K. and Ohshima, Y. (2011). Control of lifespan by food bacteria, nutrient limitation and pathogenicity of food in *C. elegans*. *Mech Ageing Dev* **132**, 210-212.

Spiegel, Y. and McClure, M. A. (1995). The surface coat of plant-parasitic nematodes: chemical composition, origin, and biological role-a review. *J Nematol* **27**, 127-134.

Starich, T. A., Herman, R. K., Kari, C. K., Yeh, W. H., Schackwitz, W. S., Schuyler, M. W., Collet, J., Thomas, J. H. and Riddle, D. L. (1995). Mutations affecting the chemosensory neurons of *Caenorhabditis elegans*. *Genetics* **139**, 171-188.

Starich, T. A., Miller, A., Nguyen, R. L., Hall, D. H. and Shaw, J. E. (2003). The *Caenorhabditis elegans* innexin INX-3 is localized to gap junctions and is essential for embryonic development. *Dev Biol* **256**, 403-417.

Stock, S. P., Caicedo, A. M. and Calatayud, P. A. (2005). *Rhabditis (Oscheius) colombiana* n. sp. (Nematoda: Rhabditidae), a necromenic associate of the subterranean burrower bug *Cyrtomenus bergi* (Hemiptera: Cydnidae) from the Cauca Valley, Colombia. *Nematology* **7**, 363-373.

Sudhaus, W. and Hooper, D. J. (1994). *Rhabditis (Oscheius) Guentheri* Sp. N., an Unusual Species With Reduced Posterior Ovary, With Observations On the *Dolichura* and *Insectivora* Groups (Nematoda: Rhabditidae). *Nematologica* **40**, 508-533.

Sulston, J. and Hodgkin, J. (1988). Methods. In *The Nematode Caenorhabditis elegans* (ed. W. Wood), pp. 587-606. Cold Spring Harbor: Cold Spring Harbor Laboratory Press.

Sulston, J. E. and Horvitz, H. R. (1977). Post-embryonic cell lineages of the nematode, *Caenorhabditis elegans*. *Dev Biol* **56**, 110-156.

Sulston, J. E., Schierenberg, E., White, J. G. and Thomson, J. N. (1983). The embryonic cell lineage of the nematode Caenorhabditis elegans. *Dev Biol* **100**, 64-119.

Suzuki, Y., Yandell, M. D., Roy, P. J., Krishna, S., Savage-Dunn, C., Ross, R. M., Padgett, R. W. and Wood, W. B. (1999). A BMP homolog acts as a dose-dependent regulator of body size and male tail patterning in *Caenorhabditis elegans*. *Development* **126**, 241-250.

Taneja-Bageshwar, S. and Gumienny, T. L. (2012). Two functional domains in *C. elegans* glypican LON-2 can independently inhibit BMP-like signaling. *Dev Biol* **371**, 66-76.

Teichman, R. J., Fujimoto, M. and Yanagimachi, R. (1972). A previously unrecognized material in mammalian spermatozoa as revealed by malachite green and pyronine. *Biol Reprod* **7**, 73-81.

Tenor, J. L. and Aballay, A. (2008). A conserved Toll-like receptor is required for *Caenorhabditis elegans* innate immunity. *EMBO Rep* **9**, 103-109.

Thein, M. C., McCormack, G., Winter, A. D., Johnstone, I. L., Shoemaker, C. B. and Page, A. P. (2003). *Caenorhabditis elegans* exoskeleton collagen COL-19: an adult-specific marker for collagen modification and assembly, and the analysis of organismal morphology. *Dev Dyn* **226**, 523-539.

Tong, Y. G. and Burglin, T. R. (2010). Conditions for dye-filling of sensory neurons in *Caenorhabditis elegans*. *Journal of neuroscience methods* **188**, 58-61.

Tuck, S. (2014). The control of cell growth and body size in *Caenorhabditis elegans*. *Experimental cell research* **321**, 71-76.

Urdaneta-Marquez, L., Bae, S. H., Janukavicius, P., Beech, R., Dent, J. and Prichard, R. (2014). A *dyf-7* haplotype causes sensory neuron defects and is associated with macrocyclic lactone resistance worldwide in the nematode parasite *Haemonchus contortus*. *Int J Parasitol* **44**, 1063-1071.

Van der Bend, R., Duetz, W., Colen, A.-M., Van Dam, K. and Berden, J. (1985). Differential effects of triphenyltin and 8-azido-ATP on the ATP synthesis, ATP-P_i

exchange, and ATP hydrolysis in liposomes containing ATP synthase and bacteriorhodopsin. *Arch Biochem Biophys* **241**, 461-471.

Vashlishan, A. B., Madison, J. M., Dybbs, M., Bai, J., Sieburth, D., Ch'ng, Q., Tavazoie, M. and Kaplan, J. M. (2008). An RNAi screen identifies genes that regulate GABA synapses. *Neuron* **58**, 346-361.

Verhoeven, K., Van Laer, L., Kirschhofer, K., Legan, P. K., Hughes, D. C., Schatteman, I., Verstreken, M., Van Hauwe, P., Coucke, P., Chen, A., et al. (1998). Mutations in the human alpha-tectorin gene cause autosomal dominant non-syndromic hearing impairment. *Nature genetics* **19**, 60-62.

Visser, R., Kant, S. G., Wit, J. M. and Breuning, M. H. (2009). Overgrowth syndromes: from classical to new. *Pediatr Endocrinol Rev* **6**, 375-394.

von Mende, N., Bird, D. M., Albert, P. S. and Riddle, D. L. (1988). *dpy-13*: a nematode collagen gene that affects body shape. *Cell* **55**, 567-576.

Vowels, J. J. and Thomas, J. H. (1992). Genetic analysis of chemosensory control of dauer formation in *Caenorhabditis elegans*. *Genetics* **130**, 105-123.

Walhout, A. J., Temple, G. F., Brasch, M. A., Hartley, J. L., Lorson, M. A., van den Heuvel, S. and Vidal, M. (2000). GATEWAY recombinational cloning: application to the cloning of large numbers of open reading frames or ORFeomes. *Methods Enzymol* **328**, 575-592.

Wang, J., Tokarz, R. and Savage-Dunn, C. (2002). The expression of TGFβ signal transducers in the hypodermis regulates body size in *C. elegans*. *Development* **129**, 4989-4998.

Wassarman, P. M. (1988). Zona pellucida glycoproteins. *Annu Rev Biochem* **57**, 415-442.

Wenick, A. S. and Hobert, O. (2004). Genomic cis-regulatory architecture and trans-acting regulators of a single interneuron-specific gene battery in *C. elegans*. *Developmental cell* **6**, 757-770.

Wilkin, M. B., Becker, M. N., Mulvey, D., Phan, I., Chao, A., Cooper, K., Chung, H. J., Campbell, I. D., Baron, M. and MacIntyre, R. (2000). Drosophila dumpy is a gigantic extracellular protein required to maintain tension at epidermal-cuticle attachment sites. *Curr Biol* **10**, 559-567.

Wolstenholme, A. J. and Rogers, A. T. (2005). Glutamate-gated chloride channels and the mode of action of the avermectin/milbemycin anthelmintics. *Parasitology* **131 Suppl**, S85-95.

Woodring, J. L. and Kaya, H. K. (1988). Steinernematid and heterorhabditid nematodes: a handbook of biology and techniques. In *Southern cooperative series bulletin*. Fayetteville: Arkansas Agricultural Experiment Station.

Wu, M. Y. and Hill, C. S. (2009). Tgf-β superfamily signaling in embryonic development and homeostasis. *Developmental cell* **16**, 329-343.

Wyeth, R. C., Croll, R. P., Willows, A. O. and Spencer, A. N. (2009). 1-Phenoxy-2-propanol is a useful anaesthetic for gastropods used in neurophysiology. *Journal of neuroscience methods* **176**, 121-128.

Yoeli, M. (1957). Observations on agglutination and the thigmotaxis of microfilariae in bancroftian filariasis. *Trans R Soc Trop Med Hyg* **51**, 132-136.

Yoshida, S., Morita, K., Mochii, M. and Ueno, N. (2001). Hypodermal expression of *Caenorhabditis elegans* TGF-β type I receptor SMA-6 is essential for the growth and maintenance of body length. *Dev Biol* **240**, 32-45.

Zuckerman, B. M., Kahane, I. and Himmelhoch, S. (1979). *Caenorhabditis briggsae* and *C. elegans*: Partial characterization of cuticle surface carbohydrates. *Exp Parasitol* **47**, 419-424.

Zugasti, O. and Ewbank, J. J. (2009). Neuroimmune regulation of antimicrobial peptide expression by a noncanonical TGF-β signaling pathway in *Caenorhabditis elegans* epidermis. *Nat Immunol* **10**, 249-256.

APPENDIX

VISUALIZATION OF *CAENORHABDITIS elegans* CUTICULAR STRUCTURES USING THE LIPOPHILIC VITAL DYE DII*

Introduction

The cuticle of *C. elegans* is a highly resistant structure that surrounds the exterior of the animal (Cox et al., 1981a; Cox et al., 1981b; Hall and Altun, 2008; Page and Johnstone, 2007). The cuticle not only protects the animal from the environment, but also determines body shape and plays a role in motility (Kramer et al., 1988; Page and Johnstone, 2007; von Mende et al., 1988). Several layers secreted by epidermal cells comprise the cuticle, including an outermost lipid layer (Blaxter, 1993).

Circumferential ridges in the cuticle called annuli pattern the length of the animal and are present during all stages of development (Costa et al., 1997). Alae are longitudinal ridges that are present during specific stages of development, including L1, dauer, and adult stages (Cox et al., 1981b; Sapio et al., 2005). Mutations in genes that affect cuticular collagen organization can alter cuticular structure and animal body morphology (Johnstone, 2000; Kramer et al., 1990; Kramer et al., 1988; von Mende et al., 1988). While cuticular imaging using compound microscopy with DIC optics is possible, current methods that highlight cuticular structures include fluorescent

---

*Reprinted with permission from "Visualization of *Caenorhabditis elegans* cuticular structures using the lipophilic vital dye DiI" by Schultz, R. D. and Gumienny, T. L., 2012. *J Vis Exp*, e3362. Copywright 2012 by Journal of Visualized Experiments. DOI 10.3791/3362.

transgene expression (Thein et al., 2003), antibody staining (McMahon et al., 2003), and electron microscopy (Cox et al., 1981a). Labeled wheat germ agglutinin (WGA) has also been used to visualize cuticular glycoproteins, but is limited in resolving finer cuticular structures (Link et al., 1988). Staining of cuticular surface using fluorescent dye has been observed, but never characterized in detail (Tong and Burglin, 2010). We present a method to visualize cuticle in live *C. elegans* using the red fluorescent lipophilic dye DiI (1,1'-dioctadecyl-3,3,3',3'-tetramethylindocarbocyanine perchlorate), which is commonly used in *C. elegans* to visualize environmentally exposed neurons. This optimized protocol for DiI staining is a simple, robust method for high resolution fluorescent visualization of annuli, alae, vulva, male tail, and hermaphrodite tail spike in *C. elegans*.

Protocol

Preparation of DiI stain

1. Prepare a stock solution of 20 mg/mL DiI (Biotium, Inc., Hayward, CA) in DMF. DiI is light sensitive, so protect DiI from light by wrapping in foil.
2. Create a working dilution of DiI by adding 0.6 μL DiI stock to 399.4 μL M9 for each population. This should give a final working dilution of 30 μg/mL DiI in M9. This can be scaled up for staining multiple populations simultaneously. Shield DiI from light by wrapping the tube(s) in foil.

Preparation of nematodes

3. Use a 60 mm plate containing a population of uncontaminated nematodes. Wash animals from plate using a solution of 0.5% Triton X-100 in M9 buffer by gently swirling liquid in a circular motion across the surface of the plate to loosen all larval and adult animals. Transfer wash into a sterile 1.5 mL tube.
4. Immediately spin down the animals at 2000 rpm for 30 sec. Remove and discard as much supernatant as possible without disturbing the mass of animals at the bottom of the tube.
5. To reduce residual Triton X-100, rinse animals using M9 buffer, spin, and remove supernatant. Repeat the rinse.
6. Add 400 μL of working DiI solution in M9 to the tube and vortex briefly to resuspend animals in the solution.
7. Shake tube at 20°C horizontally for 3 hours at 350 rpm in a light-protected environment. If desired, animals can be incubated up to 16 hours for staining.
8. To reduce the amount of unbound dye, spin down the animals at 2000 rpm for 20 sec. Remove and discard as much supernatant as possible without disturbing the mass of animals.
9. Resuspend animals in 400 μL M9 buffer and pour liquid onto a bacteria-free portion of a NGM agar plate seeded with OP50 *E. coli*. Allow animals to recover at least 30 minutes. During the recovery time the animals should crawl away from the DiI staining liquid and onto the food. This step reduces background fluorescence from free DiI.

Mounting and observation of specimens

10. Melt 4% agar in water using an autoclave or a microwave.
11. Create reusable spacers, which can be used to ensure uniform thickness of the agar pad, by layering two pieces of lab tape on a glass slide. Make two spacer slides total.
12. Arrange a clean glass slide between two spacer slides. Pipette about 150 µL (four drops) of molten 4% agar onto the center of the clean glass slide. Quickly cover the molten agar using an additional slide to form an agar pad. Carefully remove the cover slide, keeping the pad centered on the top of the mounting slide.
13. Pipette about 5 µL of nematode anesthetic (100 µM - 1 mM levamisole, for example) onto the pad.
14. Mount 8 – 12 animals in the anesthetic and cover with a microscope coverslip.
15. Observe animals using a compound or confocal microscope fitted with at least a 40x objective and a DSRed/TRITC (or other compatible) filter. The fluorescence excitation maximum of DiI is 549 nm and its emission maximum is 565 nm for bound dye (Biotium, Inc., Hayward, CA).

Representative Results

DiI stains the cuticle of wild-type and mutant *C. elegans*. The cuticular surface contains annuli separated by circumferential furrows and, in some stages, longitudinal ridges called alae. Each developmental stage has cuticular structures with distinct compositions (Cox et al., 1981b). Ridges or furrows of both alae and annuli fluorescently stain, depending on surface composition, throughout larval and adult stages

and remain visible up to a day after recovery using this method. Background fluorescent speckles are sometimes observed (Figures A.2F, G), but not routinely (Figure A.1, Figure A.2A-E, H, I). All images were taken with spinning disk confocal or, when noted, widefield (wf) compound microscopy.

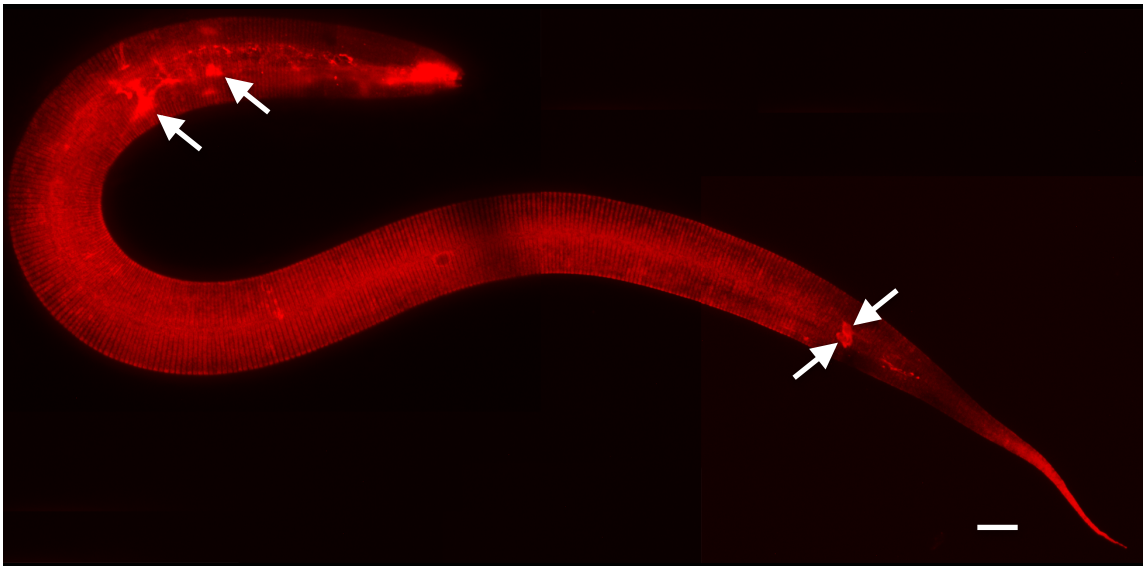

Figure A.1 DiI stains cuticle and environmentally exposed neurons. L2 stage animal. 630x magnification. Mosaic image parts were captured using iVision-Mac™ software (BioVision Technologies, Exton, PA). Images were joined using Adobe® Photoshop® CS3 (Adobe Systems, Inc., San Jose, CA). Scale bar = 10 μm. DiI also fluorescently stains amphid and phasmid sensory neurons in the head and tail respectively (arrows mark some) (Schultz and Gumienny, 2012).

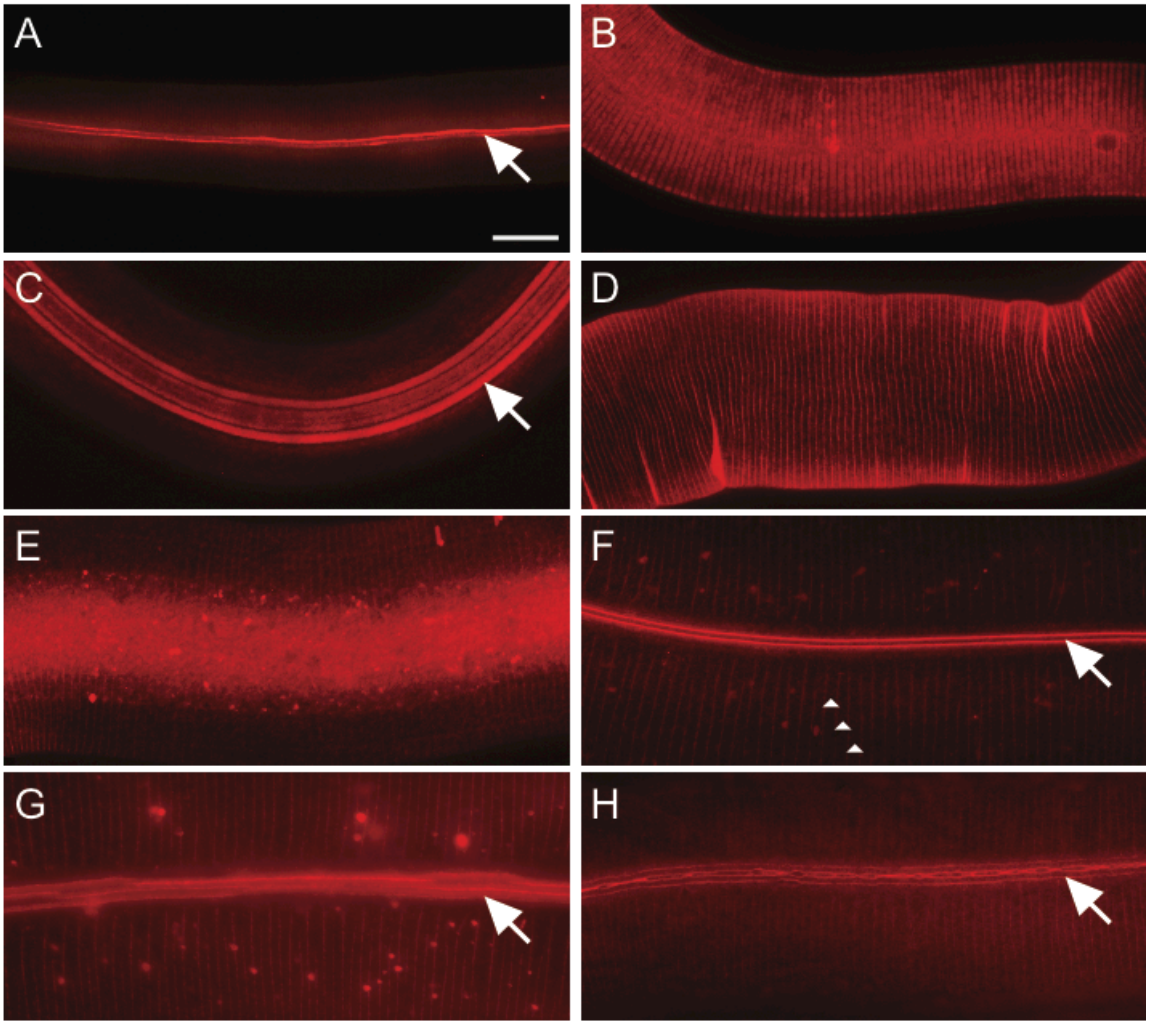

Figure A.2 DiI fluorescently stains *C. elegans* cuticle at all stages of post-embryonic development. 630x magnification. Scale bar = 10 μm. Staining of wild-type animals in A) L1; B) L2; C) dauer; D) L3; E) L4; and F) adult stages. The alae and annular ridges are fluorescently stained in L1 and dauer animals (A, C). DiI stains annular ridges in L2 animals (B). Annular furrows stain in L3 and L4 animals (D, E). The furrows of the alae and annuli are stained in adult animals (F-H). Alae are composed of two, five, or three ridges (in L1, dauer, or adult animals, respectively) that run the length of the animal (arrows). Annuli create circumferential ridges around the animal (arrowheads, F and J). The cuticle of adult mutant animals display moderate cuticular organization defects (G-H). G) Ridges of alae are discontinuous (wf). H) Supernumerary alae ridges are fused and branched or bifurcated (wf). Collagen gene mutants exhibit alae and annular organization defects (I-J). I) In transgenic animals overexpressing pRF4 (*rol-6(su1006)*), ridges of alae lie at an angle to the length of the animal. J) Annuli in transgenic animals overexpressing pRF4 (*rol-6(su1006)*) display an irregular pattern (Schultz and Gumienny, 2012).

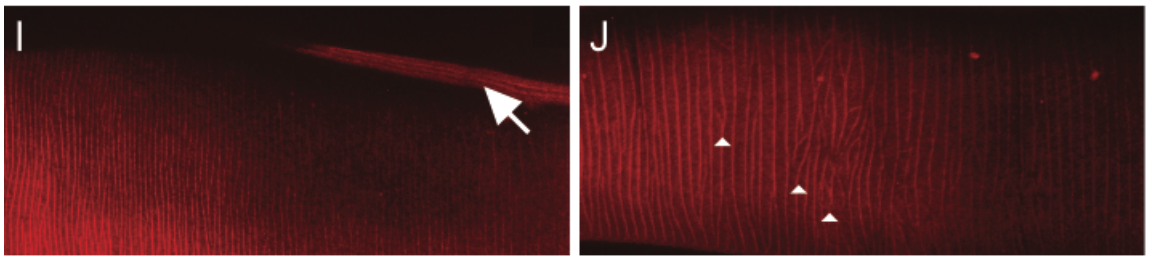

Figure A.2 Continued.

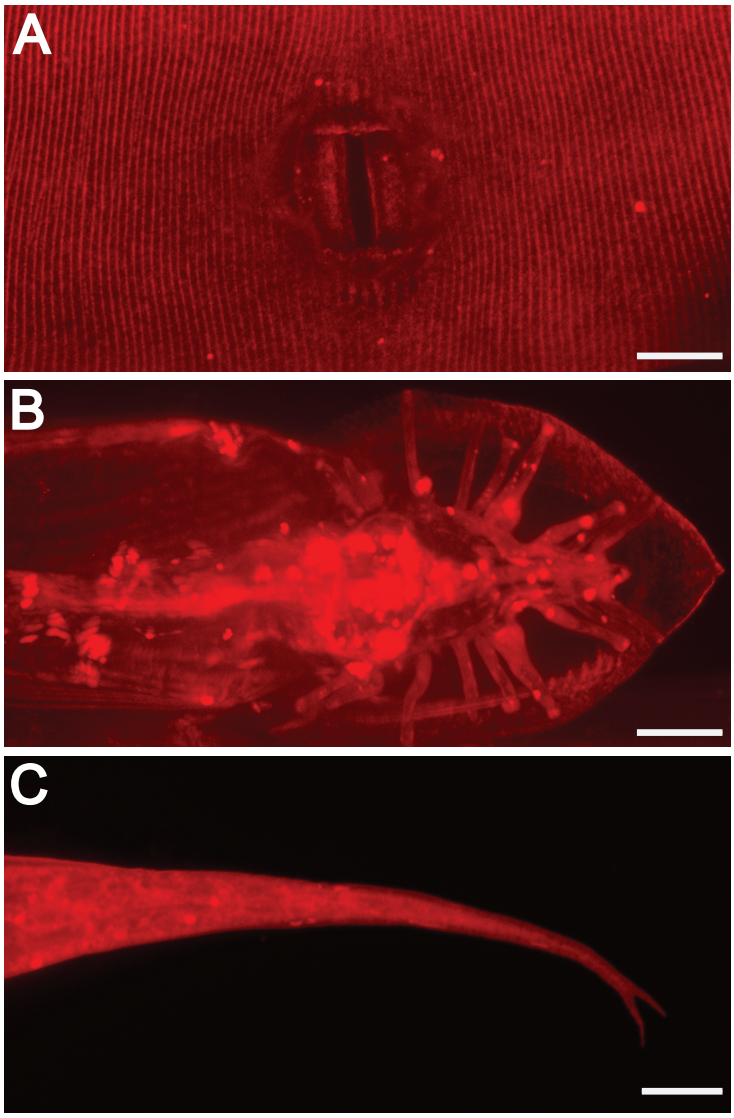

Figure A.3 External morphological structures are illuminated by DiI staining. 630x magnification. Scale bars = 10 μm. DiI also highlights other exterior features, including A) adult hermaphrodite vulva, B) adult male tail rays and fan, and C) hermaphrodite tail spike (forked in this mutant background) (Schultz and Gumienny, 2012).

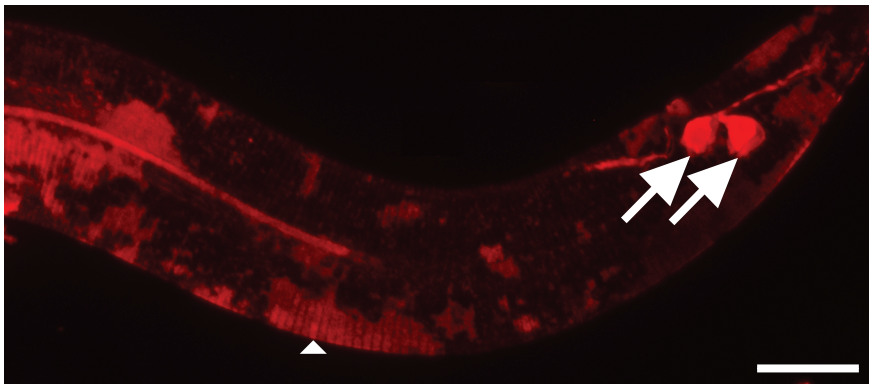

Figure A.4 Cuticle takes longer to stain with DiI than environmentally exposed neurons. 630x magnification. Scale bar = 10 μm. After two hours of staining, amphid (not shown) and phasmid sensory neurons (arrows) are sufficiently stained. In contrast, the cuticle of younger animals is only partially stained in patches (arrowhead) (Schultz and Gumienny, 2012).

Table A.1 Cuticular staining under different conditions.

Wash	Stain solution (+ DiI)	Incubation time	Cuticle stained
M9 + 0.5% Triton X-100	M9 + 0.5% Triton X-100	2 hrs	no
M9 + 0.5% Triton X-100	M9 + 0.5% Triton X-100	3 hrs	no
M9 + 0.5% Triton X-100	M9	2 hrs	partial
M9 + 0.5% Triton X-100	M9	3 hrs	**yes**
M9 + 0.5% Triton X-100	H_20	2 hrs	partial
M9 + 0.5% Triton X-100	H_20	3 hrs	yes

Various incubation solutions and times were tested to optimize cuticular staining in animals. H_20, sterile distilled water. Partial staining indicates patchy staining of larval cuticle (Figure A.4), though adult cuticle stains consistently.

Discussion

The DiI staining method presented here allows for a relatively quick and convenient way to visualize the cuticle in *C. elegans*. By repurposing and optimizing a method commonly used to image environmentally exposed sensory neurons (Collet et al., 1998; Tong and Burglin, 2010), DiI can be used to fluorescently stain both alae and annular structures (Figures A.1 and A.2), as well as the vulva, male tail, and hermaphrodite tail spike (Figure A.3). We have found that the incubation solution and time influence the ability of DiI to consistently stain the cuticle (Table A.1, Figure A.4). The method for DiI staining environmentally exposed neurons uses a two-hour incubation time in M9 with Triton X-100 (Tong and Burglin, 2010). An initial wash of M9 with the surfactant Triton X-100 helps remove contamination from the cuticular surface and prevents the animals from clumping. However, incubating the animals three hours in a staining solution in the same buffer prevents the dye from staining the cuticle (Table A.1). This may be caused by lipids on the nematode surface being stripped off by the longer treatment in the detergent solution. Incubation of animals in water with DiI stains the cuticle, indicating that the M9 salt solution is not required for DiI staining of cuticle. Although a water-based protocol is recommended for neuronal DiI staining (Tong and Burglin, 2010), we find that animals treated this way often appear unhealthy. Washing animals briefly in 0.5% Triton X-100 in M9, followed by a three-hour incubation in staining solution made with M9, provides consistent staining of cuticular structures and maintains the well-being of the animals.

Animals can be rescued after observation and maintained, permitting direct downstream analyses. This method is a convenient tool that can be used in many studies, including, but not limited to, cuticular secretion and organization, epidermal cell development, heterochronic gene pathways, and nematode evolution.